REPUBLIC OF TÜRKİYE

YILDIZ TECHNICAL UNIVERSITY

GRADUATE SCHOOL OF SCIENCE AND ENGINEERING

DEVELOPMENT OF HIGH NEAR-INFRARED (NIR) REFLECTIVE BLACK PIGMENTS

Emre TOY

MASTER OF SCIENCE THESIS

Department of Metallurgical and Materials Engineering

Material Program

Supervisor

Assoc. Prof. Dr. Buğra ÇİÇEK

August, 2024

REPUBLIC OF TÜRKİYE

YILDIZ TECHNICAL UNIVERSITY

GRADUATE SCHOOL OF SCIENCE AND ENGINEERING

DEVELOPMENT OF HIGH NEAR-INFRARED (NIR) REFLECTIVE BLACK PIGMENTS

A thesis submitted by Emre TOY in partial fulfillment of the requirements for the degree of **MASTER OF SCIENCE** is approved by the committee on 07.08.2024 in Department of Metallurgical and Materials Engineering, Program of Material.

Assoc. Prof. Dr. Buğra ÇİÇEK
Yildiz Technical University
Supervisor

Approved by the Examining Committee

Assoc. Prof. Dr. Buğra ÇİÇEK, Supervisor
Yildiz Technical University _____

Asst. Prof. Dr. Hakan YILMAZER, Member
Yildiz Technical University _____

Prof Dr. Recep ARTIR, Member
Marmara University _____

I hereby declare that I have obtained the required legal permissions during data collection and exploitation procedures, that I have made the in-text citations and cited the references properly, that I haven't falsified and/or fabricated research data and results of the study and that I have abided by the principles of the scientific research and ethics during my Thesis Study under the title of Development of High Near-Infrared (NIR) Reflective Black Pigments supervised by my supervisor, Assoc. Prof. Dr. Buğra ÇİÇEK. In the case of a discovery of false statement, I am to acknowledge any legal consequence.

Emre TOY

Signature

Dedicated to my family

and my best friends

ACKNOWLEDGEMENTS

I would like to express my gratitude to everyone who contributed to the completion of this thesis. Firstly, I sincerely thank my advisor, Assoc. Prof. Dr. Buğra ÇİÇEK, for his support throughout my graduate studies. Without his wisdom, guidance, and encouragement, this thesis would not have been possible.

My special thanks go to Dr. Oğuz KARAAHMET, Kumru KARAMAN-ÜNLÜTÜRK, Mete ÜNLÜTÜRK, Dr. Nurullah ÇÖPOĞLU, Zeynep ADAR, and my non-blood-related family who have always been by my side and supported me.

I would like to extend my deep gratitude to my family. Their loving support and encouragement have been invaluable throughout this journey. I owe them endless thanks.

Additional, I would like to thank Akcoat Advanced Chemical Coating Co. Pigment R&D team for their endless support, all the information they did not hesitate to share, and industrial guidance.

Emre TOY

TABLE OF CONTENTS

LIST OF SYMBOLS vii
LIST OF ABBREVIATIONS viii
LIST OF FIGURES x
LIST OF TABLES xii
ABSTRACT xiii
ÖZET xv
1 INTRODUCTION 1
1.1 Literature Review 1
1.2 Objective of the Thesis 4
1.3 Hypothesis 4
2 PIGMENT 6
2.1 Definition and Classification of Pigments 6
2.2 Properties of Pigments 9
2.3 Characterization of Pigments 11
2.4 Pigment Applications 17
3 TYPES OF INORGANIC PIGMENTS 19
3.1 Types of Inorganic Pigments 19
3.1.1 Iron Oxide Pigments 19
3.1.2 Chromium Oxide Pigments 20
3.2 Metal Complex Pigments 21
3.2.1 Rutile Pigments 22
3.2.2 Spinel Pigments 23
3.2.3 Zirconium Based Pigments 24
3.3 Carbon Black Pigments 24
4 NEAR-INFRARED REFLECTIVE PIGMENTS 27
4.1 Cool Pigments 27
4.2 NIR Reflective Pigments for Polymer Sorting 28
5 COLOR 29
5.1 Overview of Color Science 29

5.2 Color Formations 30
5.2.1 Color Formation by The Effect of Crystal Field 30
5.2.2 Color Formation with Charge Transfer 31
5.2.3 Color Forming Through Band Gaps 31
5.2.4 Color Measurement 32
6 EXPERIMENTAL STUDIES 34
6.1 Raw Materials 34
6.2 Preparation of Reactants 34
6.3 Preparation of Pigment 35
6.4 Calcination 35
6.4.1 Milling 35
6.4.2 Drying 36
6.4.3 Color Application 36
6.5 Characterization 39
6.5.1 Crystallography/Determination of Crystalline Structures 39
6.5.2 Elemental Analysis/ Determination of the Chemical Composition . 40
6.5.3 Particle Size Distribution 40
6.5.4 Morphology 41
6.5.5 Color Measurement 41
6.5.6 UV-Vis-NIR Spectroscopy 42
7 RESULTS AND DISCUSSION 44
7.1 Prestudies for NIR Reflective Black Pigments 44
7.1.1 Inorganic Black Pigment Trials 44
7.2 Fe-Cr Inorganic Pigments 50
7.2.1 Effect of Calcination Temperature on Properties of Fe-Cr Pigments 50
7.2.2 Effect of Fe:Cr Ratio on Properties of Pigments 58
7.2.3 Effect of Particle Size Distribution on Properties of Fe-Cr Pigments 67
7.3 NIR Reflective Black Pigments for Polymers 73
7.3.1 NIR Sorting of Polymers 73
7.3.2 Effect of Particle Size of Pigments 75
8 CONCLUSION 78
REFERENCES 81
PUBLICATIONS FROM THE THESIS 93

LIST OF SYMBOLS

Å	Angstroms
E_g	Band gap energy
*C**	Chroma
°C	Degree Celsius
eV	Electronvolt
*h**	Hue angle
*a**	In CIE *L* a* b** color space, *a** indicates red-green
*b**	In CIE *L* a* b** color space, *b** indicates yellow-blue
*L**	In CIE *L* a* b** color space, *L** indicates lightness
μm	Micrometer
mm	Millimeter
nm	Nanometer
%	Percentage
ρ(λ)	Reflectance spectra
R(λ)	Reflectance factor curves

LIST OF ABBREVIATIONS

AAS	Atomic absorption spectroscopy
ASTM	American Society for Testing and Materials
ATR	Attenuated total reflection
atm	The standard atmosphere
BET	Brunauer, Emmett, and Teller
CICP	Complex inorganic colored pigment
CIE	International Commission on Illumination
DCMA	Dry Color Manufactures Association
DIN	Deutsches Institut für Normung
DRIFTS	Diffuse Reflectance Infrared Fourier Transform Spectroscopy
EIA	Energy Information Administration
EN	European Standards
FEGSEM	Field emission gun scanning electron microscopy
FT-IR	Fourier-transform infrared
h	hour
ICDD	International Centre for Diffraction Data
IEA	International Energy Agency
IPCC	Panel on Climate Change
IR	Infrared
IRS	Internal Reflectance Spectroscopy
ISO	International Standards Organization
MFI	Melt Flow Index
min	Minute
NIR	Near-infrared
PDF	Powder Diffraction File
PE	Polyethylene
PET	Polyethylene terephthalate
pH	Potential of hydrogen

PP	Polypropylene
REE	Rare-earth elements
R_{NIR}	Electromagnetic wave reflectance of material in NIR region
RPM	Revolutions per minute
SCE	Specular Component Excluded
SCI	Specular Component Included
SEM	Scanning electron microscopy
TEM	Transmission electron microscopy
TG	Thermogravimetry
UV	Ultraviolet
Vis	Visible
WDXRF	Wavelength Dispersive X-ray Fluorescence Spectrometry
wt.	Weight
XRD	X-ray diffraction
XRF	X-ray fluorescence techniques

LIST OF FIGURES

Figure 2.1 Classification of colorants 7

Figure 2.2 Classification of inorganic pigments 8

Figure 2.3 Classification of pigments based on chemical composition 9

Figure 2.4. Illustration of light scattering method for particle size measurement 13

Figure 2.5 Illustration of sieve method for particle size measurement 14

Figure 2.6 Illustration of BET specific surface area analysis 15

Figure 2.7 SEM micrographs of (a) active carbon (porous) and (b) carbon black (non-porous) 16

Figure 2.8 Crystalline structures of pigments with examples 16

Figure 4.1 "Cool" pigment roof application illustration 28

Figure 5.1 Reflection spectra of TiO_2 (rutile), red iron oxide (a-Fe_2O_3), chrome antimony yellow (PBr24), cobalt aluminate blue (PB28) 29

Figure 5.2 CIE *L*a*b** and *L*C*h* color space 32

Figure 6.1 Schematics of experimental studies 34

Figure 6.2 Workflow chart of experimental studies 34

Figure 6.3 Gelimat mixer to mix polymer and pigment 37

Figure 6.4 Hot and cold press to form polymeric plates 38

Figure 6.5 Pool type film applicator 38

Figure 6.6 Planetary ball milling equipment 39

Figure 6.7 Y-stabilized zirconium oxide jar 39

Figure 6.8 Red and blue lasers from the Malvern Mastersizer 3000 are directed at various detectors and scattered laser light by different size of particles 40

Figure 6.9 Illustration of diffuse and specular light for SCI and SCE method 41

Figure 7.1 XRD patterns and phases of different compositions of pigments calcined at 1000 °C for 3 hours 46

Figure 7.2 Colors of different compositions of pigments 47

Figure 7.3 UV-Vis-NIR reflectance spectrum of different composition of pigments 49

Figure 7.4 XRD analysis of samples Fe:Cr1-10, Fe:Cr1-11, and Fe:Cr1-12 51

Figure 7.5 XRD analysis of samples Fe:Cr1-10, Fe:Cr1-11, and Fe:Cr1-12 in the angle range of 33-37 52

Figure 7.6 Color hues of Fe:Cr1-10, Fe:Cr1-11, and Fe:Cr1-12 53

Figure 7.7 UV-VIS-NIR spectrums of Fe:Cr1 calcined at 1000-1200 °C 54

Figure 7.8 NIR spectrums of Fe:Cr1 calcined at 1000-1200 °C 55

Figure 7.9 UV-VIS-NIR spectrums of Cr_2O_3, Fe_2O_3, and Fe:Cr1 calcined at 1000-1200 °C 56

Figure 7.10 VIS spectrums of Fe:Cr1 calcined at 1000-1200 °C 57

Figure 7.11 XRD analysis of Fe:Cr0.5, Fe:Cr1 and Fe:Cr2 calcined at 1000 °C. 59

Figure 7.12 Calculated and experimental phase diagram of Cr–Fe–O in air at 1 atm 61

Figure 7.13 XRD analysis of samples Fe:Cr0.5-10, Fe:Cr1-10, and Fe:Cr2-10 in the angle range of 33-36.5 62

Figure 7.14 XRD analysis of Fe:Cr0.5, Fe:Cr1 and Fe:Cr2 at 1200 °C 63

Figure 7.15 XRD analysis of samples Fe:Cr0.5-12, Fe:Cr1-12, and Fe:Cr2-12 in the angle range of 33-36.5° 64

Figure 7.16 Mass colors of Fe:Mn05, Fe:Mn1 and Fe:Mn2 calcined at 1000/1200 °C 66

Figure 7.17 NIR reflectance spectrum of Fe:Cr0.5, Fe:Cr1 and Fe:Cr2 calcined at 1000 °C 66

Figure 7.18 NIR reflectance spectrum of Fe:Cr0.5, Fe:Cr1 and Fe:Cr2 calcined at 1200 °C 67

Figure 7.19 FEGSEM images of a) PS-1, c) PS-5 and e) PS-10 taken at x20,000 magnifications; b) PS-1, d) PS-5 and f) PS-10 taken at x80,000 magnifications 68

Figure 7.20 Particle size distribution of PS-1, PS-5 and, PS-10 70

Figure 7.21 Mass and tint colors of PS-1, PS-5 and PS-10 71

Figure 7.22 XRD analysis of PS-1, PS-10 and Fe:Cr1 RM 72

Figure 7.23 NIR reflectance spectrum of PS-1, PS-5, PS-10 and Carbon Black . 73

Figure 7.24 Plastic plates of a) PP, b) PE, c) PP-Fe:Cr1-10, and d) PE-Fe:Cr1-10 74

Figure 7.25 UV-VIS-NIR reflectance spectrums of PP and PE 74

Figure 7.26 UV-VIS-NIR reflectance spectrums of PP-Fe:Cr1-10, PE-Fe:Cr1-10 and PP-Carbon Black 75

Figure 7.27 The photograph of PSMP-1, PSMP-5 and PSMP-10 on light source 76

Figure 7.28 Illustration of light interaction with object a) less opaque and b) more opaque 77

LIST OF TABLES

Table 2.1 Selection criteria of pigment 18

Table 3.1 Common crystalline structures and examples of pigments 22

Table 7.1 Composition of pigments used for pre-studies 45

Table 7.2 Color measurement, NIR reflectance and chroma of different compositions of pigments 48

Table 7.3 Color coordinates, NIR reflectance and chroma of Fe:Cr1 calcined at 1000-1200 °C 53

Table 7.4 Composition of Fe-Cr pigments calcined at 1000 °C to compare effect of Fe:Cr ratio 58

Table 7.5 Crystallographic information of Fe_2O_3, Cr_2O_3 ,$FeCrO_3$ from ICDD/PDF 61

Table 7.6 Color measurements of Fe:Cr0.5, Fe:Cr1 and Fe:Cr2 calcined at 1000 and 1200 °C 65

Table 7.7 Particle size distribution of PS-1, PS-5, and PS-10 69

Table 7.8 Color values of PS-1, PS-5 and PS-10 70

Table 7.9 Color and Chroma values of PSMP-1, PSMP-5, and PSMP-10 76

Table 8.1 Properties of $(Fe,Cr)_2O_3$ pigments synthesized with different parameters 80

ABSTRACT

Development of High Near-Infrared (NIR) Reflective Black Pigments

Emre TOY

Department of Metallurgical and Materials Engineering

Master of Science Thesis

Supervisor: Assoc. Prof. Dr. Buğra ÇİÇEK

Pigments are materials used to provide color and functional properties to materials such as ceramics, glass, plastic, and paint. Carbon black is preferred in many sectors, such as paint, plastic, and rubber due to such as high coloring strength, color and stability. However, it plays a restrictive role in NIR sorting systems because it absorbs the electromagnetic waves required for the sorting of plastics. Moreover, it absorbs solar energy and causes surface and object temperatures to increase, causing global warming. To eliminate these limitations, NIR reflective inorganic black pigments have been synthesized with metal oxides. In this study, pigments were synthesized via solid state reaction at 1000-1200 °C. As a result of the preliminary studies, the pigment with the highest reflectance was selected and the effects of parameters such as composition, particle size and calcination temperature were examined. Color properties of pigments were checked with paint and plastic in the CIE *L*a*b** color space. UV-Vis-NIR spectrophotometer was used to measure the reflectivity of the pigments.

According to the results: As the calcination temperature increased, increase in the reaction efficiency and R_{NIR} were observed. A decrease in the chroma (*C**) of the pigments was observed with increasing temperature. While no major difference in

both color and R_{NIR} were observed at high temperatures due to the change in the Fe:Cr ratio, a decrease of R_{NIR} was observed with the increase in the Cr ratio in calcinations at lower temperatures. On the other hand, with the decrease in particle size, the color of the pigment moved away from black by increasing the C^* value, but no significant change was observed in the R_{NIR}. However, a significant increase in the coloring strength and the hiding power of the pigments was observed. Thus, pigments with desirable properties in different application areas were obtained.

Keywords: Pigment, black, inorganic, synthesis, NIR, recycling, cool

ÖZET

Yüksek Yakın Kızılötesi (NIR) Yansıtıcı Siyah Pigmentlerin Geliştirilmesi

Emre TOY

Metalurji ve Malzeme Mühendisliği Anabilim Dalı

Yüksek Lisans Tezi

Danışman: Doç. Dr. Buğra ÇİÇEK

Pigmentler, seramik, cam, plastik ve boya gibi malzemelere renk ve işlevsel özellikler kazandırmak için kullanılan maddelerdir. Karbon siyahı, yüksek boyama gücü, renk ve kararlılık gibi özellikleri nedeniyle boya, plastik ve kauçuk gibi birçok sektörde tercih edilmektedir. Ancak, plastiklerin ayrıştırılmasında gerekli olan elektromanyetik dalgaları emdiği için NIR (yakın kızılötesi) ayırma sistemlerinde sınırlayıcı bir rol oynamaktadır. Ayrıca, güneş enerjisini emerek yüzey ve nesne sıcaklıklarının artmasına neden olmakta ve bu da küresel ısınmaya yol açmaktadır. Bu sınırlamaları ortadan kaldırmak için metal oksitler ile NIR yansıtıcı inorganik siyah pigmentler sentezlenmiştir. Bu çalışmada, pigmentler 1000-1200 °C'de katı hal reaksiyonu ile sentezlenmiştir. Ön çalışmalardan elde edilen sonuçlara göre, en yüksek yansıtma gücüne sahip pigment seçilmiş ve kompozisyon, partikül boyutu ve kalsinasyon sıcaklığı gibi parametrelerin etkileri incelenmiştir. Pigmentlerin renk özellikleri CIE $L^*a^*b^*$ renk uzayında boya ve plastik ile test edilmiştir. Pigmentlerin yansıtıcılığını ölçmek için UV-Vis-NIR spektrofotometresi kullanılmıştır.

Sonuçlara göre: Kalsinasyon sıcaklığı arttıkça, reaksiyon verimliliği ve R_{NIR}'da bir artış gözlemlenmiştir. Sıcaklık arttıkça pigmentlerin kromasında (C^*) bir azalma

gözlenmiştir. Fe:Cr oranındaki değişim nedeniyle yüksek sıcaklıklarda hem renk hem de R_{NIR} açısından önemli bir fark gözlenmezken, daha düşük sıcaklıklarda Cr oranının artışıyla birlikte R_{NIR}'da bir azalma gözlemlenmiştir. Öte yandan, partikül boyutunun küçülmesiyle pigmentin rengi C^* değerinin artmasıyla siyahtan uzaklaşmış, ancak R_{NIR}'da önemli bir değişiklik gözlenmemiştir. Bununla birlikte, pigmentlerin boyama gücü ve örtücülüğünde önemli bir artış görülmüştür. Böylece, farklı uygulama alanlarında istenilen özelliklere sahip pigmentler elde edilmiştir.

Anahtar Kelimeler: Pigment, siyah, inorganik, sentez, NIR, geri dönüşüm, soğuk

1
INTRODUCTION

1.1 Literature Review

Pigments are organic and inorganic materials with generally small particle sizes, insoluble in application systems. They are employed to impart aesthetic properties such as color, opacity, and transparency to materials [1]–[7]. In addition to aesthetic properties, pigments are utilized in anticorrosive applications to enhance corrosion resistance [1], [3]–[5]. Some pigments are employed as 'cool' pigments due to ability to reflect electromagnetic waves in the NIR region of solar light [8]–[19].

The urban heat island effect occurs when an area exhibits higher temperatures than its surrounding urban environment. This phenomenon can be attributed to factors such as high energy consumption, the replacement of natural habitats with materials that absorb heat during urbanization, and the widespread use of dark pigments, especially on roads, roofs, and exterior wall paints [11], [20]–[27].

In particular, during the summer and in regions with sunny seasons, temperature increases are exacerbated by the elevated energy consumption for air conditioning purposes. One significant contributor to the urban heat island effect is the use of general black pigments, such as carbon black, on various surfaces. Carbon black absorbs almost all electromagnetic waves present in sunlight, leading to the accumulation of energy on the surface [18]. This accumulated energy raises the temperature of materials, subsequently increasing energy consumption for cooling systems, especially in buildings exposed to heat [20], [21], [23], [25].

It is noteworthy that sunlight comprises UV (280–400 nm), 43% Vis (400–700 nm), and 52% NIR (700–2500 nm) radiation [13], [26], [28]. Carbon black absorbs almost all radiations from sunlight. In contrast, complex inorganic colored pigments (CICPs) possess the ability to reflect radiations in the NIR region [29]–[31]. This

unique characteristic enables them to mirror the radiation of sunlight, similar to natural materials found in nature. The reflectivity in the NIR region prevents the absorption of energy responsible for contributing to global warming.

Another important feature of NIR reflective pigments is their impact on polymer recyclability. Carbon black is commonly used to color black polymeric materials. However, polymers colored with carbon black cannot be recycled as they remain undetected by NIR sensors. Each polymer exhibits a unique reflectance spectrum depending on its chemical structure in the 700-2500 nm range [32], [33]. For effective recycling, polymers must be separated based on their chemical structure. However, when carbon black is used for coloring these polymers, it hinders the reflection of the polymers by absorbing radiation, making it challenging to determine the polymer's chemistry. Consequently, many polymers like PP, PE, and PET are stored in a mixed form, unable to be separated, leading to the formation of garbage islands in nature or their destruction through incineration. Both methods pose serious threats to nature, causing environmental pollution and disrupting natural life. The incineration of non-recyclable materials releases carbon dioxide into the air, affecting the natural environment both above and below the sea surface. In contrast, when inorganic black pigments reflecting NIR are used for black coloring, the polymers can be classified because the electromagnetic waves in the NIR region are not absorbed but reflected. Classified polymeric materials can be recycled under appropriate conditions, reducing the amount of carbon dioxide released into the environment and minimizing environmental damage. Consequently, these pigments are significantly more environmentally friendly than the commonly used carbon black pigment, as their structures closely resemble those found in nature. According to research by the Intergovernmental Panel on Climate Change (IPCC), if the necessary studies are conducted to reduce the amount of carbon dioxide and other greenhouse gases in the atmosphere, it is estimated that by the end of 2100, the average global surface temperature will rise between 1.1-6.4 °C [34], [35].

In this direction, the world’s increasingly diminishing energy resources and disrupted ecological balance require the conservation and more efficient use of existing resources.

The high energy consumption used in the heating and cooling of buildings has attracted the high interest of many researchers. According to reports prepared by the Energy Information Administration (EIA), energy consumed for heating or cooling in buildings accounts for 51% of total energy consumption [36]. According to report prepared by the IEA (Internatianol Energy Agency) estimates that space cooling accounted for around 6% of total electricity demand averaged across all countries in 2016 [37]. In 2021, space cooling demand grew at the highest rate among all building end uses, representing approx. 16% of the industry's total final electrical energy use [38].

Since 2000, energy demand for space cooling has increased at an average annual rate of 4% [38]. The highest shares were in 16% in the United States, 15% in the Middle East, 14% in Mexico and 10% in Japan. In some countries, such as the Middle East and parts of the United States, the energy used for space cooling can exceed 70% of total residential energy consumption on extremely hot days [37].

Although NIR rays are not visible to the human eye, electromagnetic radiation in the NIR region can be felt as heat by the material absorbing these radiations [39]–[42]. By reducing surface temperature increases, NIR reflective pigments also slow the development of global warming while saving energy by reducing the energy demand consumed for climate change [24], [26], [27], [43]–[45].

Several studies in the United States and Europe have found that when NIR reflective materials are used instead of traditional outdoor applications, energy savings are achieved between 20% and 40% per year in the use of climate energy in buildings, depending on climate conditions [21], [41], [46].

In the literature, studies have been carried out on the NIR reflectivity properties of many colors with different compositions such as black, brown, blue and yellow [8], [11], [14], [18], [19], [47]. NIR reflectivity of pigments has an important place in air conditioning and global warming issues. In addition, black NIR reflectivity pigments are also known for their contribution to the recycling of plastic materials. S. Sadeghi-Niaraki et al. studied the NIR and color properties of $(Fe,Cr)_2O_3$ black pigment by coating it with TiO_2 [23]. The raw material mixtures were calcined at 500 and 1000 °C. Approximately 33% NIR reflectivity was achieved for $(Fe,Cr)_2O_3$ pigment. Color values are 19.8, 2.3, and 1.5 for *L**, *a**, *b**, respectively. As a result

of TiO_2 coating, the R_{NIR} value was approximately 57.8, while the color values were 51.5, 9.41 and 26.3 for *L**, *a** and *b**, respectively, and it lost its darkness and its *C** value increased and moved away from black. In another study by S. Sadeghi-Niaraki et al., $Fe_{1.5}Cr_{0.5}O_3$ black pigment was obtained by spray pyrolysis method. It reached its highest R_{NIR} value at 800 °C and this value is 49.1. The *L**, *a** and *b** values of the pigment obtained are 24.4, 2.7 and 0.5, respectively [30]. R.Oka et all. worked to obtain high NIR reflective black pigments using the formula $Ca_2Mn_{1-x}Ti_xO_4$ ($0 \leq x \leq 0.40$) [48]. While the Ca_2MnO_4 black pigment they obtained had an R_{NIR} value of 50.1, it increased to 72.5 with the increasing amount of Ti. However, while the color *L**, *a** and *b** values were 25.2, -0.82 and 0.73 for Ca_2MnO_4, they were 28.5, 11.6 and 17.5 for $Ca_2Mn_{0.60}Ti_{0.40}O_4$. With the increase in *L** value and *a*/b** values moving away from 0, the color moved away from black. M. Suwan et al. obtained $NiFe_2O_4$ black pigment at 1100 °C using the solid state method [15]. The pigment has a R_{NIR} value of 52 and the *L**, *a** and *b** values are given as 28.7, 3.3 and -0.59, respectively.

1.2 Objective of the Thesis

The scope of the study is to develop and examine the optical properties of high NIR reflective black pigments, also known as "cool" pigments. In addition to being a "cool" pigment, it is used to obtain recyclable plastic products as an alternative to carbon black, thanks to its NIR reflectivity. Parameters such as calcination temperature, particle size and composition, which have important effects on pigment production, have an impact on the color properties and NIR reflectivity of the pigment. Since the user of the final product may have different preferences, the effects of these parameters on the pigment will be examined.

1.3 Hypothesis

Pigments can have different properties according to the expectations of the end user. Black pigments can have different undertones when considered in terms of color. These undertones are determined in line with the aesthetic expectations and demands of the end user. On the other hand, the coloring strength or hiding power of the pigment affects the amount of use of the pigment and the final opacity of the

product. When pigments are examined functionally, their NIR reflectivity may vary depending on parameters such as particle size and chemical composition.

It is aimed to consider different options by examining the color and NIR reflectivity properties of pigments, which vary depending on the chemical composition and crystal structure. As a result of these studies, a high NIR reflective black pigment will be selected among the pigments obtained to be studied in detail.

Three different pigments with the structure $(Fe,Cr)_2O_3$ and different Fe:Cr ratios will be synthesized. The effect of the composition on the color properties, NIR reflectivity and reaction efficiency of the final product will be examined. The R_{NIR} values of the pigments obtained are expected to be between 30-60%.

It is aimed to examine the effects of calcination temperature on reaction efficiency and pigment color properties. Calcination will be carried out between 1000-1200 °C to examine temperature-dependent phase changes and reaction efficiency. It is expected that with increasing temperature, the reactant ratio in the final structure will decrease and the $(Fe,Cr)_2O_3$ phase will form and the color will approach black. It is expected that pigments with lower C^* will be obtained with increasing calcination temperature.

It is aimed to examine the effects of particle size on the coloring strength, color properties and NIR reflectance of the pigment. In order to examine the particle size effect, the particle size distribution (PSD) (Dv_{90}) is aimed to be smaller than 1, 5, 10 μm. An increase in NIR reflectivity and coloring strength is expected as the particle size decreases.

2
PIGMENT

2.1 Definition and Classification of Pigments

Pigments are organic and inorganic materials which are generally have small particle size and almost not soluble in application systems such polymers, glass, ceramic and etc. Pigments are used in order to give materials esthetic properties which are color, opacity/transparency, effects and etc. Moreover, they can be used as functional additives in different applications because of its anticorrosive and magnetic properties [1], [3]–[5], [49]. Furthermore, the pigments can effect the climate change and global warming positively thank to its properties which are similar to material which are exist in the nature [11], [13], [20], [32], [33], [47], [50], [51]. Pigments can be separated from dyes with properties of practically insoluble in the materials. The pigments mostly used in ceramic, glass, paints, plastics, inks, cosmetic products, construction, rubber and etc. [1], [3]–[5], [49].

"Pigment" comes from the word of Latin language “pigmentum”. The word is used with regard of a coloring material. By time, the mean of this term has been expanded to describe colored decoration. Also this is used to indicate extracts of vegetables and plants in the Middle Ages because of the ability of coloring these matters. For all these situations, the terms of “dye” or “dyestuff” are better words to indicate these matters, instead of “pigment” [1][52].

The all colored compounds can be defined in the term of “colorant” regardless of their usage, purpose or origin. Colorant are not classified as pigments and dyes, but also synthetic and natural. Some pigments or dyes exist as natural while the synthetics were exist by human being [1][52].

Pigment particles have to be dispersed or attached in some additional materials, medium or binder, in order to coloring substrate or surfaces. These additional can

be paints, coatings, solvents, plastics and etc. The pigments can directly have applied on surface or substrates such as metal, fibers, papers and etc. [1], [4].

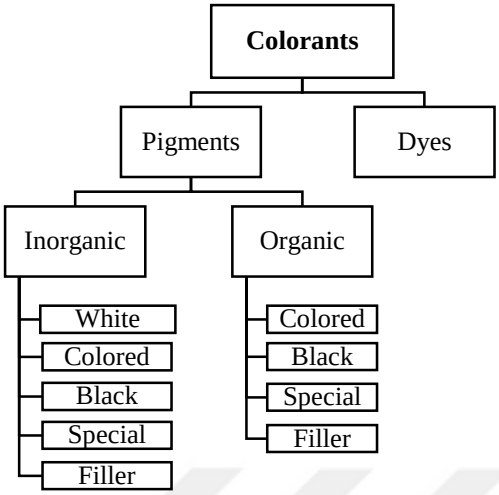


Figure 2.1 Classification of colorants [1]

Figure 2.1 shows a general classification of pigments and dyes with subcategories. Pigments are divided to two categories which are inorganic and organic while dyes are only organic. Inorganic pigments are divided into the categories which are white pigment, colored pigments, black pigments, special pigments and fillers. Organic pigments are divided to the categories which are colored pigments, black pigments, special pigments and fillers. Figure 2.2 shows a classification of the categories within the category of inorganic pigments. The most important representatives of the categories are given in Figure 2.2. Titanium oxide (TiO_2, rutile and anataese), zinc oxide, zinc sulfide, lithopone represents white pigments. Colored pigments are represented by wide range and these are mixed metal oxides, ultramarine blue iron oxide and etc. for blue pigments; chromium oxide, mixed metal oxides for green pigments; chrome yellow, nickel antimony titanate, cadmium sulfide, and praseodymium silicate for yellow pigments; iron oxides, cadmium selenides, and oxonitride for red pigments [1], [3]–[5].

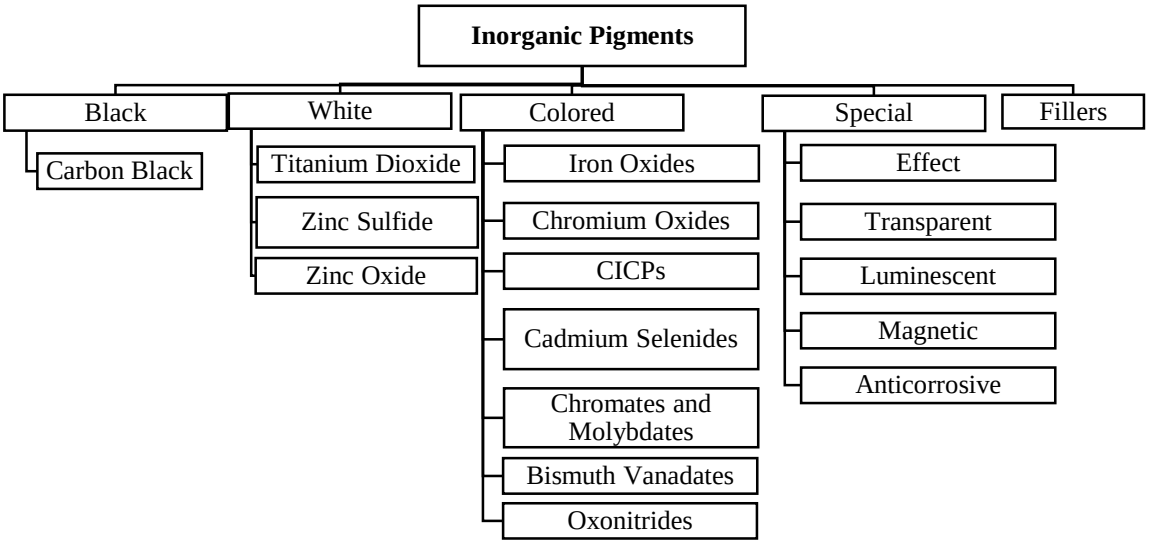


Figure 2.2 Classification of inorganic pigments [1]

Carbon black is the main representative pigment of the black pigments. The other colors shades between black and white can be obtained by combination of these black and white pigments [1].

In the field of science, pigments are classified into different categories based on their properties and functions. One such classification includes special pigments, which are further subdivided into various classes. The first class is effect pigments, also known as luster pigments, which consist of two subcategories; special and metal effect pigments. The second class is transparent pigments, which are further divided into two subcategories; fluorescent and phosphorescent pigments. The third class is luminescent pigments, which includes materials that emit light, and the fourth class is magnetic pigments. Additionally, there are others that are classified as functional pigments, such as electrically conducting, IR reflective, and UV absorbent materials. This categorization of pigments is important for understanding their properties and potential applications [1][3].

The fillers are powder materials which are not practically soluble in the application system. The property that distinguish fillers from pigments is also refractive index (RI). Although this property is not a certain distinguishing value, in general, RI of fillers is under 1.7, while refractive index of pigments is above 1.7. Fillers are not colorants in the strict sense of the word, but a material that changes the applied materials to improve its optical, color properties, and volume increases. In addition,

fillers are preferred to reduce the consumption of more expensive binder ingredients [1], [3]–[5].

An alternative way to classify inorganic pigments is categorization according to chemical compositions. Figure 2.3 shows the classification of inorganic pigments based on chemical compositions.

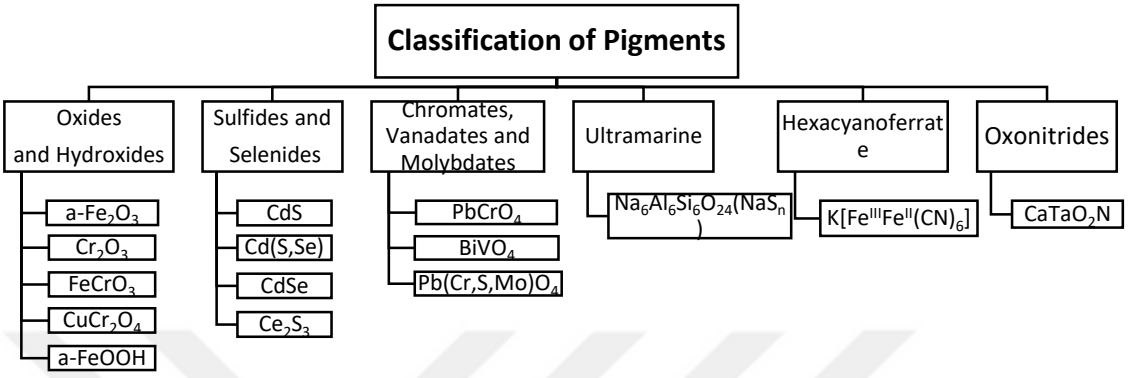


Figure 2.3 Classification of pigments based on chemical composition [1]

2.2 Properties of Pigments

The inorganic pigments are uniform chemical composition and crystalline structures in mostly. Some exceptions are layered, encapsulated and mixed pigments. These pigments are non-uniform as chemically and crystallographically. The mixed pigments consist of blending different pigments. The pigments which are blended should be similar properties due to obtain stable pigments in the application system. If the pigments have too different properties like particle size, density and durability, the pigments can be separated or reacted during application which cause non homogenous and low quality applications. Special pigments such as effect and, encapsulated pigments are formed by coating of a substrate materials [1], [3], [4].

The other case is coated pigment or layer-substrate pigments. These pigments are formed by coating a substrate material to obtain developed pigments such as better dispersionability, more stable and in the application medium as chemically or physically, preferably hydrophobic or hydrophilic surface characteristic. The interactions between coating material and substrate are strong so these pigments do not have problems during application like blended pigments [1], [3], [4].

The optical properties of pigmented systems depend on properties of pigments and application medium-binder. The properties of pigments like particle size and its distribution, refractive index of pigments, particle morphology, hiding power are determinant for final product. On the other hand, the properties of mediums are determinant for final products. The pigment volume ratio can affect the optical properties of colored system [1], [3], [4].

The pigments can be classified according to its optical effects and mechanism in 3 groups. The pigments in the first group give color or effect by scattering or absorption of light. This group includes pigments which are white, black, and colored. The white pigments scatter light without any wavelength selection, while black pigments absorb all wavelength without any selection. Otherwise, colored pigments absorb and scatter light selectively in visible range of electromagnetic waves. For example, black pigments include carbon black, black iron oxide, complex inorganic colored pigment (CICP) blacks; white pigments include TiO_2, ZnO, CaCO3, lithopone and etc.; colored pigments include cobalt blue, ultramarine blue, praseodymium yellow, cadmium red, chrome green and etc. [1], [3], [4].

The pigments in the second group, called effect pigments, give color or effect by reflection on parallel oriented, high reflection ability and platelet shaped particles. This group includes pigments which are metal effect, pearlescent and interference. Metal effect pigments regularly reflect the lights on parallel orientation. These pigments, flakes of aluminum, zinc or copper, are metallic and platelet shaped. Pearlescent pigments have very similar properties with metal effect pigments. Pearlescent and interference pigments reflect the lights regularly on parallel direction like metal effect pigments and it is highly refractive and platelet shaped. Metal oxide coated mica (iron oxide, titanium oxide coated), basic lead carbonate, tin oxide are examples for pearlescent and interference pigments [1], [3], [4], [53]–[55].

The pigments in the third group, called luminescent pigments, give color as emitting the radiation as light after absorption of the light. This group includes pigments which are fluorescent and phosphorescent pigments. The mechanism of fluorescent pigments is emitting light at longer wavelength after without delay absorption of light. On the other hand, phosphorescent pigments emit the light at longer wavelength as light, similar to fluorescent pigments, but the emission occurs after

several times. Metal doped (silver, copper) zinc sulfides can be shown as example to these pigments [1], [3], [4].

2.3 Characterization of Pigments

Chemical and physical analysis methods have an important role in the production of pigments. These analyzes are required for pigments to obtain the final product from the selection of raw materials, and sometimes pigments are need to be used and tested in the relevant substrate or medium. Determining the purity, PSD, chemical and physical structure of the raw materials to be used in pigment production plays a critical role for the final product to be obtained. Equipment to be used during production should be selected in accordance with the raw materials, chemical composition and production parameters to be used in the pigments to be obtained. Wastes or by-products (waste water, chemicals, flue gases) generated during or after production must be controlled and monitored in accordance with legal environmental requirements. Standards such as DIN, ISO, EN include definitions of national and international standards and generally accepted test and analysis methods. Properties such as optical properties (color), chemical composition, crystallographic properties, PSD and particle morphology are fundamental and important properties for pigments. In addition to these, properties such as solubility/stability in solvents, pH value, opacity/transparency, acid and alkali resistance, air and heat fastness are also important parameters for pigments [1], [3], [4].

In addition, by-products or unreacted raw materials formed during the pigment production process have an effective role in the properties of pigments. These materials or raw materials can negatively affect important properties such as color, dispersion, temperature resistance, surface quality and stability of the pigment. It may cause the color of the pigment to look dirty or pale, to react chemically with the environment in which it is used, to lose its color properties, or to negatively affect the properties of the material it is used in [1], [3], [4].

Another important feature is the toxicity of the pigments. Raw materials used during pigment production may not react, or by-products during production may cause pigments to exhibit toxic properties. Pigments caused by exceeding the required

toxicity limits may be considered toxic and may prevent their use in applications where a certificate is required [1], [3], [4].

The amount of water-soluble salts of the pigments are also the properties that significantly affect the quality and application parameters of the pigments. In water-based applications, the amount of salt dissolved in water significantly affects the conductivity, pH and thixotropic properties. The controllability of this amount is important for the user in final product applications and determinants of the application parameters [1], [3], [4].

"Particle size", which is an important term frequently used in pigments, should not be confused with "PSD". Particle sizes are a quantitative property used to specify particle size properties. PSD, on the other hand, is a term represented by a graph, histogram, curve, or table. It is the data obtained by calculating the sizes of all the particles in the pigment. Mean particle size is a value obtained by taking the average of these particles contained in the pigment. Knowing the Mean particle size of a pigment does not provide the particle size with the distribution-related information. Particle size distributions can be given by different measurement and calculation methods by volume or on the basis of pieces [1], [3], [4].

The particle size of a pigment can range from nanometer levels (0.01 μm) to micrometer (100 μm). In special cases, these values may be higher or lower [1].

Anisotropic particles require special mathematical methods and approaches to calculate the particle size, such as platelet, irregularly shaped, need-like structures. It is possible to determine the PSD and mean particle size of such geometric structures by special mathematical methods [1], [3].

The particle size of pigments can be measured by using some optical methods such as Fraunhofer diffraction and Mie scattering. The methods allow to measure particle size between 0.05 to 1500 μm. The light scattering method is based on models and assumptions when calculating the particle size of materials. It is assumed that all particles have a spherical structure and hypothetical refraction indexes are used. Validation and comparison with standard known materials is critical to determine the accuracy of this method. Figure 2.4 shows the illustration of light scattering method for particle size measurement. [1], [3] [56].

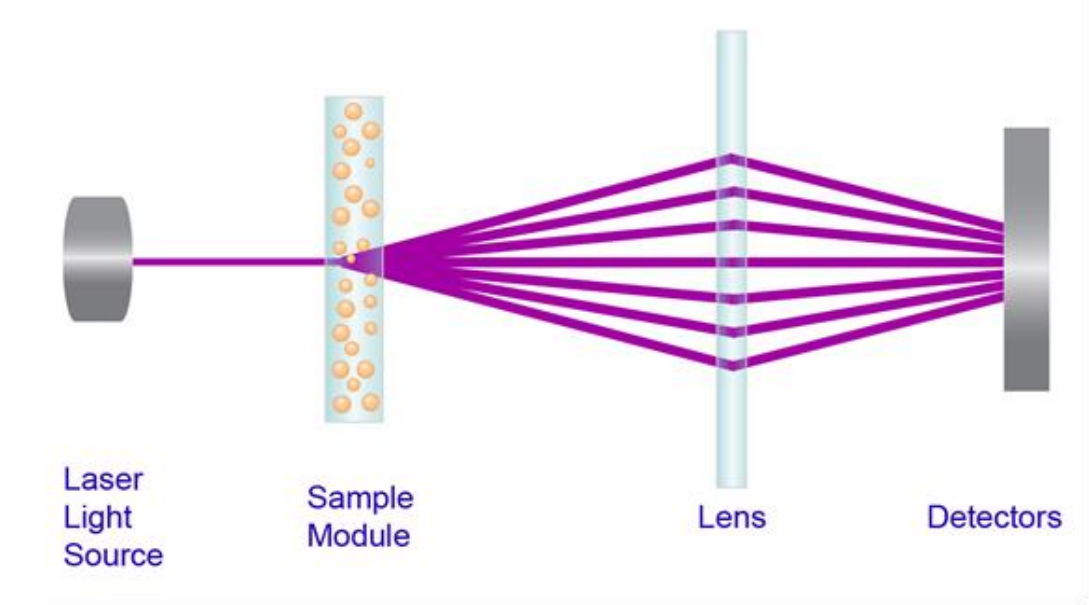


Figure 2.4. Illustration of light scattering method for particle size measurement [57]

Another particle size determination method is the sieving method. In this method, powder materials are passed through sieves of different sizes and particle size analysis is performed (Figure 2.5). This method can be applied both dry and wet. Water can be used as an aid to enable the sieve of materials with very small particle size. However, this method can be misleading in need-like structures. This may result in larger or smaller particle size measurements when due to the orientation of such structures [1][58][59].

Another different method is the Counting method. In this method, particle size measurements are made using electron micrographs. In addition to the particle size, this method can also analyze the particle size distribution and obtain information about the morphology of the particles [1][56].

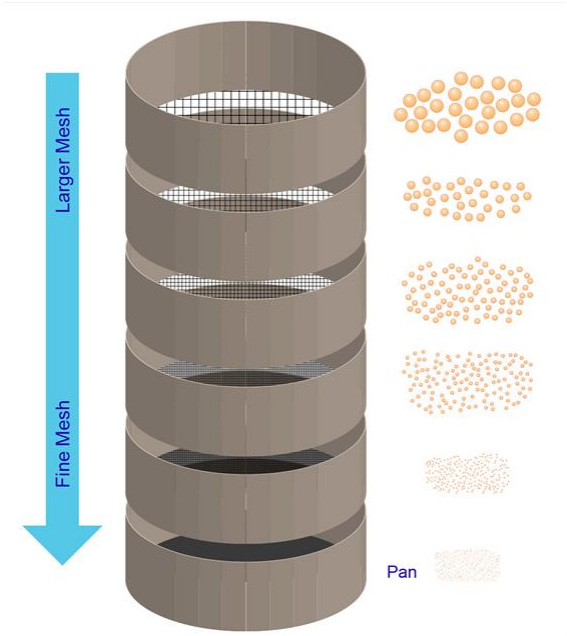


Figure 2.5 Illustration of sieve method for particle size measurement [60]

Another different method is the Counting method. In this method, particle size measurements are made using electron micrographs. Besides particle size, this method can also analyze the PSD and obtain information about the morphology of the particles. Particle size distribution analysis can be performed automatically with computer aided programs. Although this method provides information about many features of the particles structure at the same time, it has negative aspects such as long procedures required for measurement (sample preparation, vacuum, etc.) and higher infrastructure costs compared to other methods [1], [3], [61]–[63].

Optical microscope can be used instead of scanning electron microscopy (SEM) and transmission electron microscopy (TEM) for measuring materials with larger particle sizes. Optical microscope for large particle sizes has lower investment cost, faster measurement capability compared to TEM and SEM [1].

Particle size of single crystalline materials can be measured using the x-ray diffraction (XRD) method, but this method is not preferred because materials are not single crystalline in general [1].

Specific surface area (SSA) represents the surface area per unit weight of materials. This feature of the materials is very important for pigments and fillers as it will affect the behavior of the medium or material in which it is used. The SSA is measured by the Brunauer, Emmett, and Teller (BET) method (Figure 2.6). This method calculates the SSA of the materials by making calculations on the adsorption of gases properties [1][64][65].

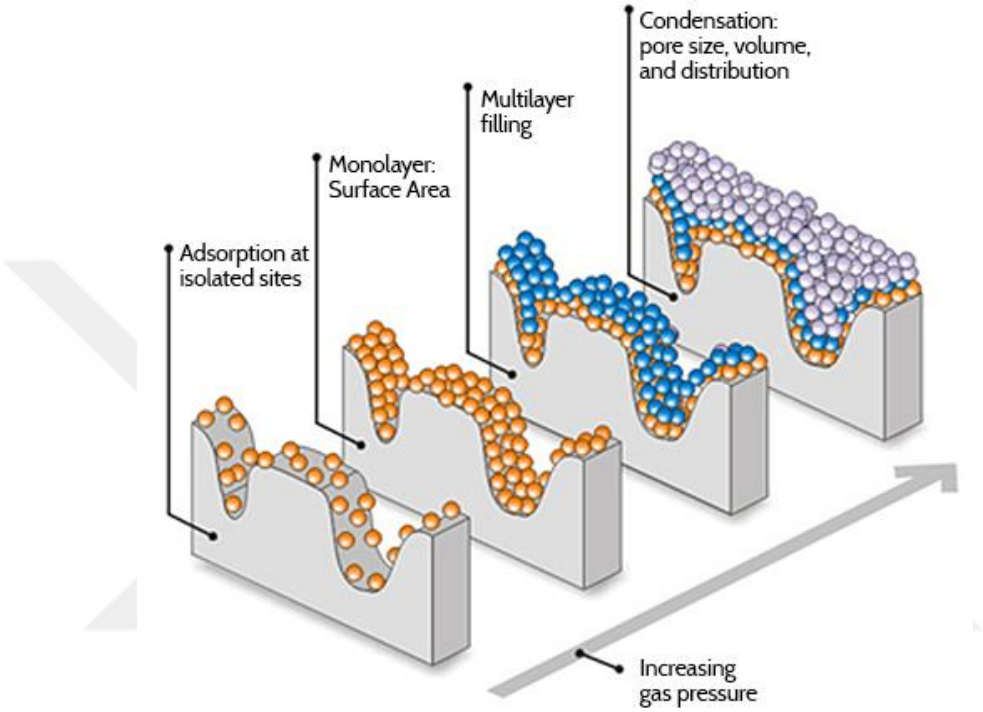


Figure 2.6 Illustration of BET specific surface area analysis [66]

In addition, this method can be used for particle size analysis. However, when it is used for particle size determination, it may not give an accurate measurement because the inner surface area and outer surface area of the material cannot be distinguished from each other. While this method can be used for non-porous materials, this method will not give accurate results for porous materials Figure 2.7 [1].

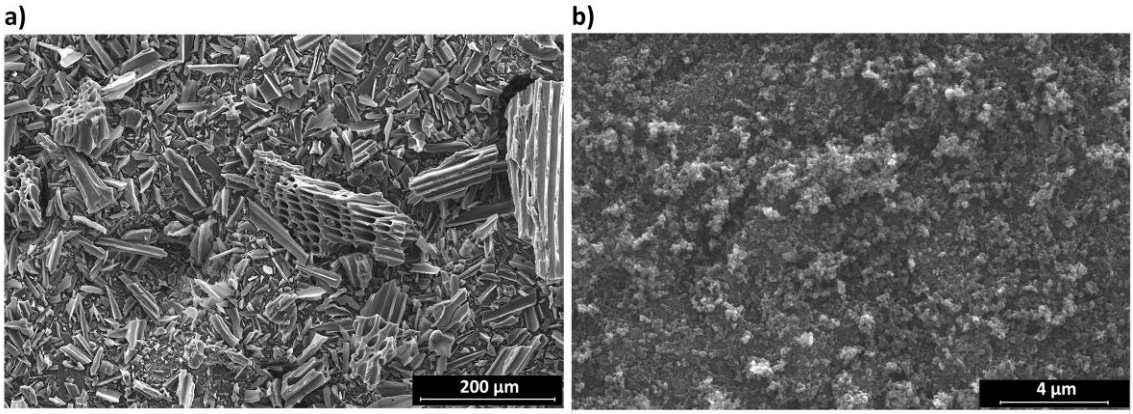


Figure 2.7 SEM micrographs of (a) active carbon (porous) and (b) carbon black (non-porous)

Inorganic pigments are composed of crystal structures, and the XRD method allows us to collect information about the crystallographic data of inorganic pigments. Diffractograms are unique to each pigment and give information about the crystal structures and compositions of the pigments and allow us to collect qualitative semi-quantitative information. It allows the determination of crystallinity and different phase structures of pigments containing multiple components. Figure 2.8 shows the crystal classes of inorganic pigments with examples [1][67].

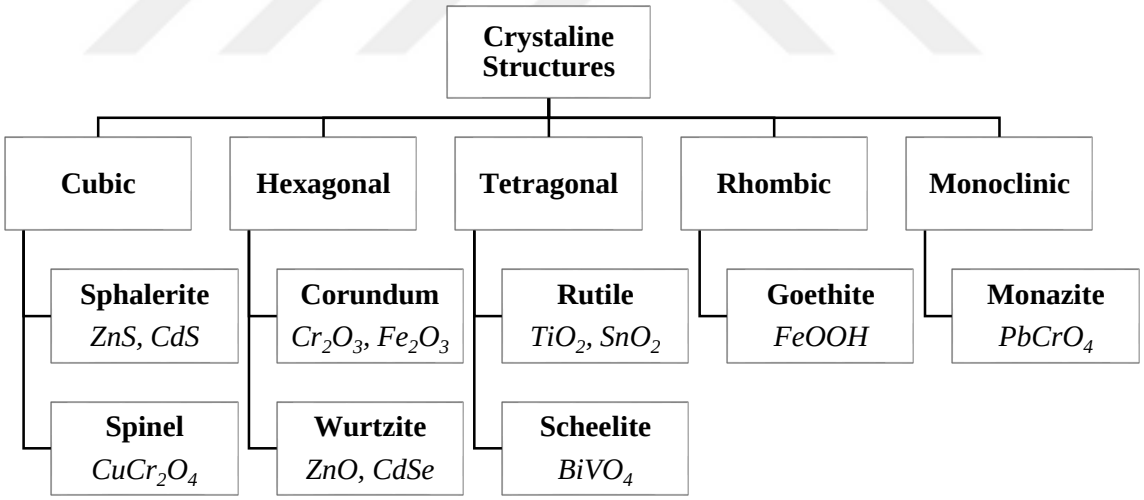


Figure 2.8 Crystalline structures of pigments with examples [1]

Thermogravimetry (TG) is used to investigate phase transformation, crystallization, decomposition, moisture, and solvent content of pigments.

Quantitative and qualitative methods such as atomic absorption spectroscopy (AAS) and x-ray fluorescence techniques (XRF) are used to examine the chemical composition of pigments.

Another study on pigments is the pH and electrical conductivity of aqueous solutions of pigments. It is used for the detection of compounds such as water-soluble.

The densities of the pigments are measured with a container of a certain volume called a pycnometer. After the pigment is completely filled into the pycnometer and the weight measurements are taken, the densities of the pigments can be calculated with the help of mathematical calculations. The measurements are performed at room temperature about 25 °C. Particle size and morphology of the pigments should be taken into consideration when calculating the density.

2.4 Pigment Applications

The usage of pigments is covered by a wide range of application systems. These systems include coating, paint, plastic, ink, cosmetics, glass, ceramic, enamel, leather, textile and etc. All systems have specific requirements to fulfill the demands such as appearance, durability, dispersion ability. For example, the coatings and paintings should be low thickness in most applications. So, the pigments used in this application systems are preferred with high tinting strength, high hiding powder and high dispersion ability to achieve necessary properties of coatings. High quality pigments are preferred in coating/painting application to provide needs such as high coloring strength, chemical stability, high dispersion ability. On the other hand, the pigments like iron oxide (natural or synthetics) and chrome oxides are used in the construction application such as cements, asphalts, bricks, and tiles. Chrome oxide green is important green pigment which provides high color stability and cheaper price compared to cobalt based green pigments [1] [3].

According to the application system, the pigments have critical properties to achieve optimum result for application. The Table 2.1 shows the criteria of color properties, stability properties, physical and chemical properties, stability properties and the interaction between binder and application systems.

Table 2.1 Selection criteria of pigment [1], [68]–[70]

Color	Chemical/Physical	Stability	Others
-Color -Color Strength -Tinting Strength -Lightening Power -Hiding Power	-Chemical Composition -Particle Size/Distribution -Density -Soluble Contents	-Heat Resistance -Light/UV Resistance -Chemicals Resistance -Corrosion Resistance	-Dispersion - Compatibility with Binders

3
TYPES OF INORGANIC PIGMENTS

3.1 Types of Inorganic Pigments

3.1.1 Iron Oxide Pigments

Synthetic iron oxides are obtained in structures such as hematite, goethite, magnetite. They have purer compositions and crystal structures compared to natural ones. Depending on the chemical composition of the ores and raw materials used in the production of pigments, iron oxide pigments may contain impurities. Elements such as aluminum, silicon, and components such as water-soluble can be found in the structure of the pigment. This rate is generally below 5 wt.%. Although synthetic iron oxides are in red, black, and yellow colors, it is possible to obtain pigments in different tones such as orange and brown with their combinations. Generally, orange pigments can be obtained by mixing red and yellow iron oxides, and brown pigments can be obtained by mixing black and red iron oxides. Yellow pigments have a need-like particle structures, while black pigments have cubic-like structures. The importance of these pigments increases due to their high tinting strength, hiding power, light and weather fastness, alkali resistance, pure hue and stable quality [1], [3], [4], [55].

Black iron oxide (Fe_3O_4) and yellow iron oxide (α-FeOOH) show phase transformation over 180 °C with increasing temperature. Black iron oxide changes from Fe_3O_4 phase to brown γ-Fe_2O_3 phase. At temperatures above 350 °C, conversion to red α-Fe_2O_3 pigment is observed. On the other hand, while the yellow α-FeOOH pigment releases the hydrogen and oxygen contained in it to the environment as water, the structure turns into red α-Fe_2O_3 pigment. The temperature resistance and decomposition behavior of the pigments obtained by the mixture of iron oxide pigments such as orange and brown vary depending on their

composition. On the other hand, red α-Fe_2O_3 pigment can provide its red color at high temperatures such as 1200 °C [1], [3], [4], [55].

Iron oxide pigments are used in many structural materials such as roof tiles, wall tiles and concrete due to their high dyeing strength. Moreover, it is preferred in many application areas such as paint, coating, plastic.

In addition, these pigments are used together with elements such as manganese, copper and chrome as raw materials in the production of black chips.

3.1.2 Chromium Oxide Pigments

Chromium oxide (Cr_2O_3) pigments are not found in the chrome (ll) oxidic structure in nature, unlike natural iron oxide. They often have a purity level of over 99% as a result of synthesizing the chrome oxide pigment. Contaminations that occur as a result of synthesis are silicon and aluminum based oxides. Since chromium oxide has high hardness (9 on the Mohs scale), it is used as grinding material. In addition to the use of chrome oxides as pigment, it is also used as raw material for the production of metallic chrome. Metallic chromium is obtained by reduction reactions of chrome oxide (ll) using the aluminothermic method [1], [3], [4], [71]–[73].

The morphology of chromium oxide, which usually varies between 0.1 µm and 3 µm in particle size, is spherical. Although the particle sizes vary according to the application area, particles with larger particle sizes are used for the refractory industry and the abrasive industry. The chromium oxide pigment is green in color and becomes darker green and bluish as the particle size increases. On the other hand, a lighter and yellowish color is obtained by decreasing the particle size. As the particle size increases, weaker pigments are obtained. Chrome oxide pigments have high light absorption and scattering ability. As a result, the pigment has high hiding power. Similar to carbon black, it can be used to improve the weather fastness properties of the structure in organic materials and polymers, thanks to its high UV absorption capability. In addition, the chromium oxide pigment has the ability to reflect electromagnetic waves in NIR zone. Since it is IR reflective, it can also be used in camouflage applications [1], [3], [4].

3.2 Metal Complex Pigments

Metal complex pigments or complex inorganic pigments are synthetical crystalline pigments similar to natural minerals as structure. These pigments are solid solution of metal oxides and the homogenous crystalline compounds are obtained by distribution of elements in the structure. These pigments contain two or more different metal elements in the structure, so called complex or mixed metal oxides pigments. Structures formed by the combination of metal elements allow the production of pigments of different colors. [1], [3][55][74].

CICPs have wide range crystalline structures such as spinel, hematite and rutile. The most decisive factor for the determination of the crystal structures of inorganic pigments is the metal/oxygen (M/O) ratio. This ratio is 0.75 for spinel structures, 0.66 for hematite structures and 0.5 for rutile pigments. Table 3.1 shows the common crystalline structures and examples of pigments according to its crystalline structures [1], [3][75].

Table 3.1 Common crystalline structures and examples of pigments [1][76]

Color Index	CI Common Name	Chemical Constituents	Structure	Color Description
PBK26	Manganese Ferrite Black	Fe-Mn-O	Spinel	**Black**
PBK27	Iron Cobalt Chromite Black	Co-Cr-Fe-O	Spinel	**Black**
PBK28	Copper Chromite Black	Cu-Cr-O	Spinel	**Black**
PBK29	Iron Cobalt Black	Co-Fe-O	Spinel	**Black**
PBK30	Chrome Iron Nickel Black	Cr-Fe-Ni-O	Spinel	**Black**
PBK33	Iron Manganese Oxide	Fe-Mn-O	Hematite	**Black**
PG17 Blk	Chromium Green Black Hematite	Cr-Fe-O	Hematite	**Black**
PG17	Chrome Oxide Green	Cr-O	Hematite	**Green**
PG50	Cobalt Titanate Green	Co-Ti-O	Inverse Spinel	**Green**
PB28	Cobalt Blue	Co-Al-O	Spinel	**Red Shade Blue**
PB36	Cobalt Chromite	Co-Cr-O	Spinel	**Blue-Green**
PBr24	Chrome Antimony Titanate	Ti-Cr-Sb-O	Rutile	**Ochre**
PY53	Nickel Antimony Titanium Yellow Rutile	Ti-Ni-Sb-O	Rutile	**Green Shade Yellow**

3.2.1 Rutile Pigments

The rutile crystalline structures, AO_2 (MO_2), have M/O ratio of 0.5. In rutile structure, metal ions are octahedrally coordinated by six oxygen ions [1], [3].

Metal ions such as nickel (Ni), antimony (Sb), chrome (Cr), manganese (Mn) are located at position of titanium. These ions of metals are used to give color to the

structure, called as coloring ions or components. For the formation of rutile structure, it is necessary to use metal ions similar to the ion radius of Ti(IV) and to maintain the ion balance. Coloring components such as Cr(lll), Ni(ll), Mn(lll) have different valence states than Ti(IV). Stabilizing ions such as Sb(V) are added to the structure in order to equalize the charge of structure. The formulas of rutile inorganic pigments are like $(Ti,Sb,Cr)O_2$ for chromium antimony yellow (PBr24), $(Ti,Ni,Sb)O_2$ for nickel antimony yellow (PY53), $(Ti,Mn,Sb)O_2$ for manganese antimony brown (PY164) and etc. The titanium ratio in the composition of rutile CICPs is in the range of 42 to 54 wt.% [1], [3].

3.2.2 Spinel Pigments

The spinel structure, AB_2O_4 (M_3O_4), can be formed by ions of metals, transition metals and oxides. Generally, the spinel structure includes divalent (+2) and trivalent (+3) ions of metals. There are two different ways to occur spinel structure. The A ion which are divalent (+2) in the AB_2O_4 structure are located tetrahedrally, while B ions which are trivalent (+3) are located octahedrally. This is the way to occur normal spinel structure. In the other hand, for inverse spinel structure, the divalent ions are located octahedrally and the trivalent ions are located tetrahedrally. Cobalt titanate green ($CoTi_2O_4$) can be given as example of inverse spinel while cobalt aluminate blue ($CoAl_2O_4$) is normal spinel [1], [3].

The most important examples for blue spinel pigment are cobalt aluminate blue ($CoAl_2O_4$) (PB28). This pigment is reddish blue with the structure of normal spinel. Addition of chromium ions to this pigment causes greenish blue pigment which is similar to turquoise blues. Otherwise, cobalt titanate green ($CoTi_2O_4$) (PG50) crystallizes in the inverse spinel structure [1], [3][14].

Brownish spinel pigments can be occurred from metal ions such as zinc (Zn), iron (Fe) and chromium (Cr). Zinc ferrite ($ZnFe_2O_4$) (PY164) can be given as example for ochre-brown pigments [1], [3][47].

Some spinel black pigment is cobalt iron ($CoFe_2O_4$) (PBk) and copper chromite ($CuCr_2O_4$) (PBk28) black CICPs. Cobalt can be replaced with manganese or copper while chromium can be replaced with iron or manganese [1], [3][10], [18][77].

3.2.3 Zirconium Based Pigments

The other structure of complex inorganic color pigments is zirconium silicate based pigments, also called zircon ($ZrSiO_4$). Generally, these pigments called ceramic pigments or color stain and these pigments are used in glass, enamel, and ceramic structures, mostly. These pigments can be used at high temperatures about 1300 °C and also have extremely stable as chemically and thermally. These colors of zircon based pigments are blue, yellow, red. Combination of these colors also allow the obtain other color tones. Examples of zirconium silicate pigments are zirconium vanadium blue (PB71) and zirconium praseodymium silicate yellow (PY159). [1], [3][78][79].

Inclusion pigments which are covered by zircon color stains are obtained by addition of coloring components to zirconium silicate structure. The ions which are giving color to the structure are not located in the zircon structure. Color providing compounds are protected with stable structures such as ZrO_2 and $ZrSiO_4$, so that the pigments can give color in the extreme conditions such as firing glaze, ceramic or enamel. Zircon iron pink and cadmium sulfoselenide yellow/red/orange can be given as representative of inclusion pigments. Other structures like silicon dioxide or tin dioxide can be used instead of zirconium silicate to protect the coloring compounds [1], [3].

Due to its high thermal stability, high weather fastness, high light fastness, high hardness, insoluble in water, acid and bases, stable against sulfur, chrome oxide green pigment is used in plastics, coatings (emulsion paints, coil coating), paints, structural materials (cements) as colorant and to obtain materials with high abrasive or wear resistance [1], [3].

3.3 Carbon Black Pigments

Carbon black, spinel (CICP) blacks and iron black are most important pigments for black. Carbon black is of higher importance compared to others because of its properties. The reasons why carbon black is important are that it is highly controllable during production, and that all carbon blacks have similar physical and chemical properties. These parameters are opposite for inorganic complex coloring pigment. Because while carbon black is a pigment consisting of a single element,

CICPs can be formed as a result of the combination of many elements with each other and can be produced with different production methods. As a result, differences in color, shade, density, coloring strength, opacity and similar may occur [1], [3].

Carbon black is a material obtained by insufficient combustion and thermal decomposition of hydrocarbons in liquid or gas form. Carbon black is practically form of carbon which is very small particle size with spherical particles. Carbon black may contain negligible contamination. These contaminations can be caused by production parameters, conditions or raw materials used. These elements, excluding carbon, are hydrogen, oxygen, nitrogen and sulfur. Carbon black has superior properties such as high stability, high light fastness and high dispersion ability in the material or medium it is used in. Besides being used as a carbon black pigment, it is also preferred as a filler. Carbon black is mostly used as filler in automotive tires and rubbers [1], [3][80].

Carbon black is a very small structure that exists as aggregates with particle sizes of 5 nm to 500nm. Due to the extremely small size of the particles, they have a high agglomeration tendency and are generally found in aggregation state. Aggregation level of carbon blacks is called structure for these pigments. Although carbon black has an amorphous structure, it contains small amounts of microcrystal sections [1], [3][81], [82].

It has a unique structure pattern like carbon black graphite. Graphite consists of a folded structure of carbon atoms bonded together as hexagons. These structures are connected by van der Waals forces, which are weak bonds. These structures that make up the graphite are aligned with each other, on the other hand, for carbon black, the structures are connected to each other to form layers in parallel. While diamond, graphite and carbon have almost the same chemical structure, they have different conductivity, which can be explained by these structural differences. While diamond has a non-conductive feature, graphite and carbon black, which have similar structures, are conductors [1], [3].

There are different types of carbon blacks. These differences are properties such as color, PSD, dispersion ability, SSA, conductivity. Carbon blacks with different properties can be preferred according to necessities for use in industries such as paint, rubber, plastic, ink, etc. [1], [3].

Carbon blacks are preferred in the rubber industry for reinforcement, coloring and modifying rheological properties of tires and rubber materials due to properties such as electrical conductivity, thermal stability. Another area of use is inks. It is used for coloring and rheology adjustments in inks due to properties suitable for high concentration, resistance to alkali and acids, dispersibility, wettability and hiding power. They are preferred in coating applications due to their hiding power, light fastness, solvent resistance and acid/alkali resistance. It is preferred in the plastics industry for increasing UV resistance, providing conductive properties, hiding power, dispersibility and excellent coloring properties. In addition to its coloring feature, it is used in components such as electrode, battery cell and carbon brushes in power units. Another feature other than coloring is that it is used as a reduction agent and carbon source in metal carbide synthesis and metal reduction processes due to low particle sizes and high specific surface are which increase surface energy [1], [3].

4
NEAR-INFRARED REFLECTIVE PIGMENTS

4.1 Cool Pigments

Natural sunlight is made up of 52% near-infrared (NIR), 43% visible and 5% electromagnetic radiation in the UV zone [31], [83], [84]. Color values are determined by the absorption and reflection of the electromagnetic spectrum of the material in the visible region. White is produced by reflecting all the radiation in this area, while black is obtained by absorbing all the rays [39], [85]. On the other hand, by absorption or reflection, colors such as red, blue, and green are produced [39], [85]. However, reflection or absorption events occurring in the NIR area have no effect on the color values of the material. However, this energy absorbed as a result of the absorption of electromagnetic waves in this region adds to the material as thermal energy, increasing the temperature of the material [39]. Pigments that can reflect electromagnetic waves in the NIR region are called NIR reflective pigments [39]. NIR reflective pigments prevent the surface temperature from rising due to the ability to reflect the rays in this region, which is why these pigments are also called “cool” pigments [31]. Thanks to these features, NIR reflective pigments are a strategic technology that can play an important role in solving global problems such as high climate energy consumption and global warming [31], [86], [87]. Especially in high-density residential areas, it is used in roof and outer front coatings to prevent the temperature of structures from rising and to cool down [39], [88]–[91]. This can reduce the energy spent in buildings from 7% to 25% [25], [31], [92]. Today, it is often used in roof coatings, outer front paint, plastics, ink and cars [31], [90], [91], [93].

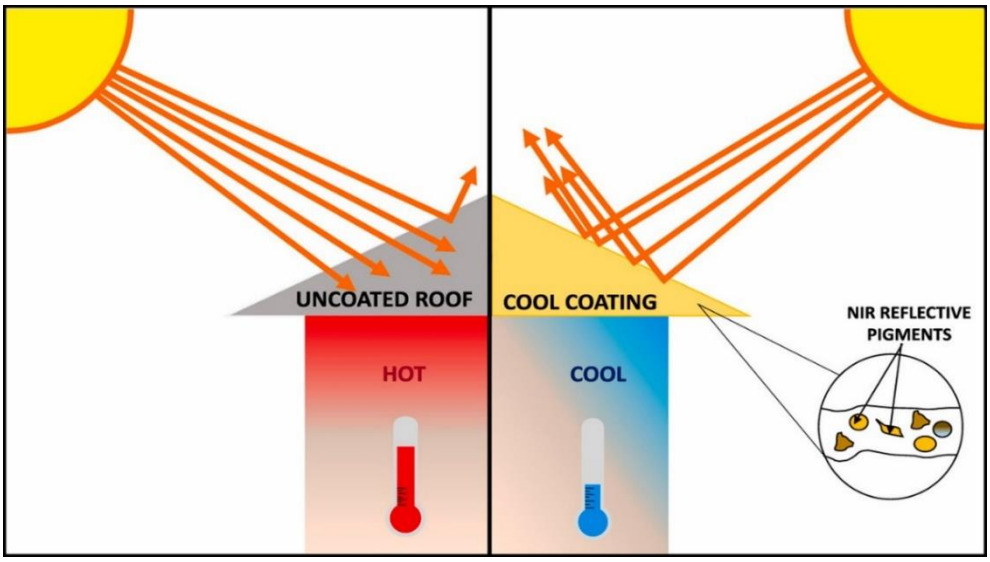


Figure 4.1 "Cool" pigment roof application illustration [20]

4.2 NIR Reflective Pigments for Polymer Sorting

Another use of pigments is to make plastic materials suitable for recycling and sorting [94]–[98]. Carbon black pigment is used in the plastic industry to give black color to materials [1], [4], [80], [99]. Carbon black is widely preferred due to its characteristics such as color stability, solvent resistance, high temperature resistance and deep black [1]. However, when these pigments are used for the coloring of plastics, the classification process, which is one of the processes necessary for recycling, cannot be carried out [48], [98], [100]–[105]. This is because carbon black absorbs electromagnetic radiations in the NIR region. Each plastic material has a specific spectrum of reflection in the NIR region, and these characteristic spectrums are used to identify and classify plastic materials [97], [98], [103]. However, when carbon black is used in the coloring of plastic materials, plastic materials cannot be detected because carbon black almost completely absorbs radiation in the NIR region. Because these materials cannot be detected, it is impossible to go through the next step of the reversal process. These plastic wastes are stored in nature as non-fill materials, as fuel by combustion or as garbage islands. The garbage islands need biological balance on land, but negatively affect the sea [106]–[111]. On the other hand, when these products are destroyed, the high CO_2 emissions come to the grocery [112]–[114]. As a solution to this problem, plastic materials can be classified using NIR reflective black pigments. Thus, classified plastics can then be recycled and these materials can be recovered by being re-functional.

5
COLOR

5.1 Overview of Color Science

Pigments show different interactions in the materials which are colored. These interactions are indicated in reflectance spectra ρ(λ) or spectral reflectance factor curves R(λ). Reflectance spectra of pigments such as titanium oxide (rutile), red iron oxide (*a*-Fe_2O_3), chrome antimony yellow (PBr24), cobalt aluminate blue (PB28) (Figure 5.1). is also shown. Theoretically, since black pigments absorb electromagnetic waves at all wavelengths in the visible region, their spectral curve is expected to be parallel to the x-axis and 0. On the other hand, unlike black pigments, white pigments are expected to reflect at all wavelengths in this region, and hence the spectral curve is still parallel to the x-axis. but it is expected to show 100% reflection. For colored pigments, different absorbance and reflectance are seen at various wavelengths as a result of the interaction of electromagnetic waves in the visible region with the valance electrons of the materials. Colors are created by various combinations of these absorbance and reflectance.

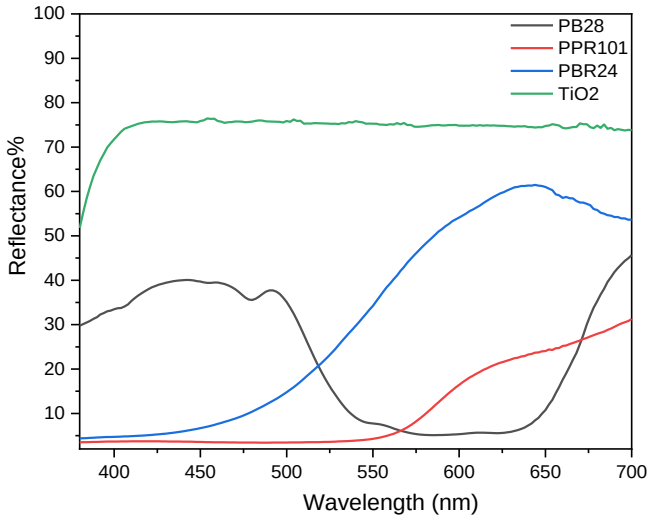


Figure 5.1 Reflection spectra of TiO_2 (rutile), red iron oxide (*a*-Fe_2O_3), chrome antimony yellow (PBr24), cobalt aluminate blue (PB28)

5.2 Color Formations

5.2.1 Color Formation by The Effect of Crystal Field

Color is explained by the development of a field of ionic crystals containing non-double ions. These are mainly generated from elements having partially filled d shells such as chromium (Cr), manganese (Mn), iron (Fe), cobalt (Co), nickel (Ni) and copper (Cu) or from other elements that have partial filled f shells, such as actinides and lanthanides. Since all electron shells, such as Cr^{+6}, and Cu^{-}, do not have non-double electrons whether they are totally filled or empty, color does not form by this method. Because characteristics such as valence state, deterioration in the crystal structure, binding forces are required for the energy account, the calculation of energy is difficult [115]–[117].

Mechanisms that create color by the effect of crystal field; color formation with transitional metals and color formation with color centers.

5.2.1.1 Color Formation with Transitional Metals

Light's transition is the most important of the mechanisms for coloring absorption by electrons by metals, also rare-earth elements (REE). Transitional metals and REE can be stimulated to higher energy levels by the light energy coming from them. The electrons obtain the energy needed for stimulation by absorbing a specific energy (color) of white light, thus causing all the minerals to appear in color. Three key examples of this mechanism are the emerald, ruby and alexandrite [115]–[117].

5.2.1.2 Color Formation with Color Centers

Color centers are formed when atoms are oxidized or removed. This usually occurs with radiation. Because the crystal must remain electrically neutral, an electron is placed in the remaining gap of the atom's escape and forms the color center. This electron comes from a neighboring atom and tends to absorb light energy because the left pair of unformed electron energy can create stimulated levels controlled by crystalline field factors and thus color is formed. Amethyst and smoky quarks are minerals colored with green diamonds, coffee topaz color centers. The coloring mechanism with color centers disappears when heated or exposed to strong light [115]–[117].

5.2.2 Color Formation with Charge Transfer

In molecules and solids, valence electrons are known to double during chemical bonding and the energy levels required for stimulation are shifted toward the ultraviolet region. In fact, this is true only when the pair-formed electrons remain fixed in the bond between two atoms. In most cases, electrons can travel longer distances, extending into a molecule or even into a macroscopic solid. When the bond is not very strong, the energy needed to create a stimulated level decreases. Electrons form molecular orbitals and form a different class of colors in nature. The mechanism that contributes to color formation in molecular orbits is the transition of the electrical load to another ion, usually a different element, that is close to the structure of one ion by the absorption of the amount of energy needed for transfer. These are known as load transfers. Valence electrons are divided between molecular structures and energy exchange is associated with the "hoping" process in the light range. Sapphire, lapis lazuli and amazonite can be given as examples [115]–[117].

5.2.3 Color Forming Through Band Gaps

The band gap colors can be obtained in insulated or semi-conductive materials. These colors require that there is a gap between the valence and the conductive energy bands within the electronic structure of an atom. The behavior of the material varies depending on the band gap energy (Eg) required to stimulate electrons from the valence band to the conductivity band by visible light absorption.

If the band space energy is smaller than the visible light energy, all visible light energies can be absorbed, in which case a dark and black color is obtained. If the energy band contains all the wavelengths of light, the material is white or pale and is an insulator. In such a material, the energy band gap range required to extract the electron in the valence band to the conductivity band is very high (>3eV), in which case the visible wavelengths are not absorbed, the material is therefore colorless.

If the band contains part of the visible spectrum, the material is semi-conductive and colorful. That is, if the band gap energy drops to the visible range, it will have a certain color. All the photons that are higher than the band gap energy are absorbed and we see the material in the color of the absorber. Some colorless insulators and semi-conductors can produce band gap colors with additional

impurities. By doping the material, the band gap energy can be reduced, thus coloring occurs as energy absorption can take place in the visible wavelength range. An impurity can be either an electron transmitter or an electron receiver. In both cases, there is an energy gap between the valence band and the conductivity band. Transitions to new levels or new levels take place in lower energy than empty intervals [115] [117].

5.2.4 Color Measurement

Colors are expressed with a three-dimensional coordinate system called color space. In the first of the three-dimensional coordinate system, color is expressed as 'lightness' without hue. In the second axis, hue is expressed such as yellow, red, green and blue. These colors are determined by the wavelength of the light emitted from the object. A third dimension, which is "chroma", is needed to distinguish two colors with the same hue and lightness. Chroma (*C**) is called color saturation. While high saturation expresses vibrant colors; low saturation causes the color to approach pale/gray tones (Figure 5.2). Color can be defined more accurately with hue, lightness and chroma [1], [3], [6], [116], [118].

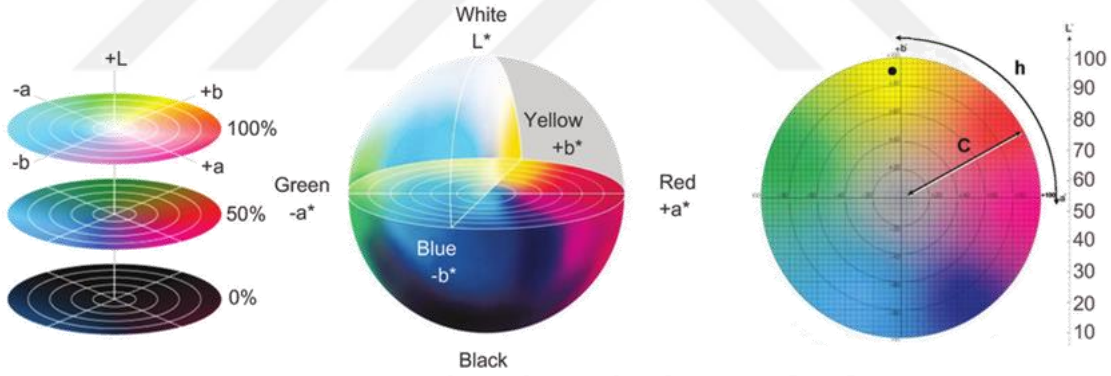


Figure 5.2 CIE *L*a*b** and *L*C*h* color space [119]

Color spaces are mathematical models used to describe colors. The CIE *L*a*b** and CIE L**C*h** systems, developed by the CIE (Commission Internationale de l'Eclairage; International Commission on Illumination) in 1976, were accepted as the international color measurement system (Figure 5.2). These systems were designed according to the principle that a color cannot be both red and green, yellow and blue at the same time. In this system, color data obtained from objects with standard illuminants A, B, C, D50, D65, E, F and observers (2°, 10°). The same color object can be observed in different tones under different light sources. The reason for this is that different light sources have different light spectra. D65 is

intended to represent average daylight illumination. The L^* value represent the lightness (absolute white=100 and absolute black=0); the a^* value represent the reddish (+a^*) and greenish hue (-a^*); the b* value represent the yellowish (+b^*) and bluish (-b^*) hue [3], [116], [120]. Additionally, to determine the saturation of the color, the chroma (C^*) parameter was calculated according to the formula (5.1) given below [14].

$$C^* = \sqrt{(a^*)^2 + (b^*)^2} \tag{5.1}$$

Color measurement with a spectrophotometer is obtained by reflection spectra in the visible region of the spectrum (380-700 nm) obtained as a result of the interaction of the light and the object [116], [118], [120]. The light coming from the source is first sent to the prism, scattered in the spectrum and then separated into monochromatic light beams with the help of a scanner. The electrical signals coming from the sensor are analyzed numerically and transferred to a graph as a function of wavelength. The spectral data received from the standard observer, standard illuminator, observer are calculated and read as $L^*a^*b^*$ color values [115].

6
EXPERIMENTAL STUDIES

6.1 Raw Materials

The required raw materials for pigment production were supplied by Akcoat Advanced Chemical Coating Company. The raw materials are; red iron oxide (Fe_2O_3, 99.9 wt.% purity), chrome oxide (Cr_2O_3, 99.9 wt.% purity), manganese oxide (MnO_2, 99.9 wt.% purity), cobalt oxide (Co_3O_4, 99.9 wt.%), copper oxide (CuO, 99.9 wt.% purity). Polypropylene (PP, MFI-25), polyethylene (PE), transparent acrylic paint base, and white acrylic paint were used for color application.

6.2 Preparation of Reactants

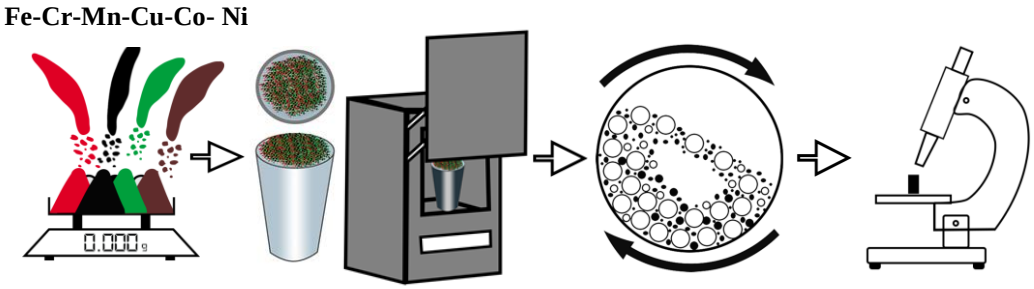


Figure 6.1 Schematics of experimental studies

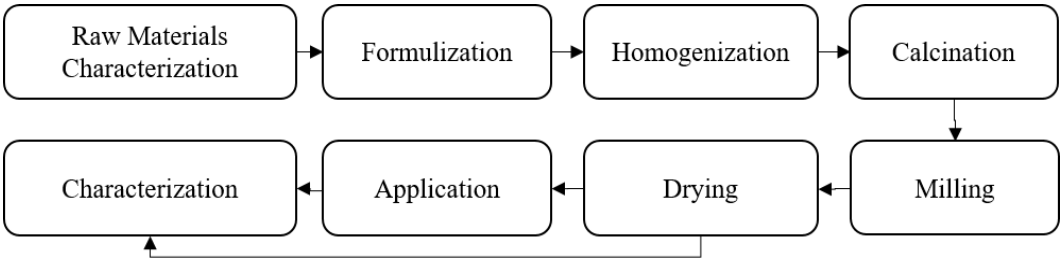


Figure 6.2 Workflow chart of experimental studies

6.3 Preparation of Pigment

The quantity of raw materials intended for calcination was determined based on molar calculations corresponding to the chemical compositions of the pigments. To achieve a more homogeneous mixture and disperse weak agglomerations, the weighted raw materials underwent homogenization using a blender equipped with blades. The resulting homogenized mixtures were subsequently deposited into corundum crucibles for the calcination process carried out at elevated temperatures. A schematic representation of the experimental procedure is provided in Figure 6.1 Schematics of experimental studies, while the experimental workflow is illustrated in Figure 6.2.

6.4 Calcination

The mixtures, composed of various metal oxides, undergo heat treatment at elevated temperatures in air atmosphere. An electric resistance furnace, capable of reaching high temperatures up to 1400 °C, is employed for the calcination process. The calcination procedures involve distinct stages, including heating, soaking, and cooling. The heating and cooling stages are executed at a rate of 5 °C/min, while the soaking stages have a duration of 3h each.

6.4.1 Milling

The pigments, resulting from the calcination of raw material mixtures, underwent milling processes to render them suitable for color applications. Milling is one of the important factor which effect the properties of pigments such as color and coloring strength. Therefore, the milling parameters are selected according to pigments. The calcination at high temperatures may form agglomerates which are difficult to break. The development of such agglomerations can be influenced by factors like chemical composition, particle size, and calcination temperature. Consequently, milling parameters may vary due to the presence of these resistant agglomerates. In order to facilitate a precise comparison of pigments, efforts were made to achieve similar particle distributions among them.

Wet ball milling was employed for milling with water as the medium, which was utilized for pigment milling. The powder-to-medium ratio was set at 1:1 by weight, and the ball-to-powder ratio was chosen as 4:1 for efficient milling. Two types of

milling machines were employed for this purpose. A high-energy planetary ball mill equipped with zirconia milling tools and a rapid pot mill equipped with alumina milling tools were utilized. The pigments underwent milling by the rapid pot mill to achieve a particle size of Dv_{90} ranging between 4-7 µm, using alumina balls with a diameter of 4-6 mm. Additionally, the high-energy planetary ball mill was employed to further reduce the particle size to Dv_{90} below 1 µm, aiming to investigate the effect of particle size. This step involved the use of zirconia balls and zirconia lined jars.

6.4.2 Drying

The drying process was employed to separate wet-milled pigments from the milling medium. Wet pigments were dried in a Refsan RK250 drying oven until the moisture content dropped below 0.1% at 120 °C. Post-drying, the pigments were sieved to a particle size of 32 µm to facilitate the breakdown of any agglomerates formed during the drying process. The Refsan RK250 drying oven was utilized for the drying procedure.

6.4.3 Color Application

For the measurements of color tones and performance of the obtained pigments, two different methods were employed. One of these methods is paint application. The paint application method was conducted to measure the color values and coloring powers of the pigments. In the mass color method, only pigment and a colorless medium were used. On the other hand, in the tint color method, a medium with white color was used along with the pigment. While the aim of the mass color method is to determine the color and tones of the pigment, the tint color method aims to collect data on both color and the coloring power of the pigment.

Another coloring method utilized involves pigments obtained through hot molding to color plastic plates. This method, commonly used in the plastic/masterbatch industries, was employed to determine both the color tones of the pigments and to conduct studies related to opacity. In addition to color studies, the plastic/masterbatch method was used to examine the NIR reflectance properties and behaviors of polymers and polymer blends colored with pigments. The devices, equipment, parameters, and materials used in the methods are detailed below.

6.4.3.1 Plastic/Masterbatch

For plastic/masterbatch application, PP and PE plastic plates with a thickness of 4 mm were obtained with the help of the devices given below (Figure 6.3 and Figure 6.4). Raw granule PP and PE were brought to dough consistency with a gelimat mixer. Gelimat mixer allows the temperature of the granules to increase and soften with the help of friction produced by the rotating blades (Figure 6.3). After adding 0.5-1 wt.% pigment into the plastic, which reaches the dough consistency, the mixing process continues. Hot/cold press was used to shape the resulting colored semi-melted plastic. While one section of the press is used for shaping, the cooling process is carried out in the other section. After the semi-melted plastic is placed in the preheated mold, a hot press is first made. Afterwards, a cold press is applied to cool the shaped plastic. While the hot pressing temperature for PP is approximately 180 °C, for PE this temperature is approximately 130 °C.



Figure 6.3 Gelimat mixer to mix polymer and pigment [121]



Figure 6.4 Hot and cold press to form polymeric plates [121]

6.4.3.2 Paint

The paint application was carried out to determine the color tones of the pigments and investigate their coloring powers. Acrylic paints and mediums were chosen as the medium for paint application. For the examination of pigment colors, mass color method was performed, using transparent acrylic base as the medium. On the other hand, tint color method was conducted to investigate the coloring power of the pigments, using white acrylic paint as the base, unlike the mass color method. The coloring power of the pigment was measured based on its ability to cover the white color.

For mass color method, in addition to the paint base, 4 wt.% of the pigment was added. For tint color, a white base was prepared first, by mixing 80 wt.% of transparent and 20 wt.% of white acrylic paint. To this mixture, 4 wt.% of the pigment was added.



Figure 6.5 Pool type film applicator

To ensure the dispersion of the pigment within the paint, the mixture was stirred using zircon grinding jars (Figure 6.7) in a planetary ball mill (Figure 6.6) for 5 min at 400 RPM.



Figure 6.6 Planetary ball milling equipment

The prepared colored acrylic base was applied to a white paper using a pool-type film applicator with a paint thickness of 0.4 mm (Figure 6.5). The coated paper had a glossy surface and a weight of 350 g/m². After application, the paint was dried under ambient conditions.



Figure 6.7 Y-stabilized zirconium oxide jar

6.5 Characterization

6.5.1 Crystallography/Determination of Crystalline Structures

The crystalline structures were characterized through X-ray Diffraction (XRD) analysis of the powdered sample using the BRUKER D8 Advance Diffractometer.

XRD functions by exposing a material to X-rays of known wavelength and subsequently measuring the intensities and scattering angles of the X-rays that distinctly diffract and reflect from the material. This process produces a diffractogram, which is utilized to identify the phases by referencing the International Centre for Diffraction Data (ICDD)- Powder Diffraction File (PDF) for crystalline phases. The measurements were conducted in the range of 10-70°.

6.5.2 Elemental Analysis/ Determination of the Chemical Composition

The elemental analysis was conducted through Wavelength Dispersive X-ray Fluorescence Spectrometry (WDXRF). Sample preparation for WDXRF involved the creation of pressed powder pellets with a 34 mm diameter. To form the pressed powder, the sample was blended with wax in a 70:30 ratio of powder to wax, and boric acid was introduced as a subtract to ensure the creation of a robust pressed powder pellet. Fluxana VANEOX 25t Automatic Press was employed for the preparation of pressed powder pellets. The measurements were performed using the S8 Tiger Series 2 WDXRF Spectrometer equipped with a Rh tube and operating at 4 kW power.

6.5.3 Particle Size Distribution

Particle size analyses of both raw materials and pigments were conducted using the Mastersizer 3000, a laser diffraction particle size analysis machine manufactured by Malvern Panalytical (Figure 6.8). The measurements were facilitated through the utilization of the Hydro EV wet dispersion unit, with water serving as the dispersant.

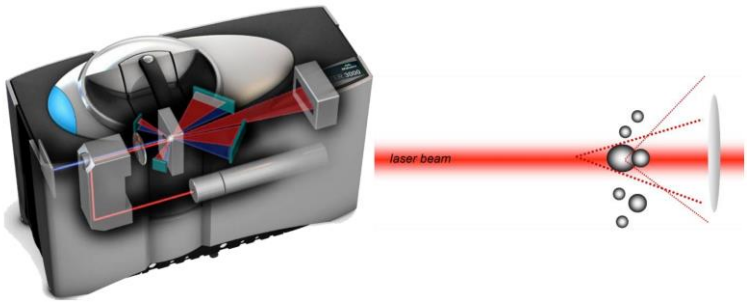


Figure 6.8 Red and blue lasers from the Malvern Mastersizer 3000 are directed at various detectors and scattered laser light by different size of particles [122]

6.5.4 Morphology

Field emission gun scanning electron microscope (FEGSEM) (FEI Quanta FEG 250) was used to examine the changes in pigment particles and the morphologies of the particles due to milling.

6.5.5 Color Measurement

For color measurements, a vertical-type portable spectrophotometer, the Konica Minolta CM-700d, was employed. The color measurement method that excludes specular reflectance is referred to as SCE (Specular Component Excluded). If specular reflectance is included in the color measurement by completing the sphere with a specular plug, it is termed SCI (Specular Component Included). In SCE mode, the specular reflectance is omitted from the measurement, and only the diffuse reflectance is considered. This provides a color assessment that corresponds to how an observer perceives the color of an object [123].

When using the SCI mode, both specular and diffuse reflectance are measured, offering a total appearance evaluation that is independent of surface conditions. In summary, the SCI mode is utilized for detecting and analyzing color components, while the SCE mode provides information about the color properties of the final product [123].

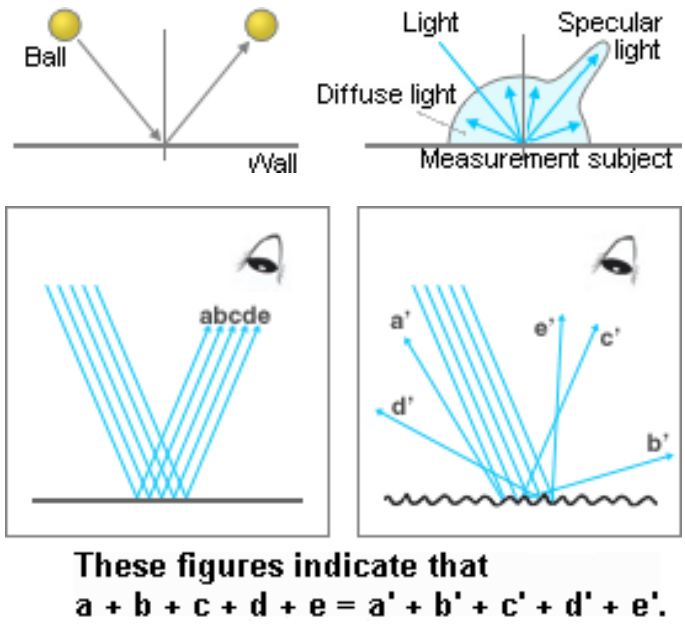


Figure 6.9 Illustration of diffuse and specular light for SCI and SCE method [123]

6.5.6 UV-Vis-NIR Spectroscopy

Ultraviolet-visible-near-infrared (UV-VIS-NIR) absorption spectroscopy serves as a vital technique for quantifying the reduction in light beam intensity following its passage through a sample or reflection from the sample's surface [124].

UV-VIS-NIR spectroscopy is frequently deployed in diverse analytical contexts, encompassing the evaluation of drinking water and wastewater, determination of anions in soluble solid substances, acquisition of spectra for organic compounds across various solvents, characterization of optical properties in thin films, and exploration of interaction and absorption bands exhibited by nanomaterials at different wavelengths [124]. For the UV-Visible-NIR spectral range, the instrumentation incorporates detectors such as the R-928 type photomultiplier, lead sulfide (PbS), and InGaAs [124]. Shimadzu UV-3600 Plus was used to measure the UV-VIS-NIR reflectance spectrum of the samples. The NIR reflectance (R_{NIR}) of pigments were calculated in a wavelength between 700 and 2500 nm following the ASTM E903-96 standard [15], [26], [47], [125].

The interaction of electromagnetic radiation with a sample surface engenders three distinct reflection phenomena: internal reflection, specular reflection, and diffuse reflection. Specular reflection transpires on smooth surfaces, akin to the reflective properties of mirrors, while diffuse reflection manifests on rough surfaces, causing light to disperse in all directions [126].

Internal Reflectance Spectroscopy (IRS), also known as attenuated total reflection (ATR) spectroscopy, pioneered by Jacques Fahrenfort and N.J. Harrick in the early 1960s, has garnered extensive utility. ATR spectroscopy involves the measurement of the interaction of the evanescent wave with the sample. If an absorbing material contacts the ATR crystal, the evanescent wave is absorbed by the sample, resulting in attenuated total reflection in the IR spectrum [126].

Diffuse reflectance spectroscopy, applied in the FT-IR region as diffuse reflectance infrared Fourier transform spectroscopy (DRIFTS), collects and analyzes electromagnetic radiation reflected by roughened surfaces. This technique is also known as "Kubelka–Munk" reflection, named after the theorists who developed a theory on radiation transport in scattering media [126].

Diffuse reflectance spectroscopy is commonly used for powders and solid samples with rough surfaces such as paper and cloth. The quality of the spectrum depends on factors like particle size, homogeneity, and packing density, with smaller particle size and narrow size distribution being preferred for obtaining a qualified spectrum [126].

7
RESULTS AND DISCUSSION

7.1 Prestudies for NIR Reflective Black Pigments

7.1.1 Inorganic Black Pigment Trials

The color and properties of pigments are influenced by parameters such as chemical composition, crystalline structures, morphology, particle size, and impurities. Various compositions can be employed to produce black inorganic pigments. Metal elements such as iron, chromium, cobalt, copper, nickel, and manganese are essential components in the manufacturing of black pigments [3], [10], [15], [18], [28], [30], [77], [105], [127]. Examples of black pigments obtained using these elements include iron chromite black (PG17 Blk), iron manganese black (PBk33), and iron chromite (PBk28) [1][76]. The ability of pigments to reflect electromagnetic waves in the NIR region can differ due to their chemical compositions, crystalline structures, particle size, and other factors (add reference). NIR reflectance spectra of pigments, which are combinations of different metal oxides, are presented in Figure 7.3 to examine the NIR reflection properties of various black inorganic pigments.

The pigments shown in Figure 7.1 and Figure 7.2 underwent a 3-hour calcination process at a temperature of 1000 °C, determined based on a literature review. The selection of these compositions was based on data obtained from the literature. When determining compositions and metal oxides, the aim was to obtain different crystal structures at similar temperatures, and the production of black or dark colors was targeted by combining different metallic elements. The heating and cooling rate was set at 5 °C per min (controlled heating and cooling were performed). Pigments were obtained through solid-state reactions using the ceramic method [30], [128].

Table 7.1 Composition of pigments used for pre-studies

Sample Name	Composition	Chemical Formula
Fe:Cr1	1 mol Fe 1 mol Cr	$FeCrO_3$
Fe:Mn1	1 mol Fe 1 mol Mn	$FeMnO_3$
Mn:Cu2	2 mol Mn 1 mol Cu	$CuMn_2O_4$
Cr:Cu2	2 mol Cr 1 mol Cu	$CuCr_2O_4$
Fe:Co2	2 mol Fe 1 mol Co	$CoFe_2O_4$
Carbon Black	C	C

The phases of the pigments in Figure 7.1 is detailed in Table 7.1. The obtained pigments undergo wet milling with a ball mill and water to achieve a suitable consistency for application after calcination. Alumina grinding jars and balls are used for the milling process, with ball sizes ranging between 4-6 mm. The weight ratio of the ball to powder in the milling process is set at 5, and the weight ratio of the powder to water is determined to be 1. The particle size distribution of the milled pigment is between 4-7 µm as Dv_{90}. Subsequently, the pigments are dried at 120 °C. After drying, the pigments are sieved through a 450-mesh (32 µm) sieve to break down any hard agglomerates formed during the drying process. Large and hard agglomerates within the pigment can lead to dispersion problems during color applications, causing deviations in color values. To ensure stable color values, each pigment is passed through a sieve to obtain a standardized powder structure.

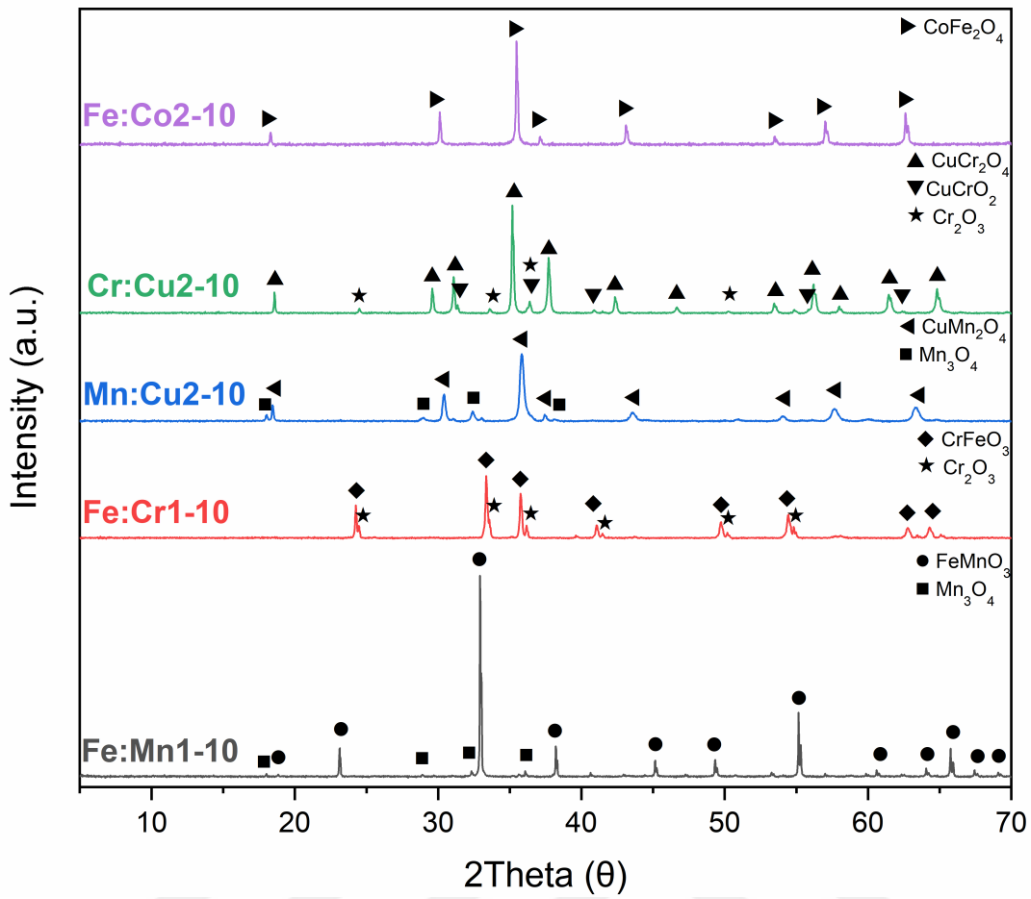


Figure 7.1 XRD patterns and phases of different compositions of pigments calcined at 1000 °C for 3 hours

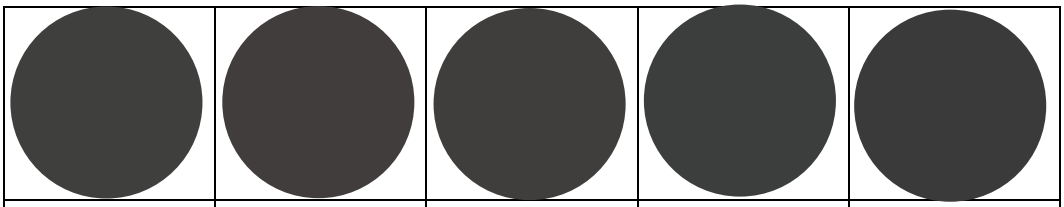
The aforementioned pigments were analyzed using the x-ray diffraction method, as illustrated in Figure 7.1. Sample nomenclature was assigned based on the metal oxides present, their quantities, and the calcination temperatures. For example, in the nomenclature Fe:Co2-10, "Fe:Co2" indicates that the molar ratio of iron to cobalt in the pigment is 2, and the "-10" code signifies that the calcination was carried out at 1000 °C.

Upon examining the Fe:Cr1-10 sample, the crystal structure was identified as iron chromium oxide $FeCrO_3$ (PDF 04-006-8200), with a low amount of unreacted metal oxide identified as Cr_2O_3 (PDF 04-015-7583). Similarly, the Fe:Mn1-10 sample exhibited the crystal structure of iron manganese oxide $FeMnO_3$ (PDF 01-083-4644), along with low amounts of residual oxides.

In the Cr:Cu2-10 sample, the primary crystal structure was identified as copper chromium oxide $CuCr_2O_4$ (PDF 00-034-0424), while the secondary phase included minor structures of $CuCrO_3$ (PDF 04-010-3330) and Cr_2O_3 (PDF 04-015-7583).

The Fe:Co2-10 sample displayed the crystal structure of cobalt iron oxide $CoFe_2O_4$ (PDF 04-015-9870).

Lastly, the Mn:Cu2-10 sample revealed the presence of copper manganese oxide $CuMn_2O_4$ (PDF 04-005-6874) in its crystal structure.



Fe:Mn1-10	Fe:Cr1-10	Mn:Cu2-10	Cr:Cu2-10	Fe:Co2-10

Figure 7.2 Colors of different compositions of pigments

After sieving, the obtained pigments underwent paint-film application to examine their color properties. A transparent acrylic paint served as the base material. The paint was blended with 4 wt.% of pigment paint and homogenized using a planetary ball mill. The resulting homogeneous colored dye was applied to a white substrate using a pool-type film applicator, with the chosen application thickness set at 0.4 mm. Subsequently, the applied paint was air-dried at room temperature.

Color measurements of the pigments were conducted using a spectrophotometer with D65 10° standard in SCI (Specular Component Included) *L*a*b** color space. The color measurement values, R_{NIR} values, and *C** values are detailed in Table 7.2. Furthermore, the colors of the pigments are visually represented in Figure 7.2.

Table 7.2 Color measurement, NIR reflectance and chroma of different compositions of pigments

Sample		*L**	*a**	*b**	C*	R_{NIR}
Mass	Carbon Black	23.58	0	-0.39	0.39	0.8
	Fe:Mn1	25.62	0.6	0	0.60	44.6
	Fe:Cr1	25.51	0.98	0.36	1.04	62.6
	Mn:Cu2	26.28	0.65	1.65	1.77	6.8
	Cr:Cu2	25.83	-0.27	-0.61	0.67	9.4
	Fe:Co2	24.44	0.33	-0.21	0.39	35.1

When examining the color values, the carbon black sample in our possession appears bluish-black with a *C** value of 0.39. (when analyzing the color values, it is observed that the carbon black sample we have is a bluish-black, with a *C** value of 0.39.) *C** is a crucial metric for black pigments, as an increase in *C** indicates a loss of deep black properties. As *C** rises, the pigment may exhibit brown or grayish tones. For instance, a positive increase in the *a** value in the *L*a*b** color space results in a color shift from deep black to brown.

Another pigment with high bluishness is $CuCr_2O_4$, located in the green region (*a<0) unlike the others. This pigment has a *C** value of 0.77 and low R_{NIR} similar to carbon black. The $FeCrO_3$ pigment, displaying the highest R_{NIR} value, possesses a reddish and yellowish-black color with a *C** value of 1.67. Meanwhile, the $FeMnO_3$ pigment, also featuring high R_{NIR}, exhibits a lower *C** of 1.01. Changes in *C** may result from unreacted oxides during calcination, with minor residual oxides observed in pigments like Mn_3O_4, Cr_2O_3, and others.

Subsequent sections will deal with the detailed study of the effect of calcination temperature on residual oxides and the corresponding changes in chromaticity. These investigations reveal that black pigments with different compositions can exhibit diverse color properties and NIR reflectance.

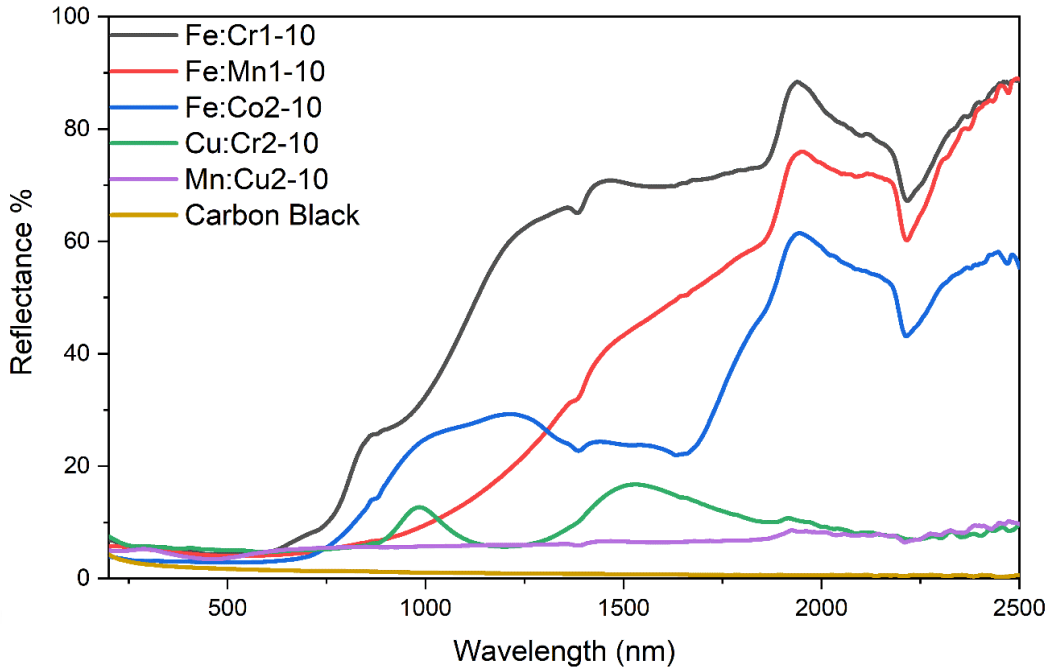


Figure 7.3 UV-Vis-NIR reflectance spectrum of different composition of pigments

The pigments were analyzed using a UV-VIS-NIR spectrometer as powder to calculate NIR reflectance, revealing that the iron chromium oxide ($FeCrO_3$) (PG17 Blk) pigment exhibited the highest R_{NIR} value at 63%. Conversely, carbon black displayed the lowest R_{NIR}, nearly 0%. Among the pigments composed of metal oxides, copper manganese oxide and copper chromium oxide pigments had the lowest R_{NIR} values at 7% and 10%, respectively. Copper chromium oxide (PBk28) pigment has been previously studied in the literature, emphasizing its NIR absorbent black inorganic pigment properties [77], [129].

On the other hand, the iron manganese oxide pigment demonstrated the second-highest reflectance value after $FeCrO_3$, approximately 45%, followed by cobalt iron oxide pigment with 35% NIR reflectance. For the future parts of the studies, it has been deemed appropriate to use Fe-Cr pigments, as $FeCrO_3$ exhibits the highest NIR reflectance. These pigments were selected for further development as they are suitable for exploring the limits of NIR reflectance and color properties.

7.2 Fe-Cr Inorganic Pigments

7.2.1 Effect of Calcination Temperature on Properties of Fe-Cr Pigments

The calcination temperatures of pigments are a critical parameter in terms of the reaction of metal oxides used in raw material mixtures to form the final phases. The temperature of the heat treatment applied to raw material mixtures affects the lattice parameters and structures of crystals. Metal oxides can react and form structures that are different from or the same as their crystal structures. Changes occur in the final product properties due to the formation of different crystal structures or differences in the ionic radius of the combined elements [130]–[133]. Temperature is of critical importance as it is the determining factor for the reaction efficiency or the formation of phases. Residual raw materials that cannot be incorporated into the structure may impact characteristics such as the color properties, chemical stability, heat resistance, toxicity, and NIR reflectance of the final product. If unreacted raw materials remain in the structure, the intended color, crystal structure or phases may not be achieved.

For example, the PG17 Blk pigment, which consists of iron oxide and chromium oxide, can turn from black to brown due to the remaining unreacted iron oxide in the structure as a result of insufficient reaction energy. On the other hand, the presence of residual chromium oxide in the structure may cause a shift towards green and a departure from black in color. Additionally, having these residual raw materials in the structure may be intentional. For instance, the PBr29 pigment deliberately includes unreacted iron oxide and chromium oxide in its structure. The unreacted iron oxide and chromium oxide, which did not enter the $(Fe,Cr)_2O_3$ structure, contribute to the brown appearance of the pigment.

Especially for applications carried out at high temperatures (600-1200 °C), unreacted raw materials in the structure are of critical importance. Residual raw materials can react with materials colored at high temperatures, leading to surface defects such as pinholes and glossiness, resembling reactions with glass. From a toxicity and compliance with standards perspective, it is necessary for residual raw material waste outside the desired structure of pigments to be below certain thresholds. Examples of these raw materials include quartz, cristobalite, or phases

outside the desired crystal structure. To investigate this effect, Fe-Cr pigments have been subjected to calcination processes at different temperatures.

7.2.1.1 X-ray Diffraction Analysis of Fe:Cr1 Pigments

After processes such as grinding, drying, and sieving following calcination, XRD analysis was conducted on the obtained pigments to examine the phases present in the structure. In Figure 7.4, XRD analysis diffractograms and phases of pigments and raw material mixtures calcined between 1000-1200 °C are provided. The diffractogram for the Fe:Cr1 pigment indicates a molar ratio of iron to chromium in the composition as 1. On the other hand, the term RM represents the raw material mixture, and the numbers 10, 11, and 12 denote calcination temperatures of 1000, 1100, and 1200 °C, respectively.

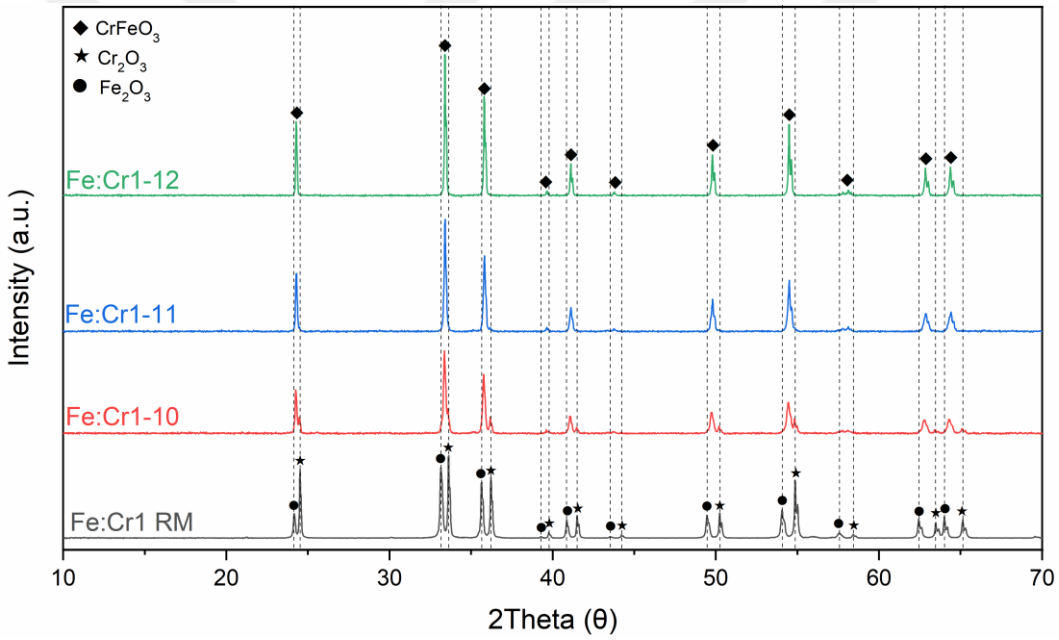


Figure 7.4 XRD analysis of samples Fe:Cr1-10, Fe:Cr1-11, and Fe:Cr1-12

Upon examining the analysis results in Figure 7.4, after calcination at 1000 °C, the Fe-Cr hematite structure and unreacted oxide materials were observed. The phases in these mentioned pigments are Fe_2O_3 and Cr_2O_3, present in the raw material. The analysis identified the main phase as $CrFeO_3$ iron chrome oxide (PDF 04-006-8200), and the residual material phases were determined as Cr_2O_3 (PDF 04-015-7583) and Fe_2O_3 (PDF 04-015-6943) through analysis. Since the peaks of Fe_2O_3 and Cr_2O_3 phases are close due to having the same crystal structure as the desired phase, the region with their highest peaks is specifically shown in Figure 7.5. In the Fe:Cr1-10 sample, the residual Cr_2O_3 phase is prominently visible, whereas in the

Fe:Cr1-11 sample, it is barely detectable, and in the Fe:Cr1-12 samples, it is almost non-existent. On the other hand, in the regions where the peaks of Fe_2O_3 are located, an indistinct diffractogram that merges with the main phase is observed. With increasing temperature, there is a decrease in the ratio of unreacted Cr_2O_3. Alongside the increasing heat treatment temperature, narrowing of the $FeCrO_3$ peak and an increase in intensity are observed. The overlapping region of Fe_2O_3 and $FeCrO_3$ peaks decreases and disappears with increasing calcination temperature. When the sample calcined at 1200 °C is examined, no residual raw material is observed. The decrease in the peaks of Fe_2O_3 and Cr_2O_3, along with the narrowing and intensity increase in the $FeCrO_3$ peaks, indicates the incorporation of unreacted raw materials into the structure with increasing temperature. This situation can support the formation of the Fe-Cr hematite crystal structure with increasing temperature. All obtained phases have the crystal structure of hematite and belong to the R-3c (167) space group.

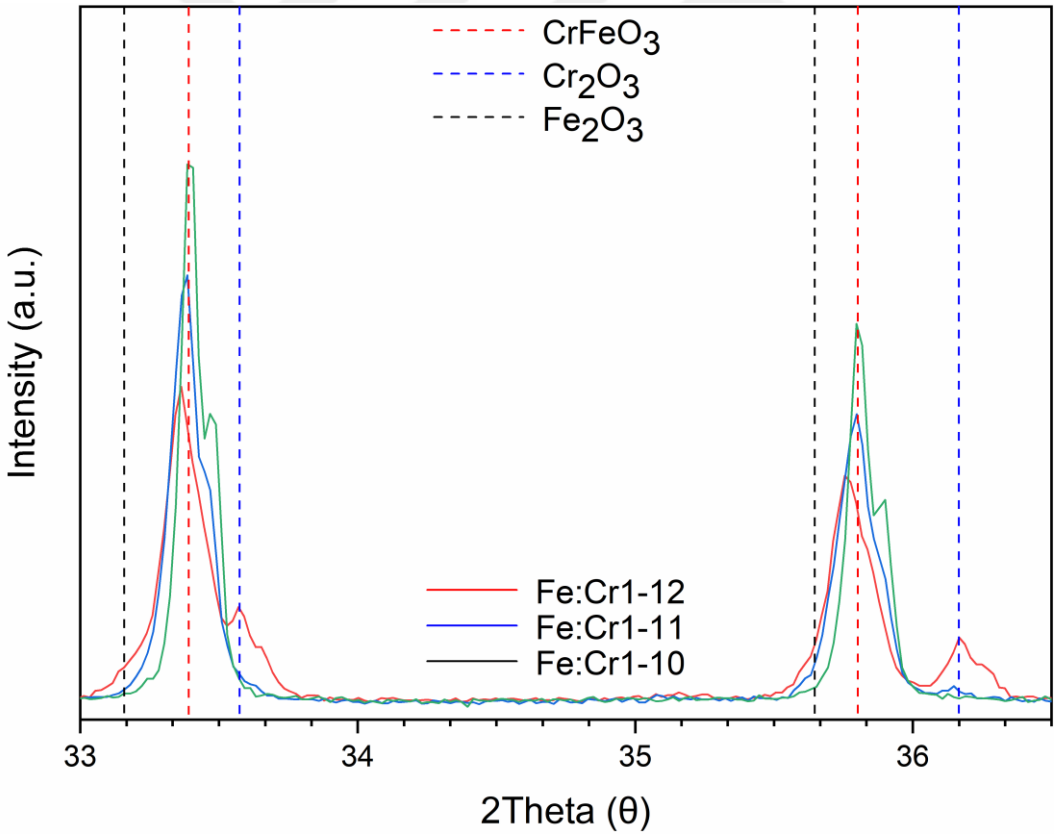


Figure 7.5 XRD analysis of samples Fe:Cr1-10, Fe:Cr1-11, and Fe:Cr1-12 in the angle range of 33-37

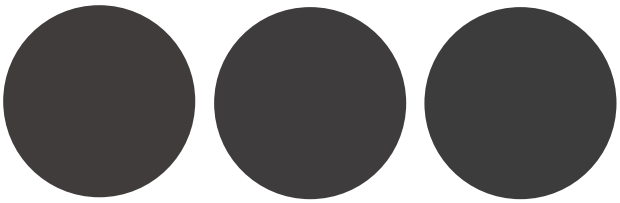
7.2.1.2 Color Properties of Fe:Cr1 Pigments

Fe:Cr1 pigments obtained by calcination at 1000-1200 °C were used for matte paint application. As a result of the application, a colored acrylic film with a thickness of 0.4 mm was obtained on white paper. Three measurements were taken from each film, and the average values were recorded. The color coordinates, chroma, and R_{NIR} values of the samples are given in Table 7.3. Additionally, the mass colors of the pigments are provided in Figure 7.6.

Table 7.3 Color coordinates, NIR reflectance and chroma of Fe:Cr1 calcined at 1000-1200 °C

Sample Name		*L**	*a**	*b**	*C**	R_{NIR}
Mass Color Paint App.	Fe:Cr1-10	25.52	1.51	0.8	1.71	62.5
	Fe:Cr1-11	25.51	0.98	0.36	1.04	64.5
	Fe:Cr1-12	25.32	0.64	0.01	0.64	65.1

When the samples are examined, the *L** value representing the lightness and darkness of the color appears similar for all three samples, with values of 25.52, 25.51, and 25.32 for Fe:Cr1-10, Fe:Cr1-11, and Fe:Cr1-12, respectively. The *a** value representing the redness and greenness of the color is 1.51, 0.98, and 0.64, respectively. The decrease in this value indicates a shift from red to green, reducing the *C** and resulting in a darker color. As the *a** value increases, the pigment appears more red, leading to a shift from black to brown. On the other hand, the *b** value, similar to the *a** value, decreases with increasing temperature, being 0.8, 0.36, and 0.01, respectively. The decrease in the b* value changes the color from yellow to blue. Similar to the a* value, approaching zero for the b* value reduces the chroma, resulting in blacker colors.



Fe:Cr1-10 Fe:Cr1-11 Fe:Cr1-12

Figure 7.6 Color hues of Fe:Cr1-10, Fe:Cr1-11, and Fe:Cr1-12

7.2.1.3 UV-VIS-NIR Reflectance Spectrums of Fe:Cr1 Pigments

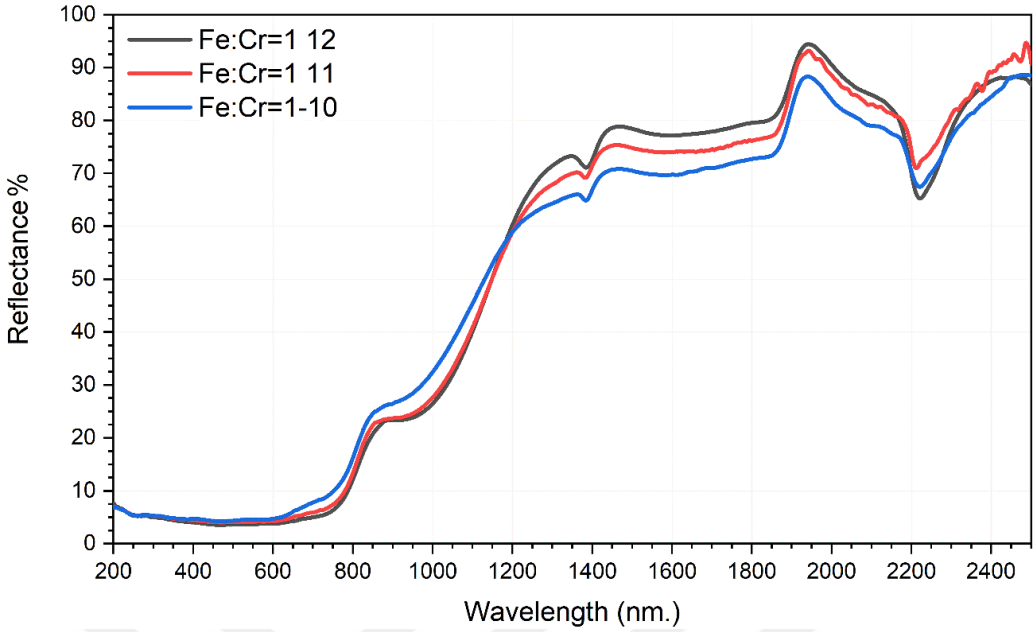


Figure 7.7 UV-VIS-NIR spectrums of Fe:Cr1 calcined at 1000-1200 °C

In Figure 7.7, UV-VIS-NIR reflectance spectra were measured to examine the NIR behavior of pigments obtained by calcination between 1000 and 1200 °C. In Figure 7.72, the region with a wavelength of 700-2500, which corresponds to the NIR region, is detailed. When the NIR reflectance of the pigments were measured, the reflections of Fe:Cr1-10, Fe:Cr1-11, and Fe:Cr-12 samples were measured as 62.5%, 64.5%, and 65.1%, respectively. When reflectance measurements are examined together with XRD analysis results, an increase in R_{NIR} value with the increase in temperature is observed, despite having the same main phases. Particularly, the Fe:Cr1-10 sample showed 2% less reflection than the Fe:Cr1-11 sample and 2.6% less reflection than the Fe:Cr-12 sample. When XRD analyses are considered alongside NIR reflectance, it is observed that the presence of unreacted raw materials in the structure can affect NIR reflectance.

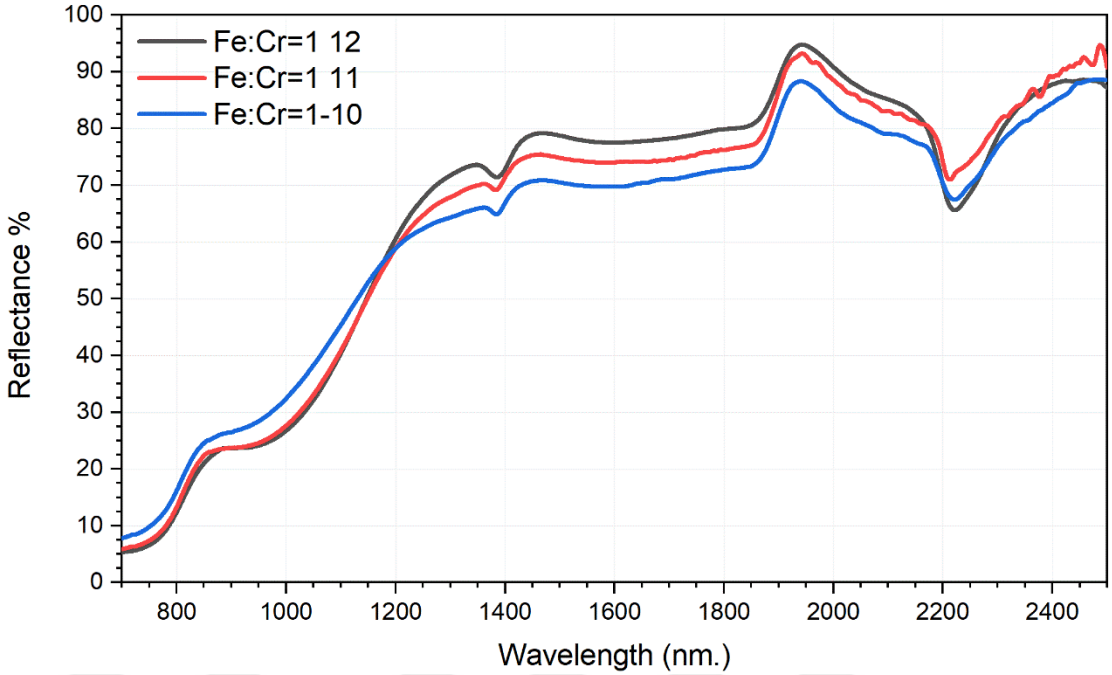


Figure 7.8 NIR spectrums of Fe:Cr1 calcined at 1000-1200 °C

The XRD patterns of Fe:Cr1-11 and Fe:Cr1-12 samples are close to each other, and similarly, there is less difference in NIR reflectance compared to the Fe:Cr1-10 sample. On the other hand, when the sample with the lowest NIR reflectance (Fe:Cr1-10) and the one with the highest NIR reflectance (Fe:Cr1-12) are compared, a significant amount of chrome oxide was detected in the XRD analysis of the Fe:Cr1-10 sample. As the amount of unreacted Cr_2O_3 increased, a decrease in R_{NIR} was observed. To demonstrate that unreacted raw materials reduce R_{NIR}, R_{NIR} of raw materials were measured and shown in Figure 7.9. The R_{NIR} reflectance of Fe_2O_3 and Cr_2O_3 were measured as 44.3% and 49.8%, respectively.

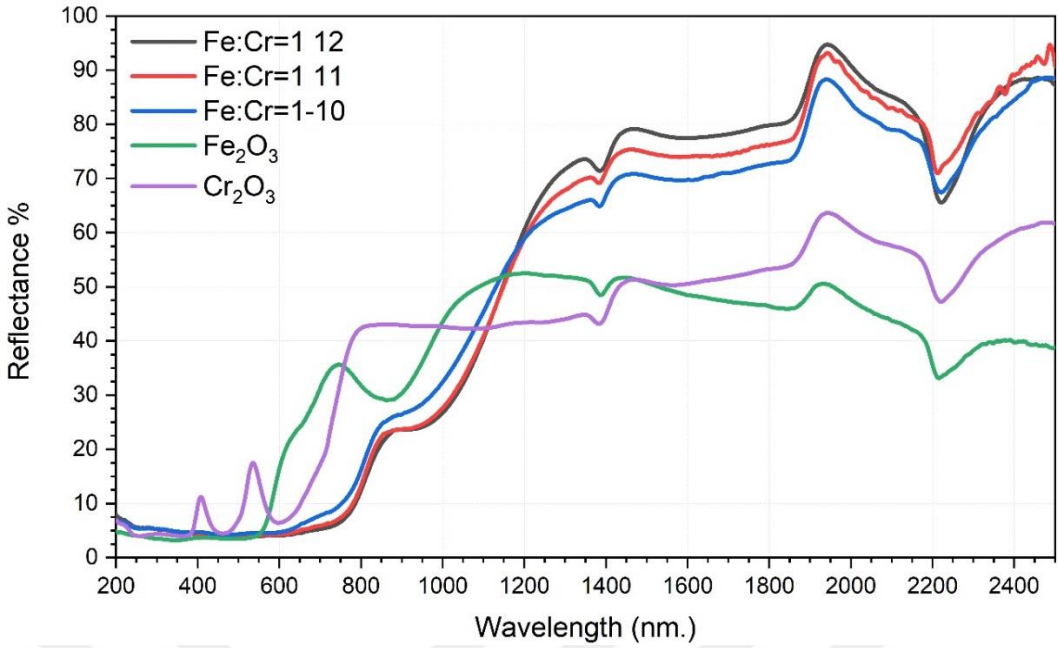


Figure 7.9 UV-VIS-NIR spectrums of Cr_2O_3, Fe_2O_3, and Fe:Cr1 calcined at 1000-1200 °C

The reflectance of Fe:Cr1-10, Fe:Cr1-11, and Fe:Cr1-12 samples in the visible (VIS) region are given in Figure 7.10. In this region, color is formed by the mixture of wavelengths reflected by the material, and it corresponds to the region with electromagnetic wavelengths visible to the human eye. In contrast, the UV and NIR regions cannot be seen by the human eye. As we move from 380 nm to 700 nm, the colors produced by the wavelengths are violet, blue, green, yellow, orange, and red. The wavelengths reflected by the reflectance and their intensities create the color formation. When examining the spectra in Figure 7.10, an overall increase is observed after 600 nm. This region includes the yellow, orange, and red areas. Higher reflectance compared to other regions, where linear reflection occurs, cause the color to shift towards red and yellow in this region.

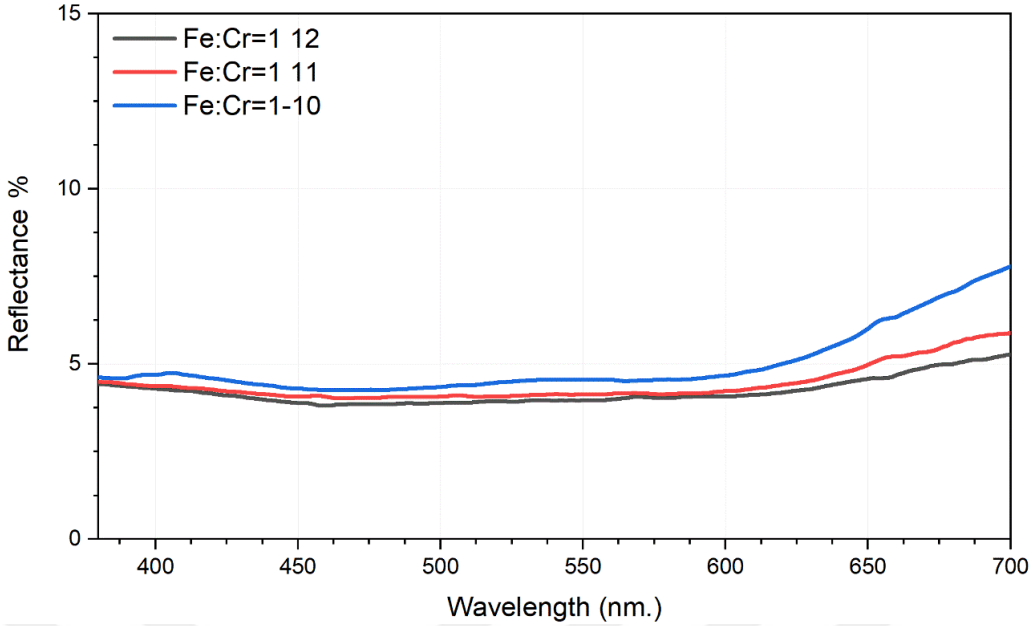


Figure 7.10 VIS spectrums of Fe:Cr1 calcined at 1000-1200 °C

Fe:Cr1-10, Fe:Cr1-11, and Fe:Cr1-12 exhibit uniform and linear reflectance characteristics within the wavelength range up to 600 nm. Notably, the reflectance spectrum of Fe:Cr1-10 demonstrates an increased reflection in the 600-700 nm range compared to the other specimens. This increase decreases with increasing calcination temperatures. The increase in C^* value at this point can be attributed to unreacted raw materials causing a noticeable shift in coloration towards yellow and red spectra. Evaluation in the CIE $L^*a^*b^*$ color space reveals that the increase in redness is summarized by the positive trend of the a^* value, while the increase in yellowness is summarized by the positive trend of the b^* value. Consistent data sets were obtained by examining the data obtained from the VIS spectrum and the measurements made via the photospectrometer. Consequently, the a^* value for the Fe:Cr1-10 specimen undergoes a reduction from 1.51 to 0.98 in the Fe:Cr1-11 specimen and further decreases to 0.64 in the Fe:Cr1-12 specimen with a rise in temperature. In parallel, the b^* value for Fe:Cr1-10, similar to the a^* value, registers at 0.8, subsequently decreasing to 0.36 for Fe:Cr1-11 and 0.01 for Fe:Cr1-12 with an increasing calcination temperature.

7.2.2 Effect of Fe:Cr Ratio on Properties of Pigments

The generation of pigments involves employing various Fe:Cr ratios, resulting in the formation of iron chrome oxide($(Fe,Cr)_2O_3$). The study delves into the investigation of NIR reflectance and color properties of pigments derived from different stoichiometric ratios. The proportions of the reactants prepared for calcination are outlined in Table 7.3.

Table 7.4 Composition of Fe-Cr pigments calcined at 1000 °C to compare effect of Fe:Cr ratio

Temperature	Sample Name	Composition
1000 °C	Fe:Cr05-10	1 mol Fe 2 mol Cr
	Fe:Cr1-10	1 mol Fe 1 mol Cr
	Fe:Cr2-10	2 mol Fe 1 mol Cr
1200 °C	Fe:Cr05-12	1 mol Fe 2 mol Cr
	Fe:Cr1-12	1 mol Fe 1 mol Cr
	Fe:Cr2-12	2 mol Fe 1 mol Cr

The $FeCrO_3$ pigment was systematically selected and denoted as Fe:Cr1. In the Fe:Cr2 sample, the iron oxide content was increased, and the raw material mixture was formulated to achieve a molar iron ratio twice that of chromium. Additionally, a raw material blend was prepared for the Fe:Cr05 sample, featuring a molar chrome amount twice that of iron. The prepared mixtures underwent calcination at two different temperatures, ranging from 1000 to 1200 °C. The purpose of calcination at these two temperatures is to examine how unreacted raw materials affect the pigment depending on the temperature. Furthermore, it aims to investigate the influence of these unreacted materials on color hues as the composition changes. Simultaneously, raw material blends with identical compositions were subjected to calcination at the higher temperature of 1200 °C, where unreacted materials could not be detected. The purpose of calcination at 1200 °C is to mitigate the impact of residual raw materials on both NIR reflectance and color properties.

7.2.2.1 X-ray Diffraction Analysis of Fe:Cr Pigments

The XRD analyses of Fe:Cr0.5, Fe:Cr1, and Fe:Cr2 samples, calcined at 1000 °C, are presented in Figure 7.11. Upon examination of these samples, unreacted raw materials were identified in each specimen. The Fe:Cr05-10 sample exhibited the highest chromium oxide content, and the analysis conducted after calcination revealed the presence of the chrome oxide phase. The intensities of the chrome oxide peaks decreased with a reduction in the chromium-to-iron ratio in the composition. On the other hand, in the Fe:Cr1-10 sample, Fe_2O_3 was detected; however, the final peaks did not provide sharp and distinct patterns due to their proximity to the peaks of the ultimate phase, resulting in observed overlapping.

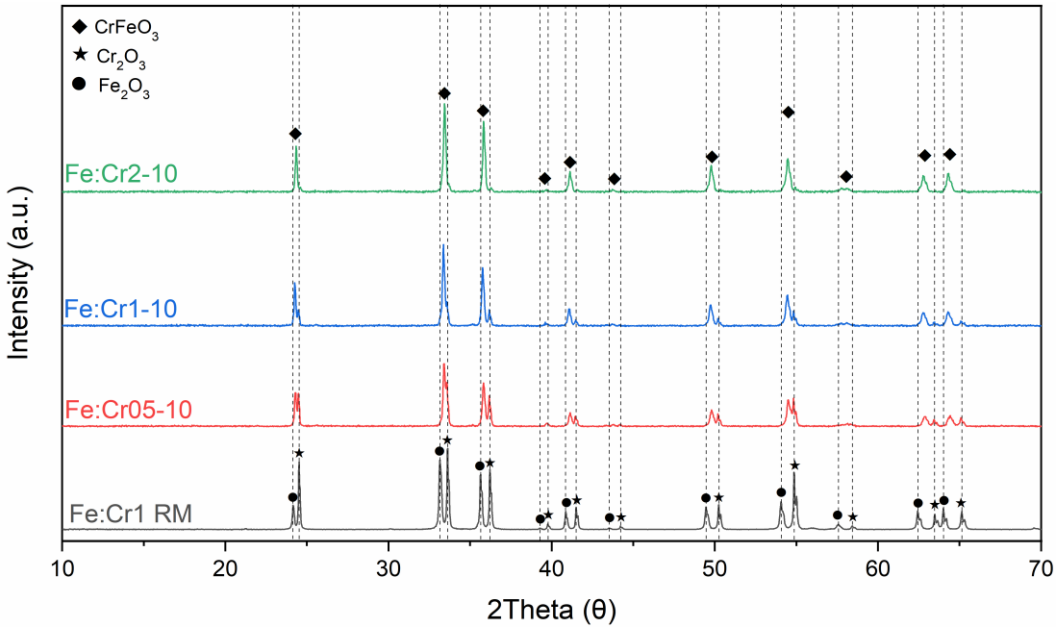


Figure 7.11 XRD analysis of Fe:Cr0.5, Fe:Cr1 and Fe:Cr2 calcined at 1000 °C

Diffractograms within the angular range of the two highest peaks were redrawn and examined in detail to further investigate the formed phases and remaining raw materials in the structure. The positions of the phases are indicated by colored and dashed lines. Iron oxide (PDF 04-015-6943) is represented by the red dashed line, chrome oxide (PDF 04-015-7583) by the black dashed line, Cr1.3Fe0.7O3 (PDF 04-006-8207) by the magenta dashed line, $FeCrO_3$ (PDF 04-006-8200) by the green dashed line, and Cr0.6Fe1.4O3 (PDF 04-026-3094) by the blue dashed line.

When examining the iron oxide phase in the samples, the highest peak was observed in the Fe:Cr2-10 sample, which has the highest Fe/Cr ratio. The peak observed here combined with the peak of the desired $(Fe,Cr)_2O_3$ phase, and therefore, a sharp peak

was not observed. The height of the peak resulting from this interaction decreased with a decrease in the Fe/Cr ratio. In the Fe:Cr05-10 sample, which has the lowest Fe/Cr ratio, the main peak of the obtained $(Fe,Cr)_2O_3$ was observed to be more to the right, yet a distinct peak of Fe_2O_3 was not observed. Similarly, the Cr_2O_3 phase is clearly visible in the Fe:Cr05-10 sample, where the Cr/Fe ratio is highest. As the Cr/Fe ratio decreased, the Cr_2O_3 peak distinctiveness decreased. In the Fe:Cr2-10 sample, where the Cr/Fe ratio is lowest, the distinct peak of Cr_2O_3 observed in Fe:Cr05-10 was not evident. These variations in Fe_2O_3 and Cr_2O_3 phases occurred depending on the composition. An increase in the composition of Fe_2O_3 resulted in distinct peaks in the unreacted Fe_2O_3 peaks, while a similar increase in the composition of Cr_2O_3 led to distinct peaks in the unreacted Cr_2O_3 peaks. When examining the intensity of the main peak and the remaining raw material's intensity in the sample with the lowest Fe/Cr ratio, it was observed that the peaks were close to each other. On the other hand, with an increase in the Fe:Cr ratio, the intensities of the main phase peaks increased, while the distinctiveness of the remaining raw material peaks decreased. Despite being calcined at the same temperature, this difference arises from the reactivity and activation energy differences between Fe_2O_3 and Cr_2O_3 structures. In comparison to Fe_2O_3, the high temperature resistance and high activation energy requirement of Cr_2O_3 led to a less pronounced reaction in samples where the chromium ratio is high. Figure 7.12 shows the phases that Cr-Fe-O can form at 1 atm pressure as a diagram. When only Fe_2O_3 is present in the structure, a transformation to a spinel structure is observed after approximately 1400 °C, while spinel formation does not seem possible when only Cr_2O_3 is present. When the phase diagram is examined, it is seen that the elements Fe, Cr and O can generate a solid solution at temperatures up to approximately 1400 °C at 1 atm [134].

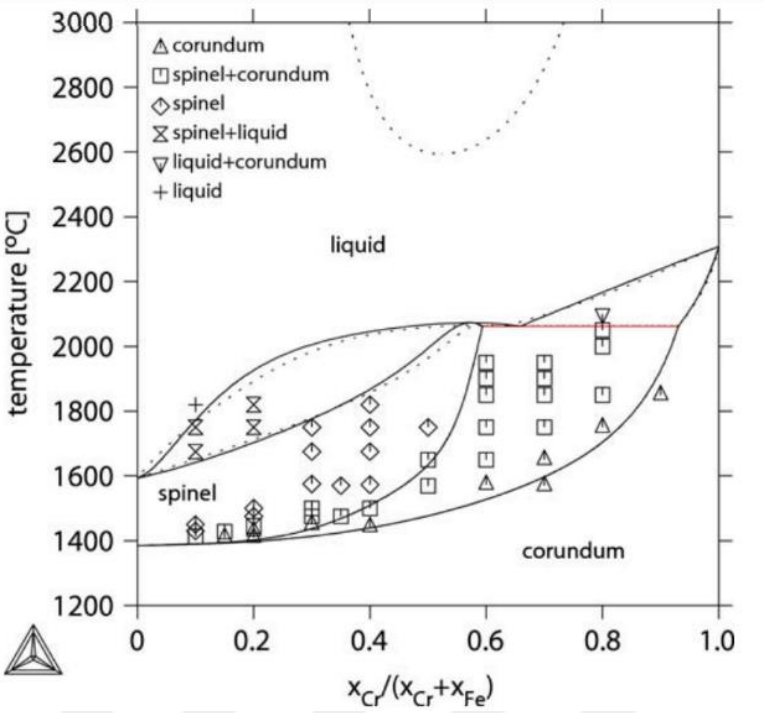


Figure 7.12 Calculated and experimental phase diagram of Cr–Fe–O in air at 1 atm [135]–[137]

Furthermore, shifts in the positions of the peaks were observed in the main phases. Due to the differences in ion diameters, Fe_2O_3 (Fe^{3+}=0.645 Å) and Cr_2O_3 (Cr^{3+}=0.615 Å), which have the same crystal structure, have different lattice parameters (Table 7.5) [138]. In the case of complete reaction, the ratios of different metal elements in the composition alter the lattice parameters of the structure, causing the peaks to shift to the right and left (Table 7.5). When a smaller radius atom dissolve into a matrix atomic structure, a lattice distortion due to contraction/shrinkage occurs [139].

Table 7.5 Crystallographic information of Fe_2O_3, Cr_2O_3 ,$FeCrO_3$ from ICDD/PDF [140], [141]

Chemical Formula	Crystal System	Space Group	Unit Cell (Å)			Volume ($Å^3$)
			a	b	c	
Fe_2O_3	Hexagonal	R-3c (167)	5.035	5.035	13.755	301.90
Cr_2O_3	Hexagonal	R-3c (167)	4.955	4.955	13.578	288.47
$FeCrO_3$	Hexagonal	R-3c (167)	5.015	5.015	13.639	297.07

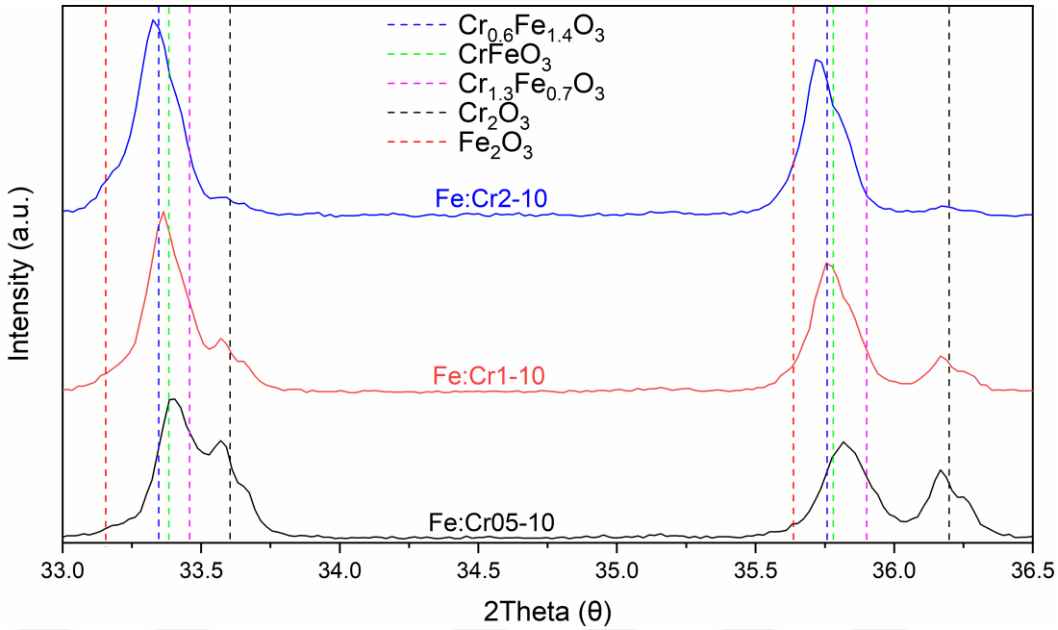


Figure 7.13 XRD analysis of samples Fe:Cr0.5-10, Fe:Cr1-10, and Fe:Cr2-10 in the angle range of 33-36.5

Nonetheless, definitive conclusions in experiments carried out at 1000 °C may be precluded due to the persistent presence of residual or unreacted raw materials within the structure. A comparative assessment of the ionic radius between Fe^{3+} and Cr^{3+} ions, denoted as 0.645 Å and 0.615 Å, respectively [138]. It presents an expected situation when Cr^{3+} with a smaller ionic radius is incorporated to the structure. The increase in the smaller ionic radius in the structure and the decrease in Fe^{3+} with a larger ionic radius in the structure cause the peaks to shift to the right. Despite the identical crystal lattice structure of Fe_2O_3 and Cr_2O_3, the variance in peak positions is attributed to disparities in ionic radius. Specifically, the principal peak of Fe_2O_3 at 33.15 contrasts with the main peak of Cr_2O_3 situated at 33.60. Consequently, an examination of the main phases of the Fe:Cr05-10, Fe:Cr1-10, and Fe:Cr2-10 samples indicates a rightward shift towards Cr_2O_3 as the Fe/Cr ratio diminishes. This shift serves as an indicator of the alterations in Fe/Cr ratios within the structure, signifying a reduction in the iron ratio accompanied by an elevation in the chromium ratio.

Section 7.7.1 scrutinizes the influence of non-reactive raw materials on color properties and NIR reflectance. Following experiments conducted at 1000 °C, discernible residual raw materials were identified in the Fe:Cr0.5, Fe:Cr1, and Fe:Cr2 samples. To mitigate the impact of non-reactive raw materials on the

targeted final phases and attain a singular-phase structure, samples with this composition underwent calcination at 1200°C.

The diffractograms and phases resulting from the XRD analysis of mixtures featuring Fe:Cr0.5, Fe:Cr1, and Fe:Cr2 compositions calcined at 1200°C are presented in Figure 7.14. The XRD analyses of Fe:Cr0.5, Fe:Cr1, and Fe:Cr2 samples subjected to calcination at 1200 °C are presented in Figure 7.7. Upon inspection of the XRD patterns of the pigments calcined at 1200 °C, no evidence of residual raw materials, which had not undergone reaction, decreasing or persisting in the structure was observed. In the examination of NIR reflectance, it was noted that the NIR reflectance exhibited an increase corresponding to the reduction in the amount of unreacted raw material. Following the alteration in composition, no notable variation was discerned in the NIR reflectance, emphasizing the absence of residues and the maintenance of an identical crystal structure. The NIR reflectance spectra of Fe:Cr0.5-12, Fe:Cr1-12, and Fe:Cr2-12 samples are illustrated in Figure 7.9.

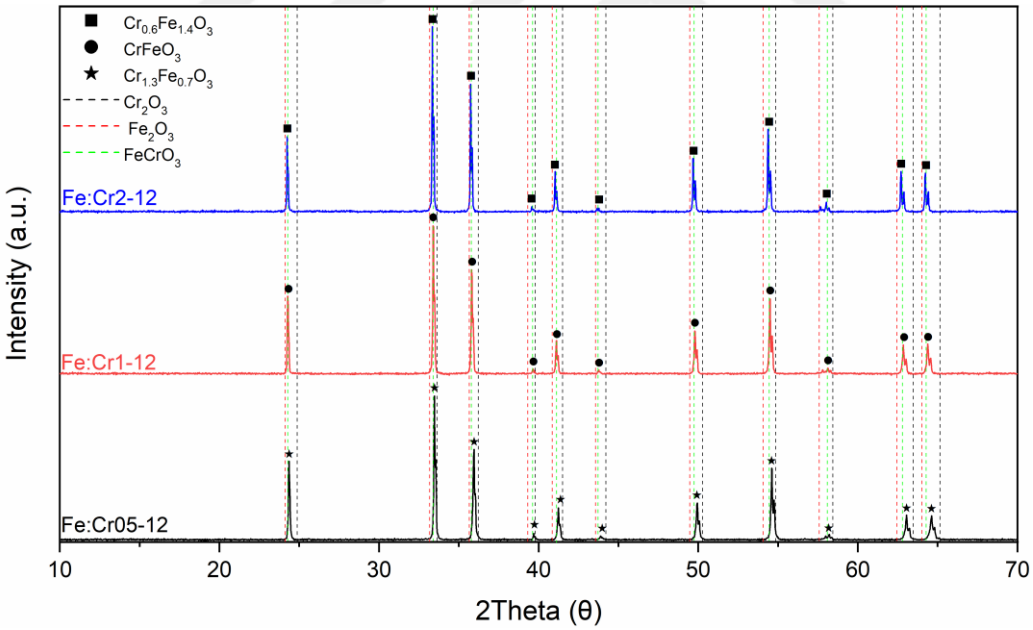


Figure 7.14 XRD analysis of Fe:Cr0.5, Fe:Cr1 and Fe:Cr2 at 1200 °C

Diffractograms obtained upon examination reveal an increase in the non-reactive raw material content with the rise in temperature across all compositions. In Fe:Cr05-12, Fe:Cr1-12, and Fe:Cr2-12 samples, a reduction in non-reactive raw materials is accompanied by a decrease in the width and an increase in the intensity of the main phase peaks. Given the proximity of peak positions for Fe-Cr pigments with different compositions, the graphs have been redrawn to focus on the region

containing the top two peaks in the diffractograms. Diffractograms drawn in the range of 33 to 36.5° are presented in Figure 7.15.

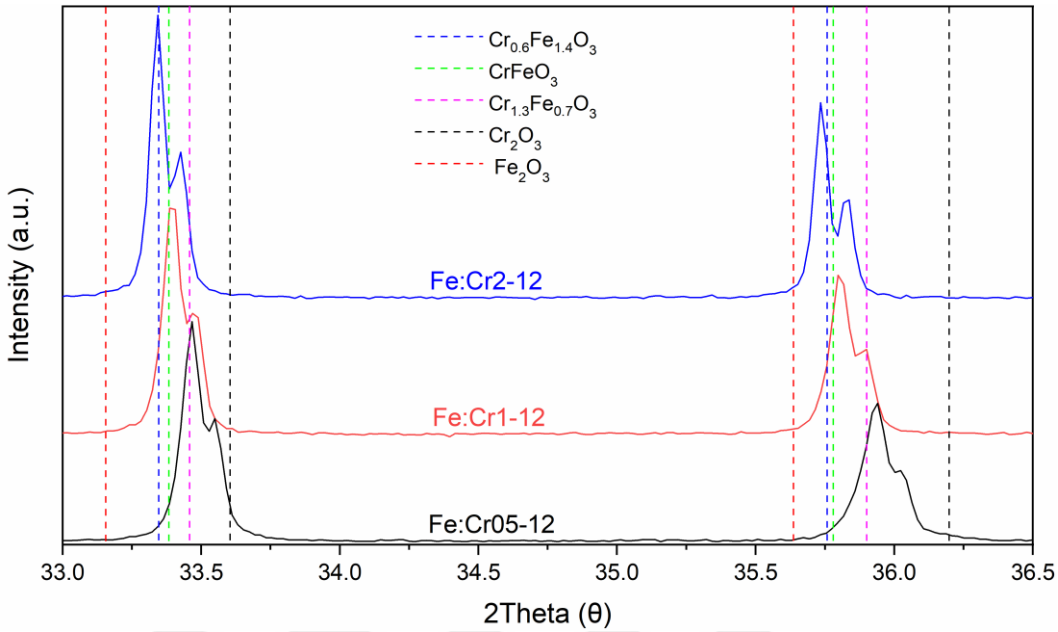


Figure 7.15 XRD analysis of samples Fe:Cr0.5-12, Fe:Cr1-12, and Fe:Cr2-12 in the angle range of 33-36.5°

Iron oxide (PDF 04-015-6943) is represented by the red color, chrome oxide (PDF 04-015-7583) by black, $Cr_{1.3}Fe_{0.7}O_3$ (PDF 04-006-8207) by magenta, $FeCrO_3$ (PDF 04-006-8200) by green, and $Cr_{0.6}Fe_{1.4}O_3$ (PDF 04-026-3094) by blue dashed lines. Upon closer examination of the Fe:Cr05-12 sample, no iron oxide and chrome oxide phases observed in the Fe:Cr05-10 sample are evident. The intensities of peaks at angles where the peaks of these phases are located have decreased towards the angles of the desired phase, rendering the peak of the desired phase more distinct with higher intensity. A similar pattern is observed for the Fe:Cr1-12 and Fe:Cr2-12 samples. When examining the final obtained phases of the Fe:Cr05-12, Fe:Cr1-12, and Fe:Cr2-12 samples, it is observed that the Fe:Cr1-12 sample has peaks of Fe_2O_3 and Cr_2O_3 located in the middle of the angles. For the Fe:Cr05-12 sample, the angles where the peaks of the final phase are located are close to those of Cr_2O_3. In comparison to the Fe:Cr1 sample, the Fe:Cr05 sample contains more Cr_2O_3 and less Fe_2O_3. On the other hand, in the Fe:Cr2 pigment, the peaks of the obtained phase are closer to Fe_2O_3. When comparing the compositions of the Fe:Cr1 sample with the Fe:Cr2 sample, the Fe:Cr2 sample contains more Fe_2O_3 and less Cr_2O_3. When the $FeCrO_3$ phase obtained in the Fe:Cr1-12 sample is taken as a reference, the $Cr_{1.3}Fe_{0.7}O_3$ phase obtained in the Fe:Cr0.5-12 sample gives peaks at higher

angles. On the other hand, the $Cr_{0.6}Fe_{1.4}O_3$ phase obtained in the Fe:Cr2-12 sample gives peaks at lower angles compared to $FeCrO_3$. The angular shifts in the positions of phases with different compositions are due to the quantitative differences in metal oxides with different ion radius in the structure, as previously mentioned. The varying ion sizes of Fe^{3+} and Cr^{3+} cause changes in crystal lattice parameters, leading to shifts in peaks.

7.2.2.2 Color Properties of Fe:Cr Pigments

The color values and *C** of the pigments subjected to calcination at 1000 and 1200 °C are provided in Table 7.6, and their corresponding colors are illustrated in Figure 7.16.

Table 7.6 Color measurements of Fe:Cr0.5, Fe:Cr1 and Fe:Cr2 calcined at 1000 and 1200 °C

Sample Name		*L**	*a**	*b**	*C**
Mass Color	Fe:Cr05-10	25.75	1.33	1.01	1.67
	Fe:Cr1-10	25.52	1.51	0.8	1.71
	Fe:Cr2-10	25.72	2.44	0.95	2.62
	Fe:Cr05-12	25.08	1.04	0.22	1.06
	Fe:Cr1-12	25.32	0.64	0.01	0.64
	Fe:Cr2-12	25.51	0.59	-0.14	0.61

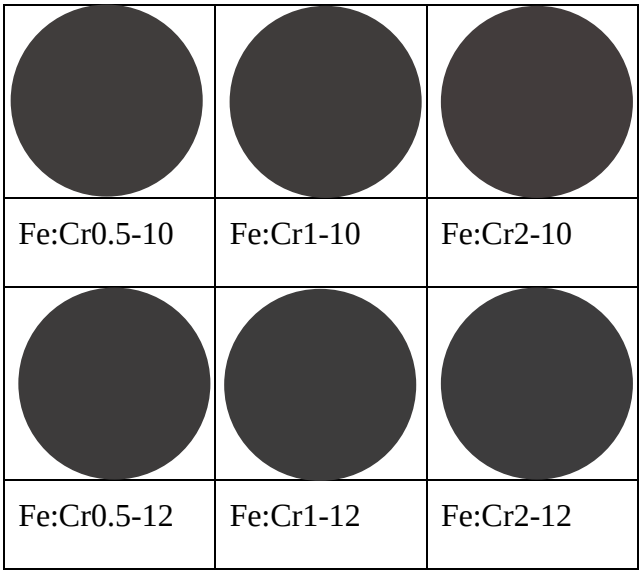


Figure 7.16 Mass colors of Fe:Mn05, Fe:Mn1 and Fe:Mn2 calcined at 1000/1200 °C

7.2.2.3 UV-VIS-NIR Reflectance Spectrums of Fe:Cr Pigments

Despite the notable alterations in composition, there was no considerable variation in the NIR reflectance values. The R_{NIR} values for the Fe:Cr05-10, Fe:Cr1-10, and Fe:Cr2-10 samples were recorded as 52.5%, 62.6%, and 61.9%, respectively. The NIR reflectance spectra of the pigments are presented in Figure 7.17.

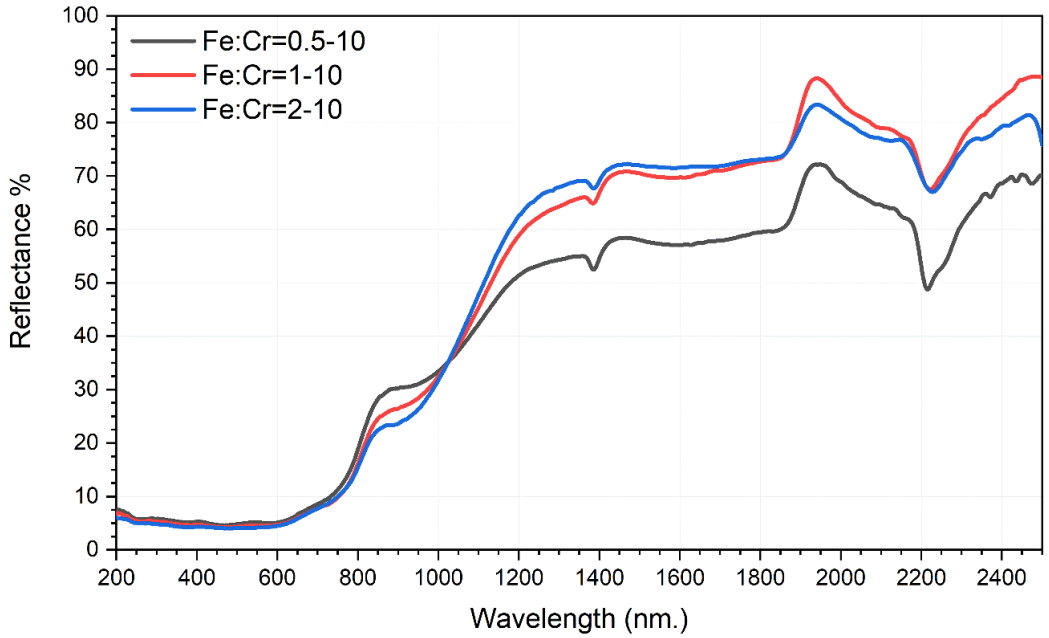


Figure 7.17 NIR reflectance spectrum of Fe:Cr0.5, Fe:Cr1 and Fe:Cr2 calcined at 1000 °C

The increase in the quantity of unreacted raw materials resulted in a decrease in the NIR reflectance values of the pigments. To ascertain the cause of this decrease, it

is essential to measure the NIR reflectance of the unreacted raw materials or achieve complete reaction. In an effort to minimize the presence of unreacted raw materials, the calcination temperature was elevated to 1200 °C. This temperature adjustment was made considering potential phase changes, yet the same crystal structures were maintained as observed at 1000 °C. The R_{NIR} values for the Fe:Cr05-12, Fe:Cr1-12, and Fe:Cr2-12 were recorded as 64.2%, 65.1%, and 65.3 %, respectively.

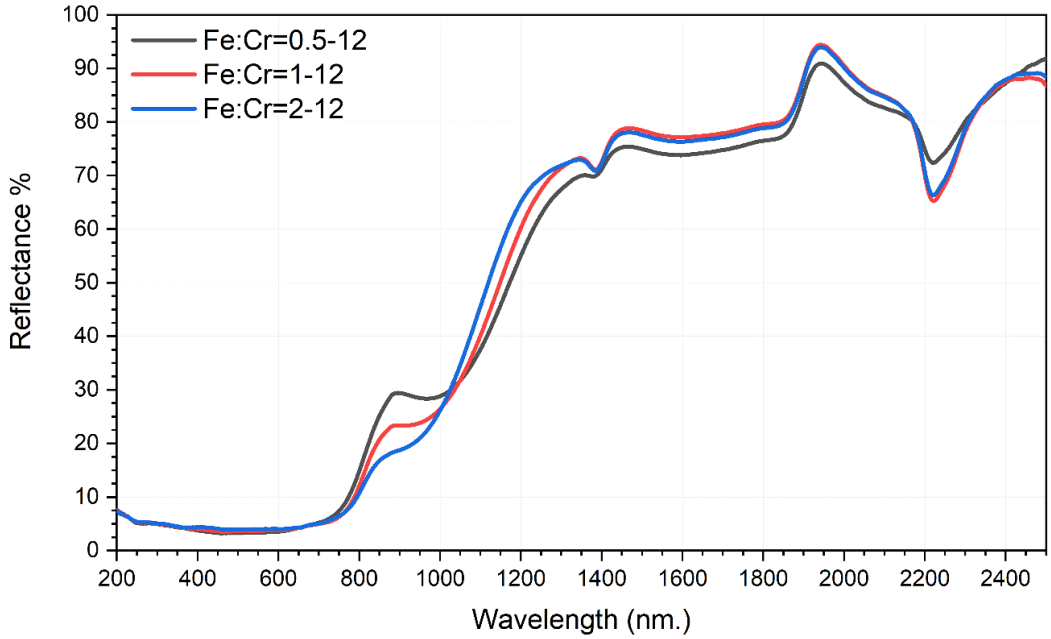


Figure 7.18 NIR reflectance spectrum of Fe:Cr0.5, Fe:Cr1 and Fe:Cr2 calcined at 1200 °C

7.2.3 Effect of Particle Size Distribution on Properties of Fe-Cr Pigments

Particle size is a crucial parameter for pigments, exerting a significant influence on various properties such as color, dispersion capability, and NIR reflectance. The literature indicates that the impact of different particle sizes on reflectance varies, with reductions in particle size resulting in both increased and decreased NIR reflectance depending on the chemical composition [142]–[145]. Additionally, studies, such as those conducted by Aslan et. all, have demonstrated that distinct particle morphologies resulting from various milling techniques can affect color values [146].

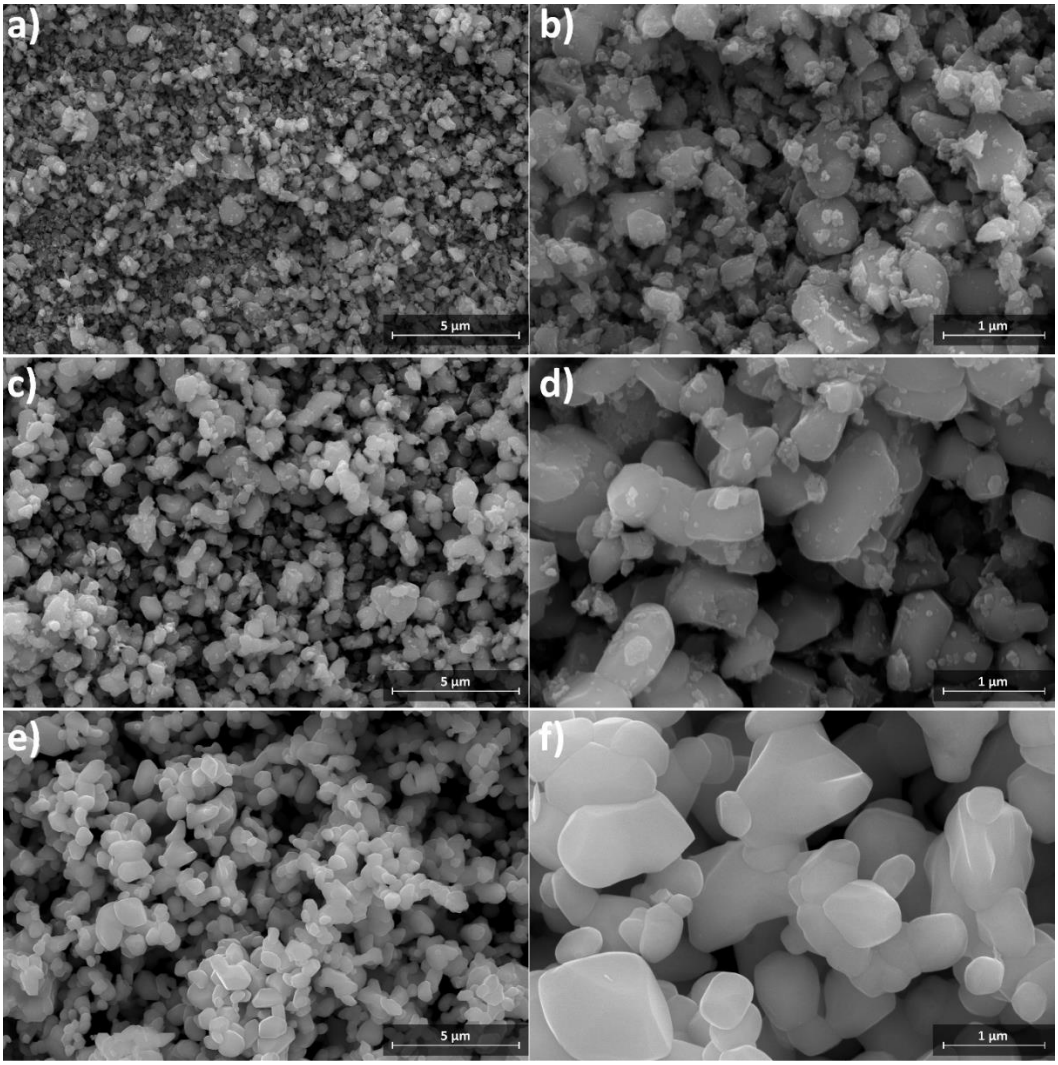


Figure 7.19 FEGSEM images of a) PS-1, c) PS-5 and e) PS-10 taken at x20,000 magnifications; b) PS-1, d) PS-5 and f) PS-10 taken at x80,000 magnifications

Figure 7.19 shows FEGSEM images of PS-1, PS-5, and PS-10 at magnifications of x20,000 and x80,000 to examine their properties, including particle size and morphology. In PS-10, the particles have smooth, oval shapes without sharp lines. Additionally, it is evident that some particles have combined to form agglomerates, likely due to reactant interactions during the reaction. These agglomerates consist of particles approximately 1 µm or smaller.

In PS-5, the smooth surfaces are less prominent, and the agglomerates have broken into smaller particles through milling. However, some agglomerates are still present. Smaller particles with fractured surfaces, not observed in PS-10, are also seen. These smaller particles may have broken off from larger particles during the milling process.

In PS-1, the agglomerates seen in PS-10 and PS-5 are no longer visible, and the smooth surfaces observed in PS-10 are almost absent. This suggests that the larger particles in PS-10 and PS-5 have fragmented into smaller particles. Compared to PS-10 and PS-5, PS-1 particles exhibit more deformed structures with sharper lines and more corners.

Table 7.7 Particle size distribution of PS-1, PS-5, and PS-10

Sample Name	Dv(10) (µm)	Dv(50) (µm)	Dv(90) (µm)	Dv(97) (µm)
PS-1	0.26	0.49	0.97	1.27
PS-5	0.87	2.13	4.98	6.69
PS-10	1.70	3.99	9.46	15.6

In this study, the Fe:Cr1-11 sample was selected to investigate the influence of particle size distribution on color and NIR reflectance properties. Raw materials, prepared with a Fe:Cr ratio of 1, underwent calcination at 1100 °C. Subsequently, the pigments were subjected to wet milling using a high-energy planetary ball mill (NETZSCH PM400 device and a 300 ml zirconium oxide milling jar). The milling process employed balls within the range of 2-4 mm, with a ball/powder ratio of 4:1 and a powder/water ratio of 1:1. Milling occurred at 400 RPM for durations ranging from 5 minutes to 1 hour. Following milling, the pigments were washed with distilled water and dried at 120 °C. The dried pigments underwent sieving through a 450 mesh (32 µm) sieve.

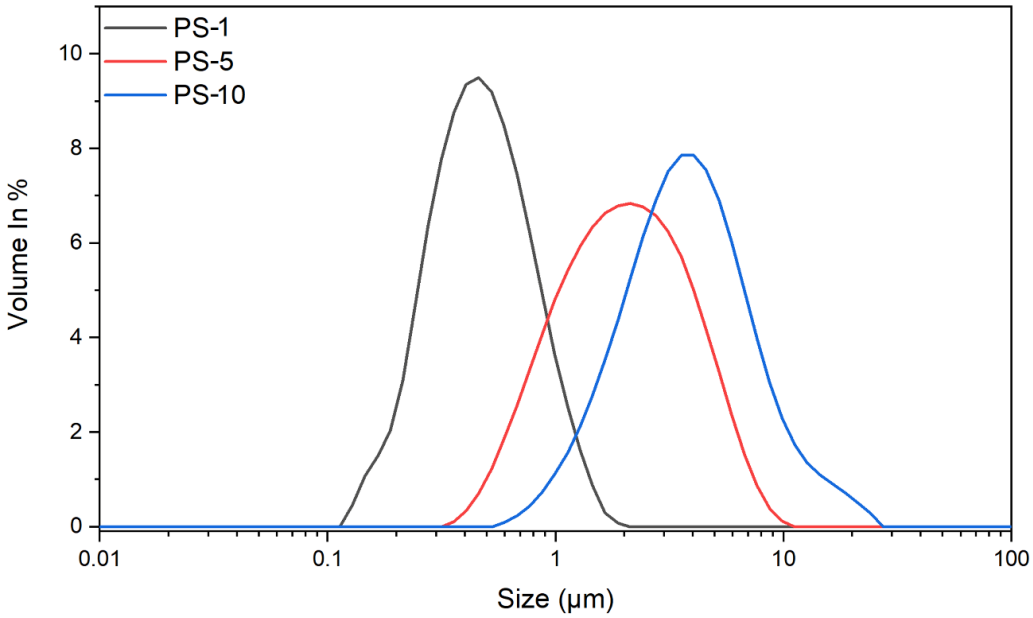


Figure 7.20 Particle size distribution of PS-1, PS-5 and, PS-10

The pigments were milled to achieve particle size distributions below 1 µm, 5 µm, 10 µm, and 20 µm, corresponding to Dv_{90} values of 90% by volume. Particle distribution measurements were conducted using the Mastersizer 3000 instrument with the wet unit HydroEV. Prior to measurement, the pigments were subjected to ultrasonic bathing for 1-5 minutes to disperse agglomerates. The measured particle size distribution values for the pigments are presented in Table 7.7, and their corresponding graphics are displayed in Figure 7.20.

Table 7.8 Color values of PS-1, PS-5 and PS-10

Sample Name		*L**	*a**	*b**	*C**
Mass Color	PSM-1	27.3	4.26	2.65	5.02
	PSM-5	25.83	2.26	1.05	2.49
	PSM-10	25.07	0.77	0	0.77
Tint Color	PST-1	43.83	4.33	-0.39	-
	PST-5	48.89	1.28	-3.69	-
	PST-10	58.42	-0.87	-5.28	-

Color measurements of the prepared pigments involved the application of paint/film, while plastic plate application was carried out for opacity measurements.

The standard procedure was followed for paint/film application, where 4 wt.% of the pigment was added to transparent paint. The film was applied using a pool-type film applicator and left to dry at room temperature. This choice aimed to prevent surface defects that might arise from rapid drying and to avoid any color changes in the base paint due to temperature fluctuations.

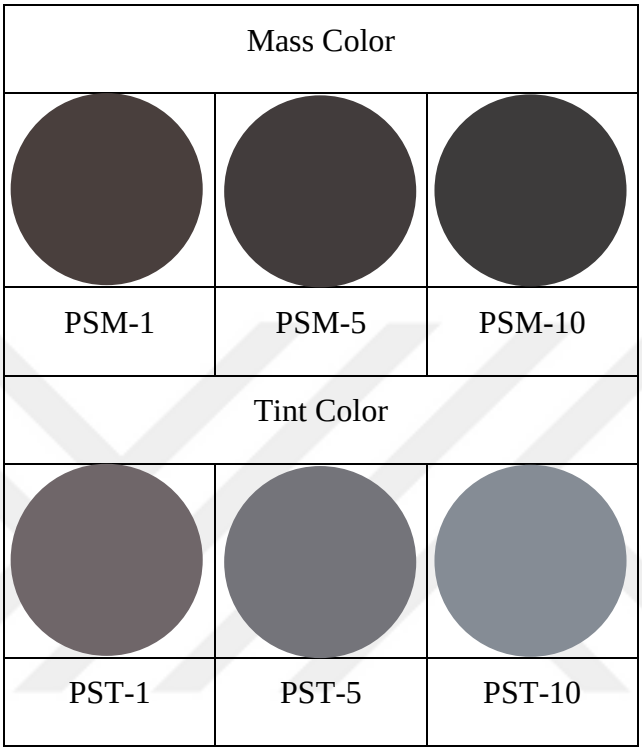


Figure 7.21 Mass and tint colors of PS-1, PS-5 and PS-10

The tint color method was performed to assess the pigment's coloring strength and hiding power. For tint, a mixture of 80% transparent acrylic paint and 20% white acrylic paint was created, and 4 wt.% pigment was incorporated. The homogenized paint, achieved with the assistance of a ball mill, was applied to white paper using a 0.4mm film applicator and dried at room temperature. The resulting color values and C^* after dye/film application are presented in Table 7.8. The mass and tint colors of the pigments are visually represented in Figure 7.21.

As the particle size decreased, there was an observable increase in the darkness and coloring strength and hiding power of the pigment. Notably, a significant rise in C^* value was observed for low particle size, especially in the PS-1. Conversely, while the PS-5 exhibited significantly higher coloring and tinting strength compared to the PS-10, no noteworthy change was observed in the C^* value.

The alterations resulting from the reduction in particle size, particularly the increase in the redness value (+a*), have been investigated. The XRD graph of the pigment obtained after calcination, along with the XRD graph and phases of the pigment milled below 1 µm, are examined in Figure 7.22. It's evident that the peaks corresponding to Fe_2O_3 and Cr_2O_3 phases in the initial material mix disappear after calcination. Comparing PS-1 and PS-10, the peaks of PS-10 exhibit greater intensity than those of PS-1. Moreover, in Figure 7.22, when comparing the XRD peaks of PS-1 and PS-10, a reduction in intensity and broadening of the peaks in PS-1 is noticeable. This reduction and broadening are attributed to the reduction in particle size from micron to nano-scale, a consequence of milling. These alterations in peak characteristics, such as reduced intensity and broadening, are commonly observed in various studies. They may stem from structural irregularities leading to less oriented crystallographic planes, lattice strains, dislocations, lattice distortions, and dispersion in diffraction angles [147]–[151].

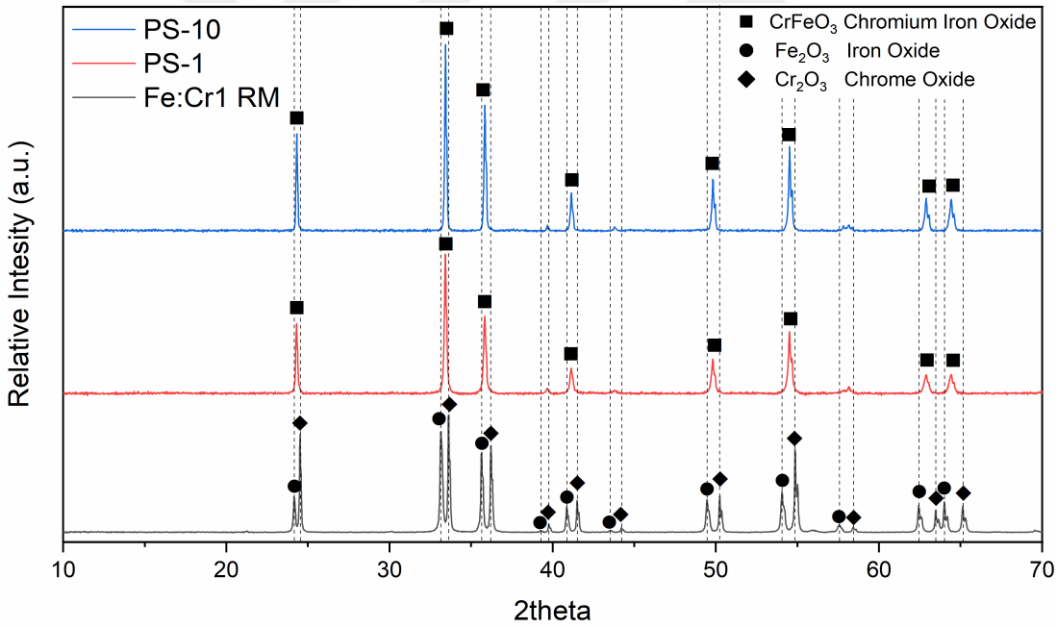


Figure 7.22 XRD analysis of PS-1, PS-10 and Fe:Cr1 RM

NIR reflectance spectrums of PS-1, PS-5, PS-10 and Carbon Black were given in Figure 7.23. The R_{NIR} values for the PS-1, PS-5, and PS-10 were recorded as 65.5%, 64.4%, and 65.3%, respectively. R_{NIR} is crucial for "Cool" pigments as it indicates their ability to deflect sunlight energy in the NIR spectrum [30], [152]. PS-1, PS-5, and PS-10 exhibit similar R_{NIR} within the 700-2500 nm wavelength range, yet notable discrepancies arise at specific wavelengths like 850, 1950, 2200, and 2400 nm. While these variations may not significantly impact plastic classification and

sorting, they hold significance when assessing pigments for the "Cool" category. On the other hand, Carbon Black absorbs almost all electromagnetic waves in the NIR. Research indicates that sunlight energy predominantly falls within the 700-1300 nm range [28], [48], [105]. Consequently, PS-1, PS-5, and PS-10, potential candidates for "Cool" pigments, were specifically analyzed within the 700-1300 nm range [45], [48], [54]. The $R_{NIR(700-1300)}$ for PS1, PS5, and PS10 within this range was calculated as 34.0%, 32.2%, and 30.4%, respectively. Notably, a decrease in particle size corresponds to an increase in R_{NIR} between 700 and 1300 nm. Literature reveals that variations in particle sizes can alter peak locations or intensities in spectra. Milling-induced particle size reduction affects properties such as surface area, scattering behavior, refractive index, and absorption coefficient, leading to phenomena like the Reststrahlen and Christensen effects [144], [145], [153]–[157].

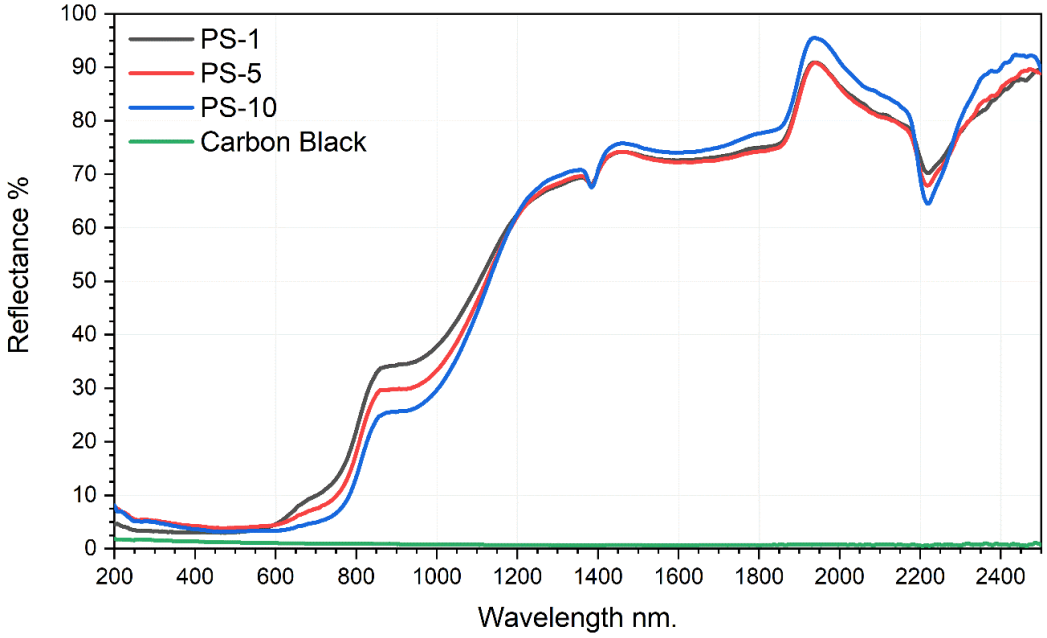


Figure 7.23 NIR reflectance spectrum of PS-1, PS-5, PS-10 and Carbon Black

7.3 NIR Reflective Black Pigments for Polymers

7.3.1 NIR Sorting of Polymers

Plastic/masterbatch applications have been made to examine the classifiability of plastic materials, which is another area of use of NIR reflective pigments, and to examine the color and optical properties of the pigments in these materials. Figure 7.24 shows photographs of uncolored and colored plastic plates with Fe:Cr1-10 pigment. Black colored PP (PP-Fe:Cr1-10) and PE (PE-Fe:Cr1-10) cannot be

distinguished from each other when visually examined. However, these two different materials can be separated from each other with the help of NIR spectra specific to plastic materials. However, when carbon black is used instead of the NIR reflective pigments synthesized in the study, every plastic will reflect in the same way and close to 0, since the electromagnetic waves that can be reflected by the plastic are absorbed by the Carbon Black. As a result of this absorption, plastic materials cannot be classified and recycled.



Figure 7.24 Plastic plates of a) PP, b) PE, c) PP-Fe:Cr1-10, and d) PE-Fe:Cr1-10

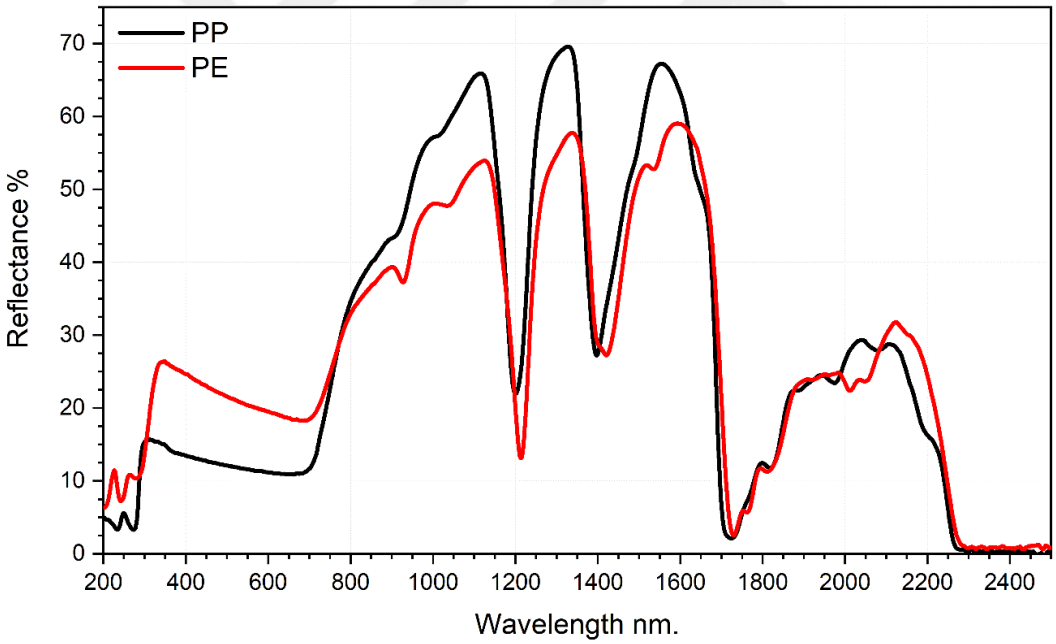


Figure 7.25 UV-VIS-NIR reflectance spectrums of PP and PE

Figure 7.25 shows the UV-VIS-NIR reflectance spectra of uncolored PP and PE plastic plates. When the spectra are examined, it is observed that they have different patterns. When the spectra at 1500 and 2000 nm were examined, it was observed that there were different reflectance and absorbance peaks. Thanks to these distinguishing features, plastics can be classified.

UV-VIS-NIR spectra of PP and PE plates colored with Fe:Cr1-10 are given in Figure 7.26. Considering the distinctive features of PP and PE mentioned above, the reflection spectra of PP-Fe:Cr1-10, PE-Fe:Cr1-10 and PP-Carbon Black plastic plates were examined. Distinctive reflection points of PP and PE were also observed on plastic plates colored with Fe:Cr1-10 pigment. Thanks to these points, even though both plastic plates appear the same to the eye, it can be distinguished which type of plastic material they are with the help of NIR electromagnetic waves. PE gives two high peaks at approximately 1950 and 2150 nm, while PP gives three main peaks at approximately 1950, 2050 and 2150 nm. While PE gives two peaks at approximately 1500 and 1600 nm, PP gives a single peak at approximately 1550 nm. Thanks to distinctive patterns and peaks like this, black colored PP and PE could be distinguished from each other. On the other hand, when the PP-Carbon Black sample colored with carbon black was examined, it was observed that there was almost no reflection and there was no obvious pattern. For this reason, it could not be determined which type of plastic material it was.

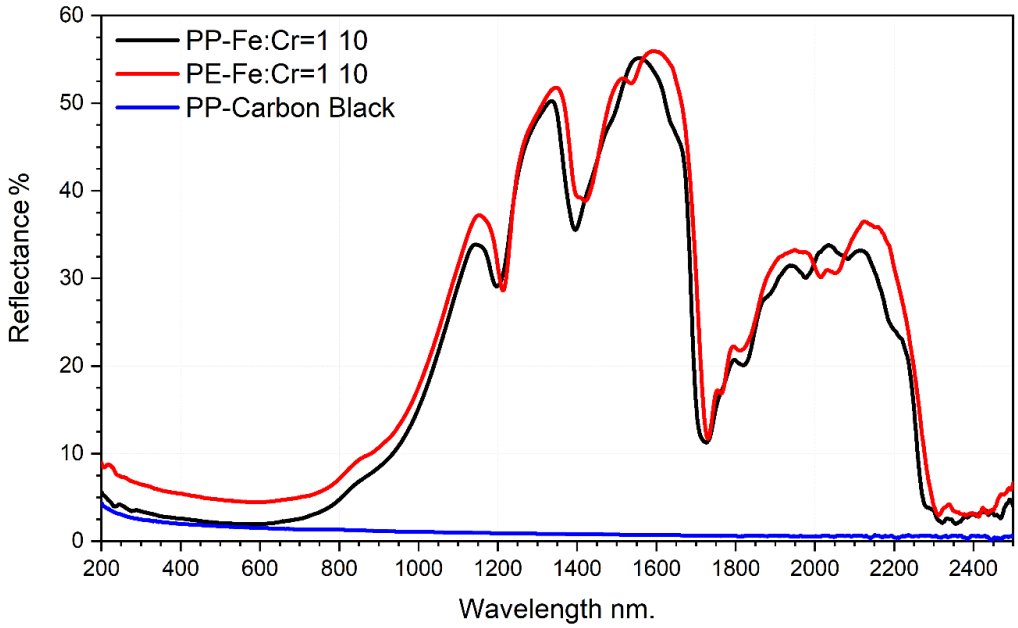


Figure 7.26 UV-VIS-NIR reflectance spectrums of PP-Fe:Cr1-10, PE-Fe:Cr1-10 and PP-Carbon Black

7.3.2 Effect of Particle Size of Pigments

7.3.2.1 Opacity and Coloring Strength

For opacity measurements, plastic plates were prepared using polypropylene (PP) polymer (25MFI). The polymeric granule material was transformed into a semi-melted plastic by increasing the temperature with the help of a device called Geli-

mat, which rotates the blades through friction. The pigment was added to semi-melted plastic at a ratio of 0.5 wt.%, and the mixture was stirred again with Gelimat. “PSMP-” represents the 1 mm PP 0.5 wt.% pigment colored plastic. Once the homogenized colored polymeric material was placed in a preheated mold at 180 °C, it underwent hot and cold pressing. The thickness of the resulting plate was 1 mm. The opacity of the colored polymers was measured using the CO.FO.ME.GRA DTP 642 Transmission Densitometer device. The opacity values of plastic plates were 3.4, 2.0 and 0.9 for PSMP-1, PSMP-5 and PSMP-10, respectively. Based on the measurements, it was observed that PSMP-1 was the opaquest sample. On the other hand, PSMP-10 exhibited much lower opacity compared to the PSMP-1. Although the PSMP-5 was close to PS-1, it could not provide opacity as much as PSMP-1. However, upon examining the color properties (Table 7.9), it was observed that the *C** of the PSMP-1 sample was significantly higher than that of the PSMP-5 sample. As the particle size of the pigments decreased, an increase in *C** was observed.

Table 7.9 Color and Chroma values of PSMP-1, PSMP-5, and PSMP-10

Sample Name		***L****	***a****	***b****	***C****
Mass Color	PSMP-1	28.59	4.59	3.1	5.54
	PSMP-5	26.71	2.65	1.33	2.96
	PSMP-10	24.74	1.01	-0.01	1.01

The opacity values and photographs of PSMP-1, PSMP-5 and PSMP-10 are presented in Figure 7.27. As seen in the graph, a decrease in particle size resulted in a substantial increase in both tinting strength and opacity from 10 µm onwards.



Figure 7.27 The photograph of PSMP-1, PSMP-5 and PSMP-10 on light source

Coloring plastic with pigments of smaller particle size leads to the production of more opaque samples due to the increase in specific surface area. When equal

weights of pigment are utilized, larger particles occupy less volume within the structure compared to smaller particles. Consequently, smaller particles cover a greater portion of the structure. The presence of more void spaces in larger particle pigments results in greater light transmission and less reflection compared to smaller particle pigments. This inability to reflect light effectively allows it to pass through the structure, indicating a higher degree of transparency and lower opacity. Figure 7.28 shows a schematic representation of two different plates with different opacity. When light hits the sample, it appears more opaque when it reflects rather than passing through the sample. In Figure 7.28, a represents the less opaque sample, while b represents the opaquer sample.

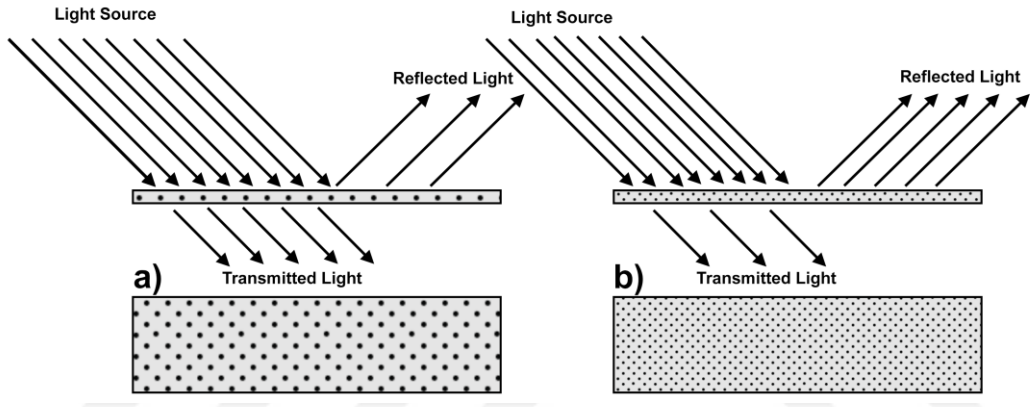


Figure 7.28 Illustration of light interaction with object a) less opaque and b) more opaque

8
CONCLUSION

As a result of the study, many black pigments with different coloring strength, hiding power, NIR reflectivity and undertones were obtained. Pigment selections can be made considering the desired properties of the final product. As a result of preliminary studies, $(Fe,Cr)_2O_3$ pigments with the highest R_{NIR} value were selected for the study and experiments continued with combinations of these two metal oxides. The properties of $(Fe,Cr)_2O_3$ pigments synthesized with different parameters were given Table 8.1.

When $(Fe,Cr)_2O_3$ pigments were examined in terms of color, it was seen that they could be obtained in different undertones. As the temperature used for pigment synthesis increased, both *a** and *b** values approached 0 on the positive side. This can be attributed to the increase in reaction efficiency with increasing temperature. For products where a more red and yellow black color is expected, products synthesized at lower temperatures may be preferred. These cases showed similar results at different Fe:Cr ratios.

When the effect of particle size was examined, independent of calcination temperature and composition, serious changes in color properties were observed. When the particle size of the pigments was reduced by milling, the color shifted from black to brown. An increase in *L**, *a** and *b** values was observed with decreasing particle size. With this increase, the color of the pigment shifted from black to brown. With the increase in a* and b* values, the pigment became more reddish and yellowish. The decrease in particle size had an effect on coloring strength, hiding power properties as well as color. As the particle size decreased, the coloring strength and hiding power of the pigments increased in line with the increasing specific surface area. While white materials colored with lower grain size pigment resulted in a darker (<*L**) color, transparent materials resulted in products with high opacity. However, the color value moved away from black, which has a low *C** value, and shifted towards brown.

When examined in terms of NIR reflectivity, the lowest reflectivity values were observed in pigments made at low temperatures and containing non-reactive raw materials. In experiments carried out at high temperatures, as the residues decreased, both color values and NIR reflectivity values became closer to each other, independent of the Fe:Cr ratio. When the connection between particle size and NIR reflectivity was examined, no significant difference was observed in R_{NIR} as the Dv_{90} value decreased from 10 μm to 1 μm. However, when the NIR values between 700-1300 nm, which have an important place for "cool" pigments, were examined, it was determined that pigments with low grain size had higher R_{NIR} values.

In line with the information given above, pigments that are suitable for the end user and have the desired properties are presented for selection. The pigments with the highest NIR reflectance coloring strength and hiding power were those with low particle size (Dv_{90} = 1 μm) and the least amount of residual raw material. However, when the colors of these pigments are examined, their *C** values are higher than other pigments with high particle sizes.

When pigments with lower *C** values are required, pigments with higher particle sizes and no residual raw materials can be preferred. The NIR reflectance of these pigments will be higher than those calcined at low temperatures, but their coloring strength and hiding power will be lower with increasing particle size.

Table 8.1 Properties of $(Fe,Cr)_2O_3$ pigments synthesized with different parameters

Fe:Cr (mol)	Temperature	Method	Dv_{90} (µm)	R_{NIR} (%)	*L**	*a**	*b**	*C**	Opacity
0.5	1000	Calcination (Solid-State Reaction)	~5	52.5	25.75	1.33	1.01	1.67	-
	1200			64.2	25.08	1.04	0.22	1.06	
1	1000			62.6	25.52	1.51	0.8	1.71	
	1100			64.5	25.51	0.98	0.36	1.04	
	1200			65.1	25.32	0.64	0.01	0.64	
2	1000			61.9	25.72	2.44	0.95	2.62	
	1200			65.3	25.51	0.59	-0.14	0.61	
1	1100		~1	65.5	27.3	4.26	2.65	5.02	3.4
			~5	64.4	25.83	2.26	1.05	2.49	2.0
			~10	65.3	25.07	0.77	0	0.77	0.9

REFERENCES

[1] G. Pfaff, *Inorganic Pigments*. De Gruyter, 2017. doi: 10.1515/9783110484519.

[2] E. Sugawara and H. Nikaido, *Pigment Compendium: A Dictionary and Optical Microscopy of Historical Pigments*, vol. 58, no. 12. 2014.

[3] G. Buxbaum and G. Pfaff, *Industrial Inorganic Pigments*. Wiley, 2005. doi: 10.1002/3527603735.

[4] R. Christie, "Azo Dyes and Pigments," in *Colour Chemistry*, The Royal Society of Chemistry, 2014, pp. 72–98. doi: 10.1039/BK9781849733281-00072.

[5] W. Funke, "Inorganic Pigments," in *Handbook of Environmental Chemistry*, vol. 3, 1980, pp. 217–229. doi: 10.1007/978-3-540-38522-6_8.

[6] J. M. Oyarzúm, *Pigment Processing: Physico-Chemical Principles*. Vincentz Network, 2016. doi: 10.1515/9783748600336.

[7] N. Eastaugh, V. Walsh, T. Chaplin, and R. Siddall, *The Pigment Compendium: Optical Microscopy of Historic Pigments*. Elsevier-Butterworth Heinemen, 2004.

[8] J. Zou, P. Zhang, C. Liu, and Y. Peng, "Highly dispersed (Cr, Sb)-co-doped rutile pigments of cool color with high near-infrared reflectance," *Dye. Pigment.*, vol. 109, pp. 113–119, Oct. 2014, doi: 10.1016/j.dyepig.2014.05.009.

[9] Z. Xu, D. Wang, M. Zhong, and Z. Zhang, "Preparation and characterization of Mg2+-doped CaCu3Ti4O12 pigment with high NIR reflectance," *Ceram. Int.*, vol. 46, no. 16, pp. 25306–25312, Nov. 2020, doi: 10.1016/j.ceramint.2020.06.324.

[10] N. Sangwong, M. Suwan, and S. Supothina, "Synthesis and optical band gap study of nir-reflective cofe2o4 black pigments doped with mgo, cao and al2o3," *Chiang Mai J. Sci.*, vol. 47, no. 4 Special Issue 2, pp. 686–699, 2020.

[11] L. Liu, A. Han, M. Ye, and W. Feng, "The evaluation of thermal performance of cool coatings colored with high near-infrared reflective nano-brown inorganic pigments: Magnesium doped ZnFe2O4 compounds," *Sol. Energy*, vol. 113, pp. 48–56, Mar. 2015, doi: 10.1016/j.solener.2014.12.034.

[12] S. Rossi, H. Lindmark, and M. Fedel, "Colored Paints Containing NIR-Reflective Pigments Exposed to Accelerated Ultraviolet Radiation Aging with Possible Application as Roof Coatings," *Coatings*, vol. 10, no. 11, p. 1135, Nov. 2020, doi: 10.3390/coatings10111135.

[13] E. S. Cozza, M. Alloisio, A. Comite, G. Di Tanna, and S. Vicini, "NIR-

reflecting properties of new paints for energy-efficient buildings," *Sol. Energy*, vol. 116, pp. 108–116, 2015, doi: 10.1016/j.solener.2015.04.004.

[14] A. A. Ali, E. El Fadaly, and I. S. Ahmed, "Near-infrared reflecting blue inorganic nano-pigment based on cobalt aluminate spinel via combustion synthesis method," *Dye. Pigment.*, vol. 158, pp. 451–462, Nov. 2018, doi: 10.1016/j.dyepig.2018.05.058.

[15] M. Suwan, "EFFECT OF Ni DOPING AND SYNTHESIS TEMPERATURE ON THE PROPERTIES OF NIR-REFLECTIVE $ZnFe_2O_4$ BLACK PIGMENTS," *Ceram. - Silikaty*, vol. 64, no. 2, pp. 172–179, Jan. 2020, doi: 10.13168/cs.2020.0006.

[16] S. Costanzini, C. Ferrari, F. Despini, and A. Muscio, "Standard Test Methods for Rating of Solar Reflectance of Built-Up Surfaces and Potential Use of Satellite Remote Sensors," *Energies*, vol. 14, no. 20, p. 6626, Oct. 2021, doi: 10.3390/en14206626.

[17] E. Coser, V. F. Moritz, A. Krenzinger, and C. A. Ferreira, "Development of paints with infrared radiation reflective properties," *Polimeros*, vol. 25, no. 3, pp. 305–310, 2015, doi: 10.1590/0104-1428.1869.

[18] N. Sangwong, M. Suwan, and S. Supothina, "Effect of calcination temperature and dolomite or Al2O3 doping on properties of NIR–reflective CoFe2O4 black pigment," *Mater. Today Proc.*, vol. 17, pp. 1595–1601, 2019, doi: 10.1016/j.matpr.2019.06.187.

[19] Y. ZHOU, X. WENG, L. YUAN, and L. DENG, "Influence of composition on near infrared reflectance properties of M-doped Cr_2O_3 (M=Ti,V) green pigments," *J. Ceram. Soc. Japan*, vol. 122, no. 1425, pp. 311–316, 2014, doi: 10.2109/jcersj2.122.311.

[20] A. Rosati, M. Fedel, and S. Rossi, "NIR reflective pigments for cool roof applications : A comprehensive review," *J. Clean. Prod.*, vol. 313, no. June, p. 127826, 2021, doi: 10.1016/j.jclepro.2021.127826.

[21] D. S. Parker and S. F. Barkaszi, "Roof solar reflectance and cooling energy use: field research results from Florida," *Energy Build.*, vol. 25, no. 2, pp. 105–115, Jan. 1997, doi: 10.1016/S0378-7788(96)01000-6.

[22] J. Qin *et al.*, "The Optical Properties of Black Coatings and Their Estimated Cooling Effect and Cooling Energy Savings Potential," *J. Power Energy Eng.*, vol. 02, no. 04, pp. 68–75, 2014, doi: 10.4236/jpee.2014.24011.

[23] S. Sadeghi-Niaraki, B. Ghasemi, A. H. Adeh, E. Ghasemi, and M. Ghahari, "Preparation of (Fe,Cr)2O3@TiO2 cool pigments for energy saving applications," *J. Alloys Compd.*, vol. 779, pp. 367–379, Mar. 2019, doi: 10.1016/j.jallcom.2018.11.114.

[24] G. M. Revel *et al.*, "Cool products for building envelope – Part I: Development and lab scale testing," *Sol. Energy*, vol. 105, pp. 770–779, Jul. 2014, doi: 10.1016/j.solener.2014.03.029.

[25] M. Zinzi and S. Agnoli, "Cool and green roofs . An energy and comfort comparison between passive cooling and mitigation urban heat island techniques for residential buildings in the Mediterranean region," *Energy Build.*, vol. 55, pp. 66–76, 2012, doi: 10.1016/j.enbuild.2011.09.024.

[26] R. Levinson, H. Akbari, P. Berdahl, K. Wood, W. Skilton, and J. Petersheim, “A novel technique for the production of cool colored concrete tile and asphalt shingle roofing products,” *Sol. Energy Mater. Sol. Cells*, vol. 94, no. 6, pp. 946–954, Jun. 2010, doi: 10.1016/j.solmat.2009.12.012.

[27] H. Akbari and H. D. Matthews, “Global cooling updates : Reflective roofs and pavements,” *Energy Build.*, vol. 55, pp. 2–6, 2012, doi: 10.1016/j.enbuild.2012.02.055.

[28] R. Oka, S. Iwasaki, and T. Masui, “Improvement of near-infrared (NIR) reflectivity and black color tone by doping Zn 2+ into the Ca 2 Mn 0.85 Ti 0.15 O 4 structure,” *RSC Adv.*, vol. 9, no. 66, pp. 38822–38827, 2019, doi: 10.1039/C9RA07849E.

[29] T. Zhang, Y. Wang, S. Ke, and Z. Pan, “Processing Research Synthesis of in-situ encapsulated ZnS x Se 1- x / ZrSiO 4 composite as cool pigment on ceramic tiles for energy saving,” vol. 23, no. 3, pp. 326–334, 2022.

[30] J. S. Hwang and K. Y. Jung, “Effect of calcination temperature and Ti substitution on optical properties of (Fe,Cr) 2 O 3 cool black pigment prepared by spray pyrolysis,” *RSC Adv.*, vol. 12, no. 1, pp. 72–77, 2022, doi: 10.1039/D1RA08300G.

[31] J. Zheng, Z. Li, Y. Zheng, W. Zhao, and F. Tan, “A novel rare-earth high-entropy RE 6 MoO 12 with high near-infrared reflectance as a promising inorganic ‘ cool pigment ,’” *Ceram. Int.*, vol. 49, no. 1, pp. 558–564, 2023, doi: 10.1016/j.ceramint.2022.09.023.

[32] F. Hollstein, M. Wohllebe, and S. Arnaiz, “Identification and Sorting of Plastics Film Waste by NIR-Hyperspectral-Imaging,” in *Near Infrared Spectroscopy: Proceedings of the International Conference*, Oct. 2015, vol. I, no. October, pp. 9–14. doi: 10.17648/nir-2015-34127.

[33] Y. Zheng, J. Bai, J. Xu, X. Li, and Y. Zhang, “A discrimination model in waste plastics sorting using NIR hyperspectral imaging system,” *Waste Manag.*, vol. 72, pp. 87–98, Feb. 2018, doi: 10.1016/j.wasman.2017.10.015.

[34] R. K. Pachauri and A. Reisinger, “Climate Change 2007: Synthesis Report,” THE INTERGOVERNMENTAL PANEL ON CLIMATE CHANGE.

[35] L. C. Lau, K. T. Tan, K. T. L. Ã, and A. R. Mohamed, “A comparative study on the energy policies in Japan and Malaysia in fulfilling their nations ’ obligations towards the Kyoto Protocol,” *Energy Policy*, vol. 37, no. 11, pp. 4771–4778, 2009, doi: 10.1016/j.enpol.2009.06.034.

[36] U.S. Energy Information Administration, “Use of energy explained,Energy use in homes.” https://www.eia.gov/energyexplained/use-of-energy/homes.php

[37] International Energy Agency, “The Future of Cooling Opportunities for energy- efficient air conditioning.” [Online]. Available: www.iea.org

[38] International Energy Agency, “Space Cooling,” 2022. www.iea.org

[39] B. Kaur, N. Quazi, I. Ivanov, and S. N. Bhattacharya, “Near-infrared reflective properties of perylene derivatives,” *Dye. Pigment.*, vol. 92, no. 3, pp. 1108–1113, 2012, doi: 10.1016/j.dyepig.2011.06.011.

[40] Glenn D. Considine, *Van nostrand's scientific encyclopedia*, 10th ed. New York: A Johon Wiley & Sons, 2008.

[41] R. Levinson, H. Akbari, S. Konopacki, and S. Bretz, "Inclusion of cool roofs in nonresidential Title 24 prescriptive requirements," *Energy Policy*, vol. 33, no. 2, pp. 151–170, Jan. 2005, doi: 10.1016/S0301-4215(03)00206-4.

[42] R. L. Ã, P. Berdahl, and H. Akbari, "Solar spectral optical properties of pigments — Part I : model for deriving scattering and absorption coefficients from transmittance and reflectance measurements," vol. 89, pp. 319–349, 2005, doi: 10.1016/j.solmat.2004.11.012.

[43] G. M. Revel *et al.*, "Cool products for building envelope – Part II: Experimental and numerical evaluation of thermal performances," *Sol. Energy*, vol. 105, pp. 780–791, Jul. 2014, doi: 10.1016/j.solener.2014.02.035.

[44] A. L. Pisello and F. Cotana, "Ac ce p te us cr t," *Energy Build.*, 2013, doi: 10.1016/j.enbuild.2013.10.031.

[45] V. C. Malshe and A. K. Bendiganavale, "Infrared Reflective Inorganic Pigments," *Recent Patents Chem. Eng.*, vol. 1, no. 1, pp. 67–79, Jan. 2010, doi: 10.2174/1874478810801010067.

[46] A. Synnefa, M. Saliari, and M. Santamouris, "Experimental and numerical assessment of the impact of increased roof reflectance on a school building in Athens," *Energy Build.*, vol. 55, pp. 7–15, Dec. 2012, doi: 10.1016/j.enbuild.2012.01.044.

[47] M. Suwan, N. Sangwong, and S. Supothina, "Effect of Co and Pr doping on the properties of solar-reflective ZnFe 2 O 4 dark pigment," *IOP Conf. Ser. Mater. Sci. Eng.*, vol. 182, no. 1, p. 012003, Mar. 2017, doi: 10.1088/1757-899X/182/1/012003.

[48] R. Oka and T. Masui, "Synthesis and characterization of black pigments based on calcium manganese oxides for high near-infrared (NIR) reflectance," *RSC Adv.*, vol. 6, no. 93, pp. 90952–90957, 2016, doi: 10.1039/C6RA21443F.

[49] N. Eastaugh and V. Walsh, "The Pigment Compendium. Optical Microscopy of Historic Pigments," p. 412p., 2004.

[50] J. Zou, P. Zhang, C. Liu, and Y. Peng, "Highly dispersed (Cr, Sb)-co-doped rutile pigments of cool color with high near-infrared reflectance," *Dye. Pigment.*, vol. 109, pp. 113–119, 2014, doi: 10.1016/j.dyepig.2014.05.009.

[51] J. S. Hwang and K. Y. Jung, "Effect of calcination temperature and Ti substitution on optical properties of (Fe,Cr)2O3cool black pigment prepared by spray pyrolysis," *RSC Adv.*, vol. 12, no. 1, pp. 72–77, Dec. 2021, doi: 10.1039/d1ra08300g.

[52] A. Towns, "Colorants: General survey," *Phys. Sci. Rev.*, vol. 4, no. 8, Jul. 2019, doi: 10.1515/psr-2019-0008.

[53] R. M. Christie, "Pigments for plastics," in *Kunstst Ger Plast*, vol. 66, no. 10, 1998, pp. 485–498. doi: 10.1007/978-94-011-5862-6_53.

[54] R. Levinson, P. Berdahl, and H. Akbari, "Solar spectral optical properties of

pigments - Part II: Survey of common colorants," *Sol. Energy Mater. Sol. Cells*, vol. 89, no. 4, pp. 351–389, 2005, doi: 10.1016/j.solmat.2004.11.013.

[55] E. B. Faulkner and R. J. Schwartz, *High Performance Pigments*. Wiley, 2009. doi: 10.1002/9783527626915.

[56] T. Allen, *Powder Sampling and Particle Size Determination*. Elsevier, 2003. doi: 10.1016/B978-0-444-51564-3.X5000-1.

[57] "Laser Diffraction." https://particletechlabs.com/analytical-testing/laser-diffraction/

[58] K. L. Dishman, "Sieving in Particle Size Analysis," in *Encyclopedia of Analytical Chemistry*, Wiley, 2000. doi: 10.1002/9780470027318.a1514.

[59] A. C. Fahrenholz, L. J. McKinney, C. E. Wurth, and K. C. Behnke, "The importance of defining the method in particle size analysis by sieving (2010)," *Kansas Agric. Exp. Stn. Res. Reports*, no. 10, pp. 261–264, Jan. 2010, doi: 10.4148/2378-5977.3435.

[60] "Analytical Testing Sieve Analysis." https://particletechlabs.com/analytical-testing/sieve-analysis/)

[61] H. Bresch, V.-D. Hodoroaba, A. Schmidt, K. Rasmussen, and H. Rauscher, "Counting Small Particles in Electron Microscopy Images—Proposal for Rules and Their Application in Practice," *Nanomaterials*, vol. 12, no. 13, p. 2238, Jun. 2022, doi: 10.3390/nano12132238.

[62] N. Pamme, R. Koyama, and A. Manz, "Counting and sizing of particles and particle agglomerates in a microfluidic device using laser light scattering: application to a particle-enhanced immunoassay," *Lab Chip*, vol. 3, no. 3, p. 187, 2003, doi: 10.1039/b300876b.

[63] G. L. Fairs, "XII.—DEVELOPMENTS IN THE TECHNIQUE OF PARTICLE-SIZE ANALYSIS BY MICROSCOPICAL EXAMINATION," *J. R. Microsc. Soc.*, vol. 71, no. 2, pp. 209–222, Sep. 1951, doi: 10.1111/j.1365-2818.1951.tb01967.x.

[64] M. Caurie, "A method to correct the wide discrepancy between Brunauer, Emmett and Teller water and N2 surface areas of adsorbents," *Int. J. Food Sci. Technol.*, vol. 47, no. 11, pp. 2366–2371, Nov. 2012, doi: 10.1111/j.1365-2621.2012.03111.x.

[65] F. S. Irwansyah *et al.*, "How to Read and Determine the Specific Surface Area of Inorganic Materials using the Brunauer-Emmett-Teller (BET) Method," *ASEAN J. Sci. Eng.*, vol. 4, no. 1, pp. 61–70, Oct. 2022, doi: 10.17509/ajse.v4i1.60748.

[66] Micromeritics, "Pore Analysis." https://www.micromeritics.com/particle-testing/analytical-testing/pore-analysis/

[67] M. F. Gazulla, M. P. Gómez, A. Barba, and M. Orduña, "Chemical and phase characterisation of ceramic pigments," *X-Ray Spectrom.*, vol. 36, no. 2, pp. 82–91, Mar. 2007, doi: 10.1002/xrs.943.

[68] A. Kiehl and H. Brendel, "Anticorrosive pigments for chemically and thermally resistant coatings," *Macromol. Symp.*, vol. 187, pp. 97–108, 2002, doi: 10.1002/1521-3900(200209)187:1<97::AID-MASY97>3.0.CO;2-P.

[69] R. A. Eppler, “Selecting Ceramic Pigments,” 2008, pp. 1139–1149. doi: 10.1002/9780470310458.ch1.

[70] S. Jose, D. Joshy, S. B. Narendranath, and P. Periyat, “Recent advances in infrared reflective inorganic pigments,” *Sol. Energy Mater. Sol. Cells*, vol. 194, no. January, pp. 7–27, 2019, doi: 10.1016/j.solmat.2019.01.037.

[71] R. Aghababazadeh, A. R. Mirhabibi, F. Moztarzadeh, and Z. Salehpour, “Synthesis and characterisation of chromium oxide as a pigment for high temperature application,” *Pigment Resin Technol.*, vol. 32, no. 3, pp. 160–165, 2003, doi: 10.1108/03699420310475629.

[72] G. Pfaff, “Chromium oxide pigments,” *Antraquinonoid Pigment. - Color Fundam.*, vol. 3, no. Iii, pp. 113–118, 2022, doi: 10.1515/9783110588071-014.

[73] J. Barnhart, “Occurrences, Uses, and Properties of Chromium,” *Regul. Toxicol. Pharmacol.*, vol. 26, no. 1 I, pp. 3–7, 1997, doi: 10.1006/rtph.1997.1132.

[74] G. Buxbaum *et al.*, “Pigments, Inorganic, 3. Colored Pigments,” in *Ullmann’s Encyclopedia of Industrial Chemistry*, Wiley, 2009. doi: 10.1002/14356007.n20_n02.

[75] J. Wang *et al.*, “Spinel to Rock-Salt Transformation in High Entropy Oxides with Li Incorporation,” *Electrochem*, vol. 1, no. 1, pp. 60–74, Mar. 2020, doi: 10.3390/electrochem1010007.

[76] Complex Inorganic Color Pigments Committee, “CPMA CLASSIFICATION AND CHEMICAL DESCRIPTIONS OF THE COMPLEX INORGANIC COLOR PIGMENTS,” 2010. [Online]. Available: www.cpma.com

[77] Y. Youn *et al.*, “Effects of metal dopings on CuCr2O4 pigment for use in concentrated solar power solar selective coatings,” *ACS Appl. Energy Mater.*, vol. 2, no. 1, pp. 882–888, 2019, doi: 10.1021/acsaem.8b01976.

[78] D. Guo, Q. Yang, P. Chen, Y. Chu, Y. Zhang, and P. Rao, “The influence of micronization on the properties of Pr-ZrSiO4 pigment,” *Dye. Pigment.*, vol. 153, pp. 74–83, 2018, doi: 10.1016/j.dyepig.2018.01.049.

[79] G. Del Nero, G. Cappelletti, S. Ardizzone, P. Fermo, and S. Gilardoni, “Yellow Pr-zircon pigments,” *J. Eur. Ceram. Soc.*, vol. 24, no. 14, pp. 3603–3611, Nov. 2004, doi: 10.1016/j.jeurceramsoc.2004.01.003.

[80] M. E. Spahr and R. Rothon, “Carbon Black as a Polymer Filler,” in *Polymers and Polymeric Composites: A Reference Series*, Berlin, Heidelberg: Springer Berlin Heidelberg, 2016, pp. 1–31. doi: 10.1007/978-3-642-37179-0_36-2.

[81] T. A. J. Kuhlbusch, S. Neumann, and H. Fissan, “Number Size Distribution, Mass Concentration, and Particle Composition of PM 1 , PM 2.5 , and PM 10 in Bag Filling Areas of Carbon Black Production,” *J. Occup. Environ. Hyg.*, vol. 1, no. 10, pp. 660–671, Oct. 2004, doi: 10.1080/15459620490502242.

[82] D. B. Blackford and G. R. Simons, “Particle Size Analysis of Carbon Black,” *Part. Part. Syst. Charact.*, vol. 4, no. 1–4, pp. 112–117, Jan. 1987, doi: 10.1002/ppsc.19870040123.

[83] W. Zhou *et al.*, “High Near-Infrared Reflectance Orange Pigments of Fe-Doped La2W2O9: Preparation, Characterization, and Energy Consumption Simulation,” *ACS Sustain. Chem. Eng.*, vol. 9, no. 36, pp. 12385–12393, Sep. 2021, doi: 10.1021/acssuschemeng.1c04799.

[84] E. Aslan, E. Toy, A. Grijalbo, and E. Yes, “Results in Chemistry The effect of various nickel oxide ratios on the color and reflectivity of PY53 nickel-titanate yellow pigment,” vol. 4, no. October, 2022, doi: 10.1016/j.rechem.2022.100662.

[85] O. F. The, “SURFEX 90,” *Pigment Resin Technol.*, vol. 19, no. 4, pp. 12–21, Apr. 1990, doi: 10.1108/eb042715.

[86] R. Madlener and Y. Sunak, “Impacts of urbanization on urban structures and energy demand : What can we learn for urban energy planning and urbanization management ?,” *Sustain. Cities Soc.*, vol. 1, no. 1, pp. 45–53, 2011, doi: 10.1016/j.scs.2010.08.006.

[87] A. Lanfranchi, H. Megahd, P. Lova, and D. Comoretto, “Multilayer Polymer Photonic Aegises Against Near-Infrared Solar Irradiation Heating,” 2022, doi: 10.1021/acsami.1c25037.

[88] E. O. Lawrence, S. E. Bretz, and H. Akbari, “Long-Term Performance of High-Albedo Roof Coatings,” vol. 25, no. March, 1997.

[89] R. Levinson *et al.*, “Methods of creating solar-reflective nonwhite surfaces and their application to residential roofing materials,” vol. 91, no. 2007, pp. 2006–2008, 2008, doi: 10.1016/j.solmat.2006.06.062.

[90] T. Thongkanluang, T. Kittiauchawal, and P. Limsuwan, “Preparation and characterization of Cr 2 O 3 – TiO 2 – Al 2 O 3 – V 2 O 5 green pigment,” vol. 37, pp. 543–548, 2011, doi: 10.1016/j.ceramint.2010.09.044.

[91] A. Han, M. Zhao, M. Ye, J. Liao, Z. Zhang, and N. Li, “Crystal structure and optical properties of YMnO3 compound with high near-infrared reflectance,” *Sol. Energy*, vol. 91, pp. 32–36, May 2013, doi: 10.1016/j.solener.2013.01.011.

[92] H. Akbari, S. Bretz, D. M. Km-n, and J. Hanford, “Peak power and cooling energy savings of high-albedo roofs,” vol. 25, 1992.

[93] S. P. Radhika and K. J. Sreeram, “Rare earth doped cobalt aluminate blue as an environmentally benign colorant,” vol. 1, no. 4, pp. 301–309, 2012, doi: 10.1007/s40145-012-0029-6.

[94] J. Milgrom, “Recycling Plastics.,” 1975, doi: 10.1007/978-1-4615-1615-6_5.

[95] D. M. Scott, “A two-colour near-infrared sensor for sorting recycled plastic waste,” *Meas. Sci. Technol.*, vol. 6, no. 2, pp. 156–159, 1995, doi: 10.1088/0957-0233/6/2/004.

[96] G. H. Now, P. Colorants, and S. C. Masterbatches, “Support the Circular Economy - Turn Former Waste into Recyclable Packaging,” pp. 3–6.

[97] Association of Plastic Recyclers, “Near infrared (NIR) sorting in the plastics recycling process,” pp. 2–4, 2018, [Online]. Available: plasticsrecycling.org

[98] T. H. E. Problem, “Arctic ® Infrared Refl ective Pigments allow for a more

sustainable solution to black plastic recycling," 2019.

[99] Ampacet, "Ampacet Provides A Second Life For Black Plastic Packaging With Carbon Black-Free Masterbatch Range REC-." https://www.ampacet.com/black-masterbatch-solutions-designed-for-near-infrared-sorting-technologies/

[100] C. Tone, "New Near-Infrared Detectable Black Masterbatch," no. May, pp. 3–5, 2018.

[101] L. I. N. Recycling, "Techmer PM launches new grades of NIR- sortable black pigment," pp. 1–5, 2021.

[102] K. Laird, "Back to black with NIR-detectable pigment," pp. 1–5, 2020, [Online]. Available: https://www.sustainableplastics.com/news/back-black-nir-detectable-pigment

[103] G. E. T. The and L. Updates, "Additives : NIR-Detectable Black Masterbatch Technology Make Dark Colors More Recyclable Join the Plastics Technology Community for Controlling Your Cycle Time : Part 3 What ' s," pp. 1–2, 2020.

[104] Ferro Corporation, "NEW NIR-REFLECTING PIGMENTS FOR SUSTAINABLE RECYCLING," pp. 1–5, 2011, [Online]. Available: https://www.ferro.com/innovation/solutions/new-nir-reflecting-pigments-for-sustainable-recycling

[105] T. Moriomoto, R. Oka, K. Minagawa, and T. Masui, "Novel near-infrared reflective black inorganic pigment based on cerium vanadate," *RSC Adv.*, vol. 12, no. 26, pp. 16570–16575, 2022, doi: 10.1039/D2RA02483G.

[106] R. C. Thompson, C. J. Moore, F. S. Saal, and S. H. Swan, "Plastics , the environment and human health : current consensus and future trends," no. 2009, pp. 2153–2166, 2010, doi: 10.1098/rstb.2009.0053.

[107] United Nations Environment Programme, "Plastic planet: How tiny plastic particles are polluting our soil." [Online]. Available: https://www.unep.org/

[108] The Vanella Group, "The Negative Effects Of Plastic On The Environment." [Online]. Available: https://www.vanellagroupmn.com/

[109] L. Parker, "Plastic pollution facts and information." [Online]. Available: https://www.nationalgeographic.com/environment/article/plastic-pollution

[110] "Five Ways That Plastics Harm The Environment (And One Way They May Help)." [Online]. Available: https://www.forbes.com/

[111] K. C. Ujeh, "The negative environmental effects of plastic shopping bags." [Online]. Available: https://www.ibanet.org/

[112] L. Sullivan, "Recycling plastic is practically impossible — and the problem is getting worse." [Online]. Available: https://www.npr.org/

[113] The Organisation for Economic Co-operation and Development, "Plastic pollution is growing relentlessly as waste management and recycling fall short, says OECD." [Online]. Available: https://www.oecd.org/

[114] Eurostat, "Plastic packaging waste: 38% recycled in 2020." [Online]. Available: https://ec.europa.eu/

[115] B. Yüksek Beyoğlu, "Yüksek Sıcaklıklarda Kararlı İnorganik Seramik Pigmentlerin Üretimi ve Karakterizasyonu," 2007.

[116] Ç. Börekcioglu, "HOMOJEN ÇÖKTÜRME YÖNTEMİYLE Fe2O3/α-Al2O3 PİGMENTLERİN ÜRETİMİ VE KARAKTERİZASYONU," 2018.

[117] K. Nassau, "The Fifteen Causes of Color," in *AZimuth*, vol. 1, no. C, Elsevier Masson SAS, 1998, pp. 123–168. doi: 10.1016/S1387-6783(98)80007-X.

[118] B. Tanışan, "Kamaralı ve Döner Fırınlarda Siyah Seramik Pigment Üretimi ve Karakterizasyonu," 2008.

[119] F. Flament, V. Hourblin, and S. Nouveau, "Skin Color Types and Indian Skin Characteristics," 2014, pp. 47–61.

[120] R. S. Berns, *Billmeyer and Saltzman's Principles of Color Technology*. Wiley, 2019. doi: 10.1002/9781119367314.

[121] "Gülnar Makina." https://www.gulnarmakina.com/

[122] A. Moroccan, "Contourite drifts and cold-water coral mounds in the Atlantic Moroccan coral province . Thomas Vandorpe," 2017.

[123] "Precise Color Communication." https://www.konicaminolta.com/instruments/knowledge/color/part3/02.html#:~:text=The method of color measurement,SCI (Specular Component Included)

[124] "UV-VIS-NIR Spektrometresi." https://daytam.atauni.edu.tr/altyapi/malzeme-sentezi-ve-karakterizasyonu/ileri-spektroskopi-laboratuvari/uv-vis-nir-spektrometresi/

[125] S. Kültür and N. Türkeri, "Assessment of long term solar reflectance performance of roof coverings measured in laboratory and in field," *Build. Environ.*, vol. 48, no. 1, pp. 164–172, Feb. 2012, doi: 10.1016/j.buildenv.2011.09.004.

[126] Z. M. Khoshhesab, "Reflectance IR Spectroscopy," in *Infrared Spectroscopy - Materials Science, Engineering and Technology*, InTech, 2012. doi: 10.5772/37180.

[127] E. Aslan, M. Bulut, A. Grijalbo, and B. Çiçek, "Effect of the milling method and particle structure on the color tone of (Cr, Fe)2O3 inorganic black masterbatch pigment," *Adv. Powder Technol.*, vol. 33, no. 2, p. 103421, Feb. 2022, doi: 10.1016/j.apt.2021.103421.

[128] O. M. Ozkendir, "Electronic and crystal structure analysis of the FeCrO3 oxide," *J. Electron Spectros. Relat. Phenomena*, vol. 191, pp. 54–59, Dec. 2013, doi: 10.1016/j.elspec.2013.10.004.

[129] P. Ma, Q. Geng, X. Gao, S. Yang, and G. Liu, "CuCr2O4 Spinel Ceramic Pigments Synthesized by Sol-Gel Self-Combustion Method for Solar Absorber Coatings," *J. Mater. Eng. Perform.*, vol. 25, no. 7, pp. 2814–2823, Jul. 2016, doi: 10.1007/s11665-016-2143-z.

[130] J. Gilabert, M. D. Palacios, V. Sanz, and S. Mestre, "Effects of composition and furnace temperature on (Ni, Co) (Cr, Al) 2 O 4 pigments synthesized by solution combustion route," *Int. J. Appl. Ceram. Technol.*, vol. 15, no. 1, pp. 179–190, Jan. 2018, doi: 10.1111/ijac.12761.

[131] Ismunandar, N. Nurdini, M. M. Ilmi, E. Maryanti, and G. T. M. Kadja, "Investigation on the Crystal Structures of Hematite Pigments at Different Sintering Temperatures," *Key Eng. Mater.*, vol. 874, pp. 20–27, Jan. 2021, doi: 10.4028/www.scientific.net/KEM.874.20.

[132] T. C. de S. Santos, D. do R. Pinheiro, C. M. L. Costa, D. C. Estumano, and N. F. da P. Ribeiro, "Synthesis and characterization of pigments based on copper-zinc aluminate (CuxZn1-xAl2O4) by combustion," *Ceram. Int.*, vol. 46, no. 2, pp. 2332–2343, Feb. 2020, doi: 10.1016/j.ceramint.2019.09.224.

[133] N. Popov *et al.*, "Influence of Cr doping on the structural, magnetic, optical and photocatalytic properties of α-Fe2O3 nanorods," *J. Phys. Chem. Solids*, vol. 148, no. May 2020, 2021, doi: 10.1016/j.jpcs.2020.109699.

[134] R. Muñoz, M. Martos, C. M. Rotaru, H. Beltrán, E. Cordoncillo, and P. Escribano, "Influence of the precursors on the formation and properties of the FexCr2-xO3 solid solution," *J. Eur. Ceram. Soc.*, vol. 26, no. 8, pp. 1363–1370, 2006, doi: 10.1016/j.jeurceramsoc.2005.02.008.

[135] J. R. Taylor and A. T. Dinsdale, "A Thermodynamic Assessment of the Cr - Fe - O System," *Int. J. Mater. Res.*, vol. 84, no. 5, pp. 335–345, May 1993, doi: 10.1515/ijmr-1993-840511.

[136] L. Kjellqvist, M. Selleby, and B. Sundman, "Thermodynamic modelling of the Cr–Fe–Ni–O system," *Calphad*, vol. 32, no. 3, pp. 577–592, Sep. 2008, doi: 10.1016/j.calphad.2008.04.005.

[137] A. MUAN and S. OMIYA, "Phase Relations in the System Iron Oxide—Cr 2 O 3 in Air," *J. Am. Ceram. Soc.*, vol. 43, no. 4, pp. 204–209, Apr. 1960, doi: 10.1111/j.1151-2916.1960.tb12982.x.

[138] A. Kelly and K. M. Knowles, *Crystallography and Crystal Defects*. Wiley, 2012. doi: 10.1002/9781119961468.

[139] G. Wang, J. Zhou, and Z. Sun, "First principles investigation on anomalous lattice shrinkage of W alloyed rock salt GeTe," *J. Phys. Chem. Solids*, vol. 137, p. 109220, 2020, doi: https://doi.org/10.1016/j.jpcs.2019.109220.

[140] D. E. Cox, W. J. Takei, and G. Shirane, "A magnetic and neutron diffraction study of the Cr2O3-Fe2O3 system," *J. Phys. Chem. Solids*, vol. 24, no. 3, pp. 405–423, Mar. 1963, doi: 10.1016/0022-3697(63)90199-9.

[141] N. Pailhé, A. Wattiaux, M. Gaudon, and A. Demourgues, "Impact of structural features on pigment properties of α-Fe2O3 haematite," *J. Solid State Chem.*, vol. 181, no. 10, pp. 2697–2704, Oct. 2008, doi: 10.1016/j.jssc.2008.06.049.

[142] P. Jeevanandam, R. S. Mulukutla, M. Phillips, S. Chaudhuri, L. E. Erickson, and K. J. Klabunde, "Near Infrared Reflectance Properties of Metal Oxide Nanoparticles," *J. Phys. Chem. C*, vol. 111, no. 5, pp. 1912–1918, Feb. 2007, doi: 10.1021/jp066363o.

[143] T. L. Myers *et al.*, "Quantitative reflectance spectra of solid powders as a function of particle size," *Appl. Opt.*, vol. 54, no. 15, p. 4863, May 2015, doi: 10.1364/AO.54.004863.

[144] Y.-F. Su *et al.*, "Infrared reflectance spectra: effects of particle size, provenance and preparation," *Opt. Photonics Counterterrorism, Crime*

Fight. Def. X; Opt. Mater. Biomater. Secur. Def. Syst. Technol. XI, vol. 9253, p. 925304, 2014, doi: 10.1117/12.2069954.

[145] J. F. Mustard and J. E. Hays, "Effects of Hyperfine Particles on Reflectance Spectra from 0.3 to 25 μm," *Icarus*, vol. 125, no. 1, pp. 145–163, Jan. 1997, doi: 10.1006/icar.1996.5583.

[146] E. Aslan, M. Bulut, A. Grijalbo, and B. Çiçek, "Effect of the milling method and particle structure on the color tone of (Cr, Fe)2O3 inorganic black masterbatch pigment," *Adv. Powder Technol.*, vol. 33, no. 2, p. 103421, Feb. 2022, doi: 10.1016/j.apt.2021.103421.

[147] S. Britto, S. Joseph, and P. Vishnu Kamath, "Distinguishing crystallite size effects from those of structural disorder on the powder X-ray diffraction patterns of layered materials," *J. Chem. Sci.*, vol. 122, no. 5, pp. 751–756, Sep. 2010, doi: 10.1007/s12039-010-0063-2.

[148] O. Sahin and V. Erturun, "The effect of ball milling on crystallite size," *Acad. Perspect. Procedia*, vol. 3, no. 1, pp. 543–549, 2020, doi: 10.33793/acperpro.03.01.103.

[149] A. A. Al-Tabbakh, N. Karatepe, A. B. Al-Zubaidi, A. Benchaabane, and N. B. Mahmood, "Crystallite size and lattice strain of lithiated spinel material for rechargeable battery by X-ray diffraction peak-broadening analysis," *Int. J. Energy Res.*, vol. 43, no. 5, pp. 1903–1911, Apr. 2019, doi: 10.1002/er.4390.

[150] N. Y. Iwata, A. Kimura, M. Fujiwara, and N. Kawashima, "Effect of milling on morphological and microstructural properties of powder particles for High-Cr Oxide dispersion strengthened ferritic steels," *J. Nucl. Mater.*, vol. 367–370, no. SPEC. ISS., pp. 191–195, Aug. 2007, doi: 10.1016/j.jnucmat.2007.03.147.

[151] V. Chikhalia, R. T. Forbes, R. A. Storey, and M. Ticehurst, "The effect of crystal morphology and mill type on milling induced crystal disorder," *Eur. J. Pharm. Sci.*, vol. 27, no. 1, pp. 19–26, Jan. 2006, doi: 10.1016/j.ejps.2005.08.013.

[152] G. George, V. S. Vishnu, and M. L. P. Reddy, "The synthesis, characterization and optical properties of silicon and praseodymium doped Y6MoO12 compounds: Environmentally benign inorganic pigments with high NIR reflectance," *Dye. Pigment.*, vol. 88, no. 1, pp. 109–115, Jan. 2011, doi: 10.1016/j.dyepig.2010.05.010.

[153] R. Prost, "The Influence of the Christiansen Effect on I.R. Spectra of Powders," *Clays Clay Miner.*, vol. 21, no. 5, pp. 363–368, 1973, doi: 10.1346/CCMN.1973.0210512.

[154] J. W. Salisbury and A. Wald, "The role of volume scattering in reducing spectral contrast of reststrahlen bands in spectra of powdered minerals," *Icarus*, vol. 96, no. 1, pp. 121–128, Mar. 1992, doi: 10.1016/0019-1035(92)90009-V.

[155] G. R. Hunt and L. M. Logan, "Variation of Single Particle Mid-Infrared Emission Spectrum with Particle Size," *Appl. Opt.*, vol. 11, no. 1, p. 142, Jan. 1972, doi: 10.1364/AO.11.000142.

[156] J. M. Olinger and P. R. Griffiths, “Effects of Sample Dilution and Particle Size/Morphology on Diffuse Reflection Spectra of Carbohydrate Systems in the Near- and Mid-Infrared. Part I: Single Analytes,” *Appl. Spectrosc.*, vol. 47, no. 6, pp. 687–694, Jun. 1993, doi: 10.1366/0003702934066965.

[157] T. L. Myers, C. S. Brauer, Y.-F. Su, T. A. Blake, T. J. Johnson, and R. L. Richardson, “The influence of particle size on infrared reflectance spectra,” in *Algorithms and Technologies for Multispectral, Hyperspectral, and Ultraspectral Imagery XX*, Jun. 2014, vol. 9088, no. 509, p. 908809. doi: 10.1117/12.2053350.

PUBLICATIONS FROM THE THESIS

Conference Papers

1. E. Toy and B. Çiçek, “Effect of Calcination Temperature on Color and NIR Reflectivity of (Fe,Cr)2O3 Black Pigment,” in *3rd International Congress on Engineering and Sciences*, Istanbul, 2024.